FINAL REPORT

"The role of PGE_2 signaling at the epithelial-mesenchymal interface in Colorectal Cancer and Inflammatory Bowel Disease"

submitted by

Marina Schernthanner BSc

University of Innsbruck

Innsbruck, November 2018

Home University:	University of Innsbruck
Supervisor:	Univ. Prof. Dr. Dirk Meyer (University of Innsbruck)
Host institution:	Yale School of Medicine
Supervisor:	Manolis Roulis, PhD (Yale School of Medicine)

Acknowledgements

First of all, I would like to thank Richard A. Flavell for giving me the opportunity to pursue my master thesis project in his laboratory at the Yale School of Medicine, allowing me to work with and alongside some incredible, extraordinarily talented minds in science. Thank you to Prof. Dirk Meyer, who willingly agreed to supervise this work and largely helped me in preparing for my stay abroad and the University of Innsbruck for providing me with a well-founded knowledge in biology besides enabling me to take on a project like this. I would also very much like to thank the Austrian Marshall Plan Foundation for their financial support, which to a great extent financed my work, studies and life in the United States. Thank you, at this point, also to Sandra Scherl, my assigned contact person in Innsbruck, to whom I could turn to for questions about organizational management and funding and Prof. Ute Rothbächer, who helped me get this thesis project by writing a warm recommendation letter.

A sincere thank you, most certainly, goes to the Flavellian community for providing such a stimulating and continuously welcoming environment. I have learned a lot during insightful weekly lab meetings and scientific discussions, while being motivated performance-wise by witnessing their constant effort, work ethic and knowledge. I am particularly grateful for all the effort and work Manolis, my supervisor at Yale, invested to grant me the best training possible. Not only did he train me in a number of basic techniques, advanced methods and technical skills, but also helped me to gradually evolve into an independent, responsible researcher, able to plan, conduct and analyze experiments. Thank you for sharpening my scientific perception during our (almost) weekly journal clubs, raising my interest in new biological fields I haven't been exposed to before and for believing in myself when I did not. It was a great year working with you and all other Flavellians on such exciting projects and an experience I will never forget.

Last but not least, a big thank you goes to my family and friends, who from the very beginning on supported me whole-heartedly in my decisions and despite the long distance were always there for me. My deepest gratitude goes to my mum, my best friend, who helped me through my initial homesickness and throughout my whole life continuously supported and believed in me.

Thank you all for enabling me to follow my dreams, accomplish my goals and on top of that make such invaluable experiences that I will carry in my heart throughout my life.

Abstract

Inflammatory bowel disease (IBD) and colorectal cancer (CRC) classify as two highly prevalent intestinal disorders affecting millions of people worldwide. Prostaglandin (PGE_2) signaling has been associated with both, primarily thought to be implemented in pro-inflammatory responses. Recent genome-wide association studies for IBD ranked the prostaglandin receptor gene *PTGER4* (EP4) among the candidate genes most significantly linked to IBD. Here, we specifically focus on a ~400 kb non-coding region upstream of *PTGER4*, which not only harbors elicited genetic variants, but also overlaps with enhancer marks and is conserved between human and mouse. Employing the CRISPR/Cas9 methodology we set up an *in vitro* system to knockout designated genetic (non-coding) elements in human cell lines, while examining the role of *Ptger4* in mouse models of IBD. Given that fibroblast-specific ablation of *Ptger4* alleviated inflammation in mice, we further established an organotypic system to model epithelial-mesenchymal cellular interactions. Since the epithelial-mesenchymal interface has also proven to be essential for intestinal tumorigenesis, we extended our studies to a murine model of CRC. Our results reveal strong effects of the PGE_2-EP4 signaling axis in both conditions. Within IBD EP4 upon immune-related stimulation with PGE_2 in fibroblasts supposedly activates downstream pro-inflammatory processes, whilst during CRC mesenchymal-derived PGE_2 via EP4 in epithelial stem/progenitor cells seems to induce a downstream Yap-mediated stemness program. Overall, we provide evidence for a molecular axis in an intimate mesenchymal-epithelial microenvironment affecting inflammation, proliferation and differentiation, thus being associated with and explanatory for the correlative incidence of IBD and CRC in humans.

Table of contents

1. Introduction

1.1. Mesenchymal-epithelial interactions within intestinal development

The gastrointestinal tract in the human body relies upon a network of various cell types implicated not only in numerous signaling pathways but also disease pathologies. Facing rapid renewal, the intestinal epithelium combines, aligned within its' typical crypt-villus architecture, differentiated and stem cells (see figure 1.1.A). Enterocytes serve for nutrient uptake and appear alongside mucin-producing goblet cells, enteroendocrine cells secreting hormones, tuft cells and M cells in lymphoid Peyer's patches (Barker, van Oudenaarden and Clevers, 2012). Paneth cells and secretory equivalents in the colon, respectively (Rothenberg *et al.*, 2012), exerting antimicrobial defense, preferably reside in the crypts of Lieberkhun with intestinal stem cells (ISCs) of either actively cycling, i.e. crypt base columnar cells (CBCs), or quiescent character (Vermeulen and Snippert, 2014). They help maintaining the intestinal stem cell niche (Barker, van Oudenaarden and Clevers, 2012; Vermeulen and Snippert, 2014). In addition, the subjacent intestinal microenvironment, primarily composed of heterogeneous mesenchymal cells, basement membrane and soluble cell- or matrix-associated growth factors, contributes to intestinal stem cell dynamics (Powell *et al.*, 2011).

Bidirectional signaling between the epithelium and mesenchyme postnatally is required for intestinal development. Signaling gradients, encompassing predominant Wnt, bone morphogenetic protein (BMP) and hedgehog (Hh) signaling, help shape the typical villus-crypt axis of the intestine (Powell *et al.*, 2011; Karlsson *et al.*, 2000; Kurahashi *et al.*, 2013). Primarily expressed in intestinal epithelial cells, hedgehog molecules are implicated in the generation of mesenchymal cells in the lamina propria, subjacent to the epithelium (Madison *et al.*, 2005). Similarly to Hh agonists, canonical Wnts are secreted by the epithelium, particularly Paneth cells, whilst noncanonical ones together with Wnt antagonists originate in mesenchymal cells. The mesenchyme seems to locally concentrate Wnt and downstream β-catenin signaling to stem and progenitor cells in the intestinal crypt base. Hh and Wnt signaling gradients, however, appear to be opposing, with the latter one exerting its highest signal strength in pericryptal regions ensuring stem cell proliferation (see figure 1.1.B). BMP molecules, just as Hh, antagonize Wnt and thereby restrict its proliferative capacity to the crypt, whilst BMP antagonists, expressed by myofibroblasts proximal to the crypt, help maintain the stem cell niche (Powell *et al.*, 2011). In addition, stem cell

proliferation and survival is impacted by Notch signaling activity (Sancho, Cremona and Behrens, 2015). Taken together, mesenchymal cells supposedly are required for accurate dosing and localization of the mentioned signaling agonists within the frame of intestinal morphogenesis and subsequent maintenance of the respective cell populations. *In vitro* their implication in these processes has been remodeled in organotypic cultures (see 1.2.1.), rendering a cocktail of extracellular matrix-associated and BMP antagonistic molecules as crucial for organoid development from Lgr5+ intestinal stem cells (Sato *et al.*, 2009).

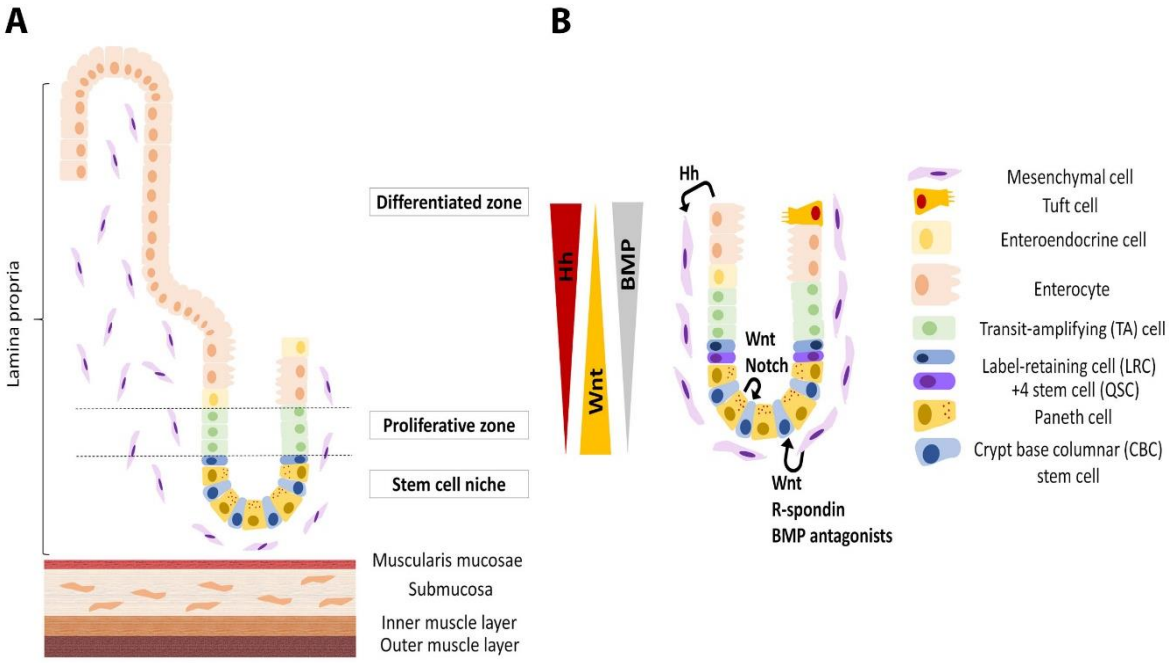

Figure 1.1. Schematic overview of the intestinal morphology and signaling gradients. (A) The intestine appears in crypt-villus units. The epithelial layer thereby is lying on top of a network of fibroblasts and extracellular matrix components (lamina propria), followed by layers of *Muscularis mucosae*, submucosa, inner (circular) and outer (longitudinal) muscular layers. Stem, progenitor and Paneth cells make up the stem cell niche on the bottom of crypts, succeeded by an adjacent proliferative and differentiated zone **(B)** Major signaling gradients shaping the cellular compartments predominantly in pericryptal regions of the intestine. Paneth and mesenchymal cells serve as Wnt signaling agents. Hh molecules are secreted by the epithelium towards the subjacent stromal compartment, Notch signaling occurs between epithelial cells, R-spondin and BMP antagonists from fibroblasts additionally support the Wnt source within cryptal region (adapted from Powell *et al.*, 2011; Roulis and Flavell, 2016)

1.2. The role of the mesenchyme in intestinal disorders – IBD and colorectal cancer in the focus

With the intestinal mesenchyme changing in morphology and function along the crypt-villus axis (Desaki and Shimizu, 2000) and impacting epithelial cell populations, dysfunction of it often underlies common intestinal pathologies. Inflammatory bowel disease (IBD) in its two clinically defined forms of ulcerative colitis (UC) and Crohn's disease (CD), is emblematic for

a gastrointestinal chronic progressive or remittent inflammatory condition, originating in an immunologically dysregulated microenvironment following epithelial barrier disruption and subsequent entry of microbiota from the lumen (Kaser, Zeissig and Blumberg, 2010). Whilst CD is characterized by an alternating pattern of inflamed and uninflamed areas throughout the gastrointestinal tract, although most commonly affecting the distal small intestine (ileum), UC, exhibiting continuous lesions, is usually restricted to rectal and colonic parts of the gut. Inflammation in CD may proceed transmurally, whereas in UC it is limited to the mucosa (Boyapati, Satsangi and Ho, 2015; Liu and Stappenbeck, 2016). With fibroblasts being involved in immune cell trafficking processes (Toyoda *et al.*, 1997) and fistula development in Crohn's disease (Powell *et al.*, 2011), a role of mesenchymal cells in inflammatory conditions in the intestine appears reasonable.

Within IBD, fibroblasts have been shown to react to detrimental proinflammatory cues like tumor necrosis factor (TNF) (Armaka *et al.*, 2008), commonly upregulated in the epithelium (Roulis *et al.*, 2011), by increasingly producing matrix-metalloproteases (MMPs) or secreting collagens (Bamba *et al.*, 2003) and thereby remodeling the extracellular matrix. Apart from that, mesenchymal cells may also be involved in immune cell recruitment and secrete cytokines, be it immuno-attractants or -suppressors such as interleukin-10 (IL-10), themselves. Based upon their adjacent microenvironment fibroblasts thus are capable of exerting immunosuppressive or -stimulatory effects, which complicates our understanding of mechanisms underlying inflammatory conditions such as IBD (Powell *et al.*, 2011).

Besides immunoregulatory function, however, stromal cells, upon proinflammatory cues, may also counteract progredient damage of the intestinal epithelium by signaling-induced repair mechanisms (Roulis *et al.*, 2014), re-localization in cryptal proximity (Brown *et al.*, 2007) or stimulating epithelial proliferation in addition to promoting stem cell differentiation (Grégoire *et al.*, 2017). Recent data from single-cell RNA sequencing on colonic mesenchyme from human IBD patients versus healthy individuals elucidated two fibroblast-like subsets, one of which displayed reduced Wnt signaling activity influencing stem cell self-renewal in IBD patients (Kinchen *et al.*, 2018), which is consistent with the description of stromal cells as potent Wnt-signaling niche upon injury (Degirmenci *et al.*, 2018; Greicius *et al.*, 2018). IBD condition was aggravated by the expansion of the second subset secreting pro-inflammatory factors interfering with the resolution phase of the wound-healing process (Kinchen *et al.*,

2018). In conclusion, mesenchymal cells via matrix remodeling and signaling towards immune or epithelial cells, including cryptal progenitor and stem cells, vastly engage in regenerative processes in the gut. Whilst a return to proliferative capacities, linked to active Wnt signaling, tendentially is viewed as beneficial for epithelial repair, an excessive deregulation of this pathway may cause a shift towards tumorigenic processes, though, closely linking inflammatory processes (IBD) with the formation of (colorectal) cancer.

Given its role for stem cell proliferation Wnt signaling represents the most frequent and earliest pathway facing deregulation in colorectal carcinogenesis, being vastly dependent on the stromal niche (Powell *et al.*, 2011; Degirmenci *et al.*, 2018; Greicius *et al.*, 2018). Indeed, upregulated Wnt signaling in cells of the crypt base, i.e. LGR5+, PROM1+ or BMI1+ cells, is a designated sign of adenomatous growth in the small intestine (Vermeulen and Snippert, 2014). Consistently, the perception of tumors as products of aberrantly growing cancer stem cells (CSCs) with metastatic capacities while maintaining their potential to self-renew and differentiate (Dalerba *et al.*, 2007), gains popularity. The compartmentalization of actively cycling stem cells in the intestine is believed to establish a balance between necessary regenerative capacities and dissipation of tumorigenic mutations in oncogenes or tumor suppressor genes at homeostatic state. Mutations like these, however, may assign a competitive advantage, i.e. increased proliferative potential, to a stem cell, enabling it to colonize a crypt. Once fixation is achieved, expansion of the mutated lineage via crypt fission follows. Most often, this competitiveness is highly context-dependent, raising the possibility for cancer formation in an inflammatory milieu, like f.e. in colitis, as opposed to homeostatic conditions (Vermeulen and Snippert, 2014). Based upon their pericryptal localization (see figure 3.1.) and their identification as a potent Wnt-signaling niche, mesenchymal cells thus represent an interesting target population, likely causative also in intestinal tumorigenesis.

1.2.1. How to model intestinal tumorigenesis – organoid culture

A major caveat in cancer research long has been the inadequacy of tumor models. Neither murine models, unrepresentative of the genetically as well as histologically heterogeneous complexity of human cancer, nor *in vitro* cancer cell lines poorly recapitulating in vivo mechanisms, have solved this issue. Also, patient-derived tumor xenografts (PDTXs) discount variable engraftment efficacy and mouse-specific effects (Drost and Clevers, 2018).

Exploiting a cocktail (ENR) of epidermal growth factor (EGF), BMP-inhibitor noggin and Wnt activator R-spondin1, all reportedly stimulating crypt proliferation, in combination with laminin-rich Matrigel, reducing *anoikis* of isolated intestinal cells, Sato and colleagues (2011) developed an *in vitro* system highly resembling the *in vivo* crypt-villus morphology in the intestine. This long-term culture method allows for organoid growth from both, murine and human intestinal tissue (Sato *et al.*, 2011) and requires LGR5+ intestinal stem cells (Sato *et al.*, 2009), known to continuously give rise to transit-amplifying (TA) cells, which will subsequently undergo differentiation (Mustata *et al.*, 2013). Aligning with the cell populations *in vivo*, organoids harbor crypt-like progenitor niches and villus-like domains with all of the differentiated cell types in the epithelium (Spence *et al.*, 2011). Intriguingly and of clinical relevance, organoids are also associated with regenerative potential, given that they reconstituted epithelial disruption after transplantation into colonic injury models (Miura and Suzuki, 2017). If taken from fetal intestinal tissue, organoids even omit their typical budding and exhibit a so-called spheroid morphology, characterized by an increased amount of progenitor and stem cells, fewer differentiated epithelial cells and an altered expression profile (Mustata *et al.*, 2013). The suggested stemness potential does not exclusively evolve as a consequence of reinforced Wnt signaling (Van der Flier *et al.*, 2007), considering Notch signaling as an alternative pathway to maintain the spheroid state (Noah and Shroyer, 2013). In fact, stem cells in spheroids, most accurately defined as Trop2/Cnx43+ for now, differ from Lgr5+ ones and are hypothesized to display a progenitor population, converting into conventional stem cells as development proceeds (Mustata *et al.*, 2013). This appears relevant in the light of reported interconversion processes between intestinal stem cell subsets of disparate proliferative potential, specifically during regenerative mechanisms and requires further investigation.

1.3. Prostaglandin E_2 and *PTGER4* – suspects in IBD and CRC

Crohn's disease and ulcerative colitis, the two common forms of IBD, affect millions of people worldwide with rising prevalence (Boyapati, Satsangi and Ho, 2015). Genome-wide association studies (GWAS) represent a relatively novel methodology, comparing the genotypes of numerous cohorts of different ancestry, encompassing IBD patients and aim at identifying a genetic profile inducing inflammatory pathogenesis. Through GWAS genetic

variants (SNPs) within haplotypes that are associated with the disease course, help identify candidate (risk) genes linked to IBD. The number of revealed susceptibility loci steadily increases (Jostins *et al.*, 2012; Liu and Stappenbeck, 2016; de Lange *et al.*, 2017; Huang *et al.*, 2017), amounting to 241 IBD risk loci as derived from the most recent analysis. Intriguingly, many SNPs linked to UC and CD also confer substantial risks for alternative immune-regulated diseases such as ankylosing spondylitis or arthritis (Verstockt, Smith and Lee, 2018). To definitively assess the genetic driver of IBD, finemapping studies (Huang *et al.*, 2017) based upon immunochips, i.e. microarrays containing a set of variants specifically linked with immune diseases, ideally ameliorate the resolution of genetic risk loci via high-density mapping and assist in the identification of causal variants (Liu and Stappenbeck, 2016). GWAS has helped uncover numerous susceptibility loci linked to IBD pathology, however, owing to cohort-specific effects and disease course variabilities it often remains difficult to deconvolute functional implications associated with variants (Verstockt, Smith and Lee, 2018). Notably, finemapping studies have shown that the majority of potentially causal SNPs, partially identified through compensatory expression quantitative trait loci (eQTL) analyses, resides within non-coding regions (Liu and Stappenbeck, 2016). Among those, many are located in transcriptionally active genetic loci exhibiting H3K4me1 and H3K27ac marks, often specifically in disease-relevant tissues (Huang *et al.*, 2017).

PTGER4, encoding one of 4 receptors (EP4) relevant for the Prostaglandin E_2 (PGE_2) pathway, an annotated candidate gene, ranks among the most significant associations with IBD (see figure 1.2.) (Jostins *et al.*, 2012). Its synthesizing enzyme, encoded by *PTGS2*, was defined as an IBD-risk locus as well, strengthening the role of prostaglandin in chronic inflammatory conditions (McGovern, Kugathasan and Cho, 2015). Apart from immune-related disorders certain risk loci associatively mapped to colorectal cancer, often an adversary complication in UC (Huang *et al.*, 2017). Although not specifically mapped to colorectal cancer, *PTGER4* in a separate series of association studies for human cancer has been indicated as a candidate gene for SNPs found in microRNA target sequences, underscoring the regulatory potential of non-coding elements (Landi *et al.*, 2007). Taken together, prostaglandin signaling appears to be of great importance in both, inflammatory and carcinogenic manifestations (Krause and DuBois, 2000; Hull, Ko and Hawcroft, 2004). Consistently, non-steroidal anti-inflammatory drugs (NSAIDs), known to interfere with prostaglandin rate-limiting cyclooxygenases, rank among well-established medical treatments of IBD. Additionally, aspirin, exemplary of those,

is hypothesized to limit tumorigenesis via inhibitory effects on Wnt activity (Vermeulen and Snippert, 2014) and the regulation of EP4 signaling in colorectal carcinoma has been proposed as a therapeutic approach (Yokoyama *et al.*, 2013).

A

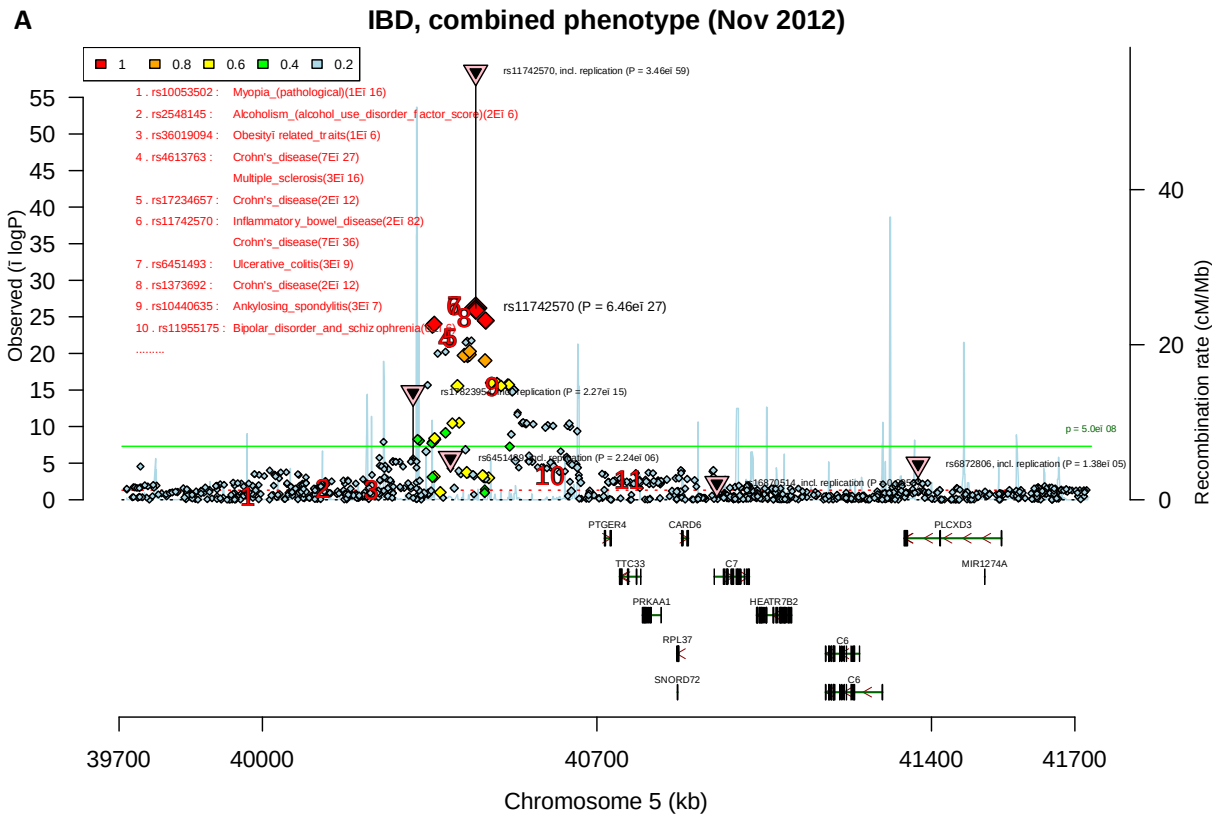

B

Phenotype	Chromosome: Position (hg19 (Mb))	SNP	Candidate genes	p-value	Odds Ratio
IBD	Chr.1: 67.68	rs11209026	*IL23R*	8.12E-161	2.013
IBD	Chr.1: 206.93	rs3024505	*IL10*	6.66E-42	1.208
IBD	Chr.5: 40.38	rs11742570	*PTGER4*	1.81E-82	1.198
IBD	Chr.9: 117.60	rs4246905	*TNFSF8, TNFSF15*	2.80E-32	1.142
IBD	Chr.9: 139.32	rs10781499	*CARD9*	4.38E-56	1.188

Figure 1.2. PTGER4 is significantly associated with both forms of IBD. (A) Ricopili plot (Ripke and Brett, 2018) showing SNPs in high linkage disequilibrium, which are highly associated with both forms of IBD alongside other immune-related diseases and lying in a gene desert region adjacent to PTGER4 (Underlying dataset was derived from Jostins *et al.*, 2012). **(B)** List of genes most significantly associated with IBD as obtained from GWA studies (adapted from Cho and Brant, 2011; Jostins *et al.*, 2012).

1.3.1. Prostaglandin synthesis and signaling in the intestine

Prostaglandin E_2, a highly unstable lipid metabolite, is synthesized from the conversion of arachidonic acid into prostaglandin intermediates via cyclooxygenases (COX) 1 and 2 in a cell-specific manner (see figure 1.3.). With COX-1 being constitutively active, COX-2, displaying the inducible isoform although known to be constitutively expressed in distinct cell types, is classified as the rate-limiting enzyme. PGE_2, one of the downstream products, is the correspondent ligand to the EP receptors 1-4 and hypothesized to signal in an auto- or paracrine fashion over relatively short distances. It has been shown, alongside COX-2, in elevated levels in colorectal adenomas and within tumorigenic environment is increasingly secreted by immune, stromal and epithelial cells (Hull, Ko and Hawcroft, 2004; Gupta and DuBois, 2001). Expression of EP4, its receptor on which we will focus in our work, showed a similar trend, suggesting a role of PGE_2-EP4 signaling in growth, motility and behavior of colorectal epithelial cells (Chell *et al.*, 2006). EP4 is a G-protein-coupled receptor upstream of several signaling cascades, initiated through G-protein subunits. Activation of cyclic AMP (cAMP) followed by protein kinase A (PKA)-mediated phosphorylation of cAMP-response element-binding protein (CREB), a transcription factor, has for instance been shown in colonic epithelial cells. Apart from that, PGE_2 via EP4 induces phosphoinositide 3-kinase (PI3K)-mediated phosphorylation of protein kinase B (Akt). Finally, mitogen-activated protein kinase (MAPK)/ extracellular signal-regulated kinase (ERK) signaling and the NFκB pathway represent additional downstream events, particularly pivotal for induction of inflammatory mediators. The receptor gene itself, *PTGER4*, based upon its genetic motifs, is highly responsive to proinflammatory agents (Yokoyama *et al.*, 2013).

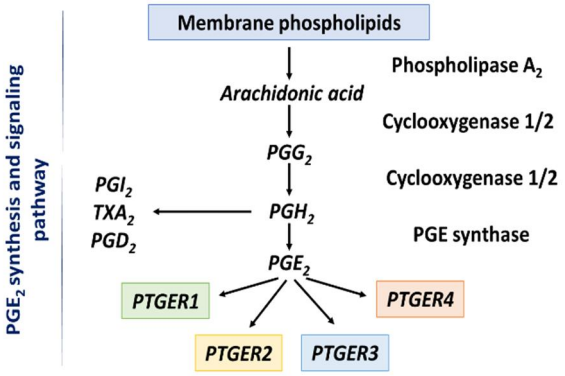

Figure 1.3. Prostaglandin E_2 synthesis and signaling pathway (based on Park, Pillinger and Abramson, 2006).

The dual role of prostaglandin signaling in epithelial regeneration (Powell *et al.*, 2011; Roulis *et al.*, 2014) and tumorigenesis (Nishihara *et al.*, 2004; Pozzi *et al.*, 2004; Holla *et al.*, 2006), underscores its modulatory effect on proliferation, which is of medical relevance for inflammation (IBD) and cancer (CRC). Due to their multifaceted roles in these conditions (see

1.2.), their localization, susceptibility to immune mediators and their (constitutive) expression of COX-2, intestinal stromal cells may account for a missing link in this context.

1.3.2. Cell specificity of the PGE_2 –EP4 signaling pathway

PGE_2 signaling has been linked to excessive proliferation, tumor angiogenesis and cancer progression in multiple studies. In mouse models of familial adenomatous polyposis (FAP) a decline in polyp number has been observed on a *Cox-2*$^{-/-}$ background (Gupta and DuBois, 2001). This appears to be consistent with a reduction in polyp burden in human FAP patients upon administration of Celecoxib, a COX-2 inhibitor (Buchanan and DuBois, 2006). Moreover, application of 16,16-dimethyl PGE_2 in the *Apc*$^{Min/+}$ mouse model of intestinal cancer not only increased adenoma formation (Wang *et al.*, 2004) but also induced the expression of the cell cycle regulator cyclin D1 and vascular endothelial growth factor (Shao *et al.*, 2005). *In vitro* studies on human cancer cell lines complement these results and further established a potential link between PGE_2 and Wnt signaling, having PGE_2 and β-catenin act in a synergistic fashion (Shao *et al.*, 2005). Particularly via EP2 and EP4 receptors, PGE_2 furthermore turned out to be able to phosphorylate glycogen synthase kinase-3 (GSK-3), involved in the destruction complex downstream of Wnt signaling (Fujino, West and Regan, 2002) and activated Wnt-regulated proliferation in epithelial progenitor cells (Castellone *et al.*, 2005). Out of the 4 receptors (EP1-4) of PGE_2, EP1 and 4 based upon genetic ablation in mouse models of CRC appear to be the most likely ones associated with colon carcinogenesis (Watanabe *et al.*, 1999, 2002; Sonoshita *et al.*, 2001). Since PGE_2 is classified as a proinflammatory mediator, it is hypothesized to promote tumor formation not only via deregulating epithelial proliferation, but also through altering the tumor microenvironment. CRC development is vastly dependent on minimal immune-surveillance, evading immune reactions and favoring immunosuppressive agonists, which is believed to be facilitated by PGE_2. In conclusion, PGE_2 appears to support tumor formation and progression, whereby EP4, given its suggested crosstalk with the Wnt pathway and implication in mouse CRC models seems to be particularly relevant. Simultaneously PGE_2 induces factor secretion from tumor cells that in combination with PGE_2 itself will help create an immunosuppressive microenvironment (Wang and DuBois, 2013).

Contrary to that, chronic inflammatory conditions like IBD originate in excessive immune mechanisms, thus raising the question, how the same signaling pathway might possibly direct two disorders of apparently opposite responses. In line with experiments on *Ptgs1*$^{-/-}$ and *Ptgs2*$^{-/-}$ mice (Morteau *et al.*, 2000), coding for the two cyclooxygenases in the prostaglandin synthesis pathway, Kabashima *et al.* (2002) proposed EP4 to be beneficial in mouse models of colitis, showing *Ptger4*$^{-/-}$ mice suffering from exacerbated DSS colitis course (see 1.4.1.). However, these results shall be analyzed critically, given the absence of littermate controls, which is common practice for DSS mouse cohort studies nowadays and the mixed genetic background (129/Ola x C57BL/6) of the mice, enabling their survival. Overall deletion of *Ptger4* on a C57BL/6 background accounts for perinatal lethality due to incomplete closure of the ductus arteriosus, a blood vessel linking the aorta with the pulmonary artery (Kabashima *et al.*, 2002). Thus, based upon the scarcity and partial inconclusiveness of these results from the literature, long-term goals, as follows, have been defined to study PGE_2 signaling within the context of IBD and colorectal cancer.

1.4. Studying the role of PGE_2 in IBD and CRC

1.4.1. Long-term goals and preliminary work in mouse models of IBD and colorectal cancer

Given its strong association with genetic risk variants in both forms of IBD and human cancer in GWA studies, *PTGER4* very likely depicts a mediator of prostaglandin signaling in the intestine, which not only affects inflammatory mechanisms but also proliferation, applicable to both, IBD and carcinogenesis. It will be interesting to elucidate the exact cellular compartments implicated and their role in these signaling processes, supposedly active at the mesenchymal-epithelial interface of the intestine. Despite extensive research in these fields, hardly anything is known about downstream events of prostaglandin signaling and in what way they differ between proinflammatory and tumorigenic microenvironment, though. Whilst investigating the impact of described SNPs on the expression of *PTGER4* will demarcate a follow-up on GWAS results in IBD, tested for relevance in a well-established murine model of UC (DSS), the *Apc*$^{Min/+}$ mouse model of colorectal cancer will help deconvolute signaling cues triggering tumorigenesis. Within this context, the following experiments were performed in advance to this thesis and consequently served as preliminary data for upcoming work on prostaglandin signaling in the intestine.

DSS colitis seems to be resolved upon *Ptger4* deletion in fibroblasts

Colitis phenotype, mirroring one of the IBD subtypes (UC) in humans, is induced by the administration of dextran sodium sulfate (DSS), an anticoagulant polysaccharide toxic to intestinal epithelial cells of the basal crypts, for usually 7 consecutive days. Given that an acute colitis, i.e. bloody diarrhea, ulceration and immune cell infiltration following epithelial barrier breakage, is triggered in a T- and B-cell independent fashion (Tennyson and Bucy, 1994), this model serves to study innate immune aspects (Wirtz *et al.*, 2007; Chassaing *et al.*, 2014).

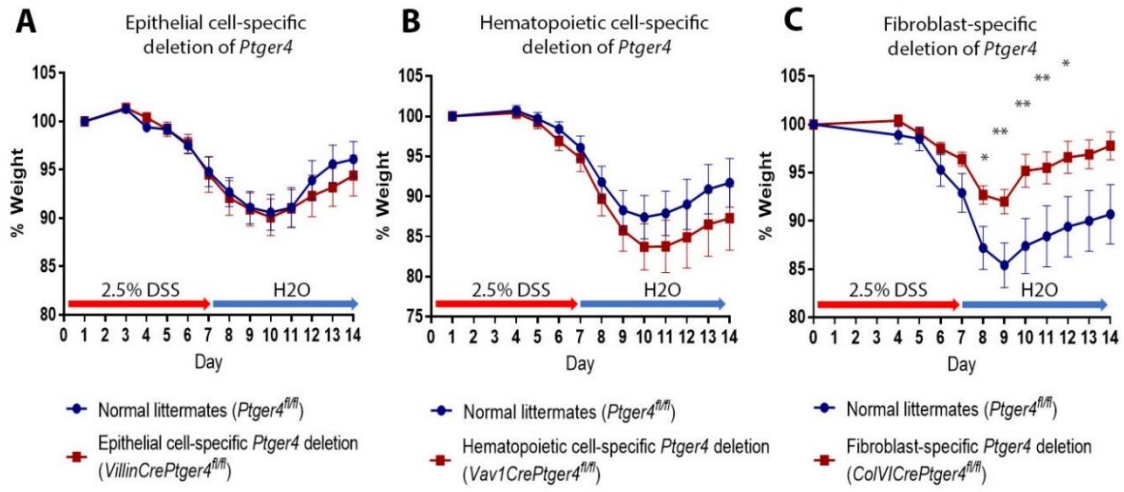

Figure 1.4. DSS weight loss curves from three conditional *Ptger4*$^{-/-}$ mouse lines. Cell type-specific *Ptger4* deletion was achieved by crossing *Ptger4*$^{flox/flox}$ mice with conditional Cre lines. **(A)** *VillinCrePtger4f*$^{lox/flox}$ mice were used with *Ptger4*$^{flox/flox}$ littermates for epithelial cell-specific deletion. Numbers used were n = 11 *Ptger4*$^{flox/flox}$ and n = 10 *VillinCrePtger4*$^{flox/flox}$ (2 experiments) **(B)** For hematopoietic cell-specific deletion n = 6 *Vav1CrePtger4*$^{flox/flox}$ and n = 6 *Ptger4*$^{flox/flox}$ mice (2 experiments) were used **(C)** For fibroblast-specific deletion n = 15 *ColVICrePtger4*$^{flox/flox}$ and n = 14 *Ptger4*$^{flox/flox}$ mice (3 experiments) were used. DSS (2.5 %) was administered in the drinking water for 7 consecutive days, followed by water for 7 days. Weight was monitored daily.

Based on concepts proposed by Kabashima *et al.* (2002), genetic ablation of *Ptger4* aggravated DSS colitis course, we however could not build on these results when crossing *Ptger4*$^{fl/fl}$ with constitutively active *EIIaCre* mice on a 129P3/J background. Lethality of overall *Ptger4*$^{-/-}$ mice could not be overcome, therefore we opted for examining the effect of *Ptger4* in distinct cell types via employing murine conditional Cre recombinase lines (Le and Sauer, 2001). No difference in colitis course, as determined by weight loss, between recombinase negative mice (*Ptger4*$^{fl/fl}$) and their conditional knockout littermates for epithelial cell-specific deletion of *Ptger4* (*VillinCrePtger4*$^{fl/fl}$) (see figure 1.4.) was observed, similarly to hematopoietic cell specific deletion of *Ptger4* (*Vav1CrePtger4*$^{fl/fl}$). Fibroblast-specific deletion (*ColVICrePtger4*$^{fl/fl}$), though, resulted in ameliorated colitis course, indicative

of a detrimental role of *Ptger4* in IBD. These results, demarcating a likely proinflammatory mechanism of prostaglandin E_2 signaling, contrast with previous ones from the literature (Kabashima *et al.*, 2002).

Tumor formation in *Apc*$^{Min/+}$ mice depends on a mesenchymal-epithelial pathway

In comparison, PGE_2 signaling in the *Apc*$^{Min/+}$ mouse model of colorectal cancer, predisposed to intestinal adenoma formation (Moser *et al.*, 1995), mirrored the expected results from the literature, showing a decreased number of adenomas per mouse (see figure 1.5.) upon deletion of the EP4 receptor from the intestinal epithelium, attributing it with tumorigenic potential. Interestingly, fibroblasts have also been established as crucial cell type in this model, displaying them as a major source of PGE_2 and thus suggesting a mesenchymal-epithelial signaling network in the context of intestinal tumor formation.

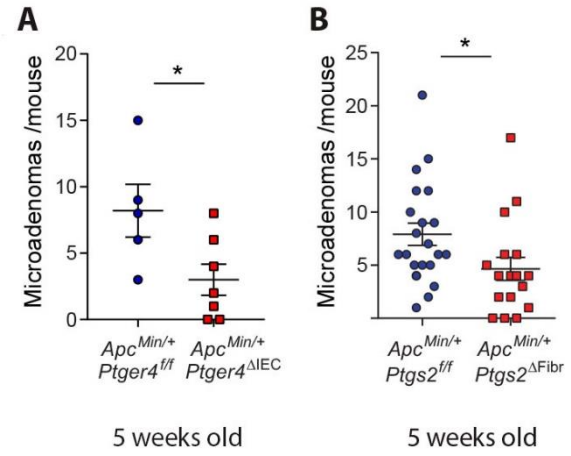

Figure 1.5. Mesenchymal-epithelial PGE_2 signaling accounts for tumorigenesis in *Apc*$^{Min/+}$ mice. Number of microadenomas per mouse in the small intestine of *Apc*$^{Min/+}$ mice (5 weeks old) **(A)** Number of microadenomas per mouse in (n = 7) mice bearing a deletion of *Ptger4* (EP4) in the intestinal epithelium (*Apc*$^{Min/+}$ *Ptger4*$^{\Delta IEC}$ = *Apc*$^{Min/+}$ *VillinCrePtger4*$^{flox/flox}$) is reduced compared to (n= 5) *Apc*$^{Min/+}$*Ptger4*$^{flox/flox}$ controls **(B)** Number of microadenomas per mouse in (n = 17) mice bearing a deletion of *Ptgs2* (Cox-2) in fibroblasts (*Apc*$^{Min/+}$*Ptgs2*$^{\Delta Fibr}$ = *Apc*$^{Min/+}$*ColVICre Ptgs2*$^{flox/flox}$) is reduced compared to (n = 21) *Apc*$^{Min/+}$*Ptgs2*$^{flox/flox}$ controls.

1.4.2. Aims specifically addressed in this study

Based upon these preliminary data from published GWAS datasets, models of colitis and colorectal cancer, confirming PGE_2 (via EP4) to play a pivotal role in both, inflammatory and carcinogenic settings, we, for this study, specifically aimed at…

1) Prioritizing and studying the role of putative enhancer elements within IBD-associated GWAS risk loci through genetic ablation in human cell lines and mice via CRISPR/Cas9.
2) Modeling mesenchymal-epithelial interactions as suggested for intestinal disorders in an *in vitro* organoid system.

3) Specifying molecular mechanisms downstream of PGE_2-EP4 signaling and potential differences of those dependent on the respective cell type and disease.

2. Materials and methods

2.1. Cells and cell culture

2.1.1. Human cell lines

Human cell lines used included CCD18-Co (ATCC), HEK-293T (Flavell lab), THP-1 (ATCC), Caco-2 (ATCC) cells. CCD18-Co, HEK-293T and Caco-2 cells were cultured in Dulbecco's Modified Eagle Medium (DMEM) by Gibco™ (ThermoFisher Scientific), supplemented with 10% fetal bovine serum (FBS), 1% Penicillin/Streptomycin (Gibco™) and 1% L-Glutamine (Gibco™) (DMEM10). THP-1 cells were grown in Roswell Park Memorial Institute (RPMI) – 1640 medium by Gibco™ (ThermoFisher Scientific) supplement with 10% fetal bovine serum (FBS), 1% Penicillin/Streptomycin (Gibco™) and 1% L-Glutamine (Gibco™) (RPMI10). THP-1 cells were split as indicated by ATCC, CCD18-Co, HEK-293T and Caco-2 cells were grown until ~90% confluency and then split accordingly. For splitting cells were washed once in Dulbecco's Phosphate Buffered Saline (Gibco™), trypsinized for 2 minutes at 37°C using Trypsin-EDTA (0.25%) (Gibco™), collected in DMEM10, spun at 1200 rpm for 5 minutes and then reseeded as required in DMEM10.

2.1.1.1. Stimulation with PGE_2

To establish cell line readouts THP-1, HEK-293T, CCD18-Co and Caco-2 cells were stimulated for the indicated timespans with 0.1 µM 16,16-dimethyl Prostaglandin E_2 ($dmPGE_2$) (Cayman, #14750) or 100% ethanol as vehicle control. If required, EP4 inhibitor (ONO-AE3-208) (Cayman, #14522) was added at a final concentration of 10 µM for 1 hour prior to $dmPGE_2$ stimulation, DMSO (Sigma-Aldrich, #276855) was used as vehicle control. For Western Blot analyses cells were starved overnight in DMEM supplemented with 0.5% FBS, Penicillin/Streptomycin and L-glutamine before stimulation.

2.1.2. Murine mesenchymal cells

Murine fibroblasts were derived from C57BL/6 wildtype mice bred at the Yale Animal Resources Center. For isolation of mouse intestinal stromal cells the intestine was dissected, flushed with ice-cold Dulbecco's Phosphate Buffered Saline (Gibco™), opened longitudinally and cut into 1 cm pieces. Tissue pieces were incubated in Hank's Balanced Salt Solution (HBSS) (Gibco™) containing 1 mM EDTA, 1 mM DTT, 0.2 % fetal calf serum (FCS), 4-5 times, 10 minutes each, at 37 °C, 200 rpm. Intestinal epithelial cells were released through vigorous shaking after each step and discarded. After the last incubation step tissues were washed twice in DPBS, resuspended in DMEM10 containing 300 units/ml Collagenase XI (Sigma #C7657, 1100 u/mg), 0.1 mg/ml Dispase II (Sigma, #D4693) and 50 u/ml DNase II type V (Sigma, #D8764, 1100 u/mg) and incubated at 37°C, 200 rpm for 1 hour. Cells released after vigorous shaking were passed through a 70 µm strainer (Corning) (filtered mouse fibroblasts) or not (unfiltered mouse fibroblasts), spun at 1200 rpm for 7 minutes at 4°C, washed with DMEM10 and DPBS containing 2% sorbitol at 200 g. Cell pellets were directly resuspended in DMEM10 for unfiltered fibroblasts or filtered, washed and resuspended in DMEM10 for filtered ones. Fibroblasts were plated on 100 mm^2 cell culture dishes and expanded *in vitro* prior to ongoing experiments (Roulis, M. *et al.,* unpublished).

2.1.2.1. Immunocytochemistry on murine fibroblasts

Mouse intestinal fibroblasts were seeded onto autoclaved lamellas. Cells were washed in DPBS, fixed with 4% paraformaldehyde (PFA) for 30 minutes at room temperature, washed in DPBS and permeabilized with 0.025% TritonX100 for 15 minutes at room temperature. Cells were blocked for 1 hour at room temperature in DPBS 0.025% TritonX100 with 5% FBS. Primary antibodies were added in blocking buffer for overnight incubation at 4°C. The following day cells were washed 3 times in DPBS 0.025% TritonX100 before adding the secondary antibodies (goat anti-rabbit biotinylated IgG (Vector Laboratories, #BA-1000) (1:200), anti-biotin/Streptavidin-FITC conjugated Ab (Life Technologies, #S32354) (1:500)) for 1 hour at room temperature. Cells were washed 3 times in DPBS 0.015% TritonX100, DPBS and water before mounting on a glass slide with Gel Aqueous Mounting Medium (Sigma-Aldrich, #G0918) containing DAPI. Primary antibodies included YAP (D8H1X) XP® Rabbit mAb (Cell Signaling, #14074) (1:100).

2.1.2.2 Cyclical pressure experiments

Murine fibroblasts (P8) were seeded onto 60 mm^2 cell culture dishes in DMEM10 on the day prior to the experiment. Cells were prepared in biological duplicates and were left untreated (no pressure), treated with static (constant) pressure (30 mmHg) or cyclical pressure (55-115 mmHg) for 6 hours in a pressure chamber that was placed at 37°C. Cells were placed on ice and lysed for protein or RNA extraction as described in 2.4. and 2.5. The cyclical pressure machine and monitoring software (Schipke, Filip To and Warnock, 2011) were kindly provided by Angel Solis, a PhD-Student in the Flavell lab and experiments were performed in cooperation with him.

2.2. Mice

Wildtype (WT) mice were bred in the facilities of the Yale Animal Resources Center (YARC) and used for immunostainings and organoid experiments unless indicated otherwise. *Ptger4*$^{fl/fl}$ mice crossed with *EIIaCre, ColVICre, VillinCre* or *Apc*$^{Min/+}$ mice as well as *Col1α2CreERRosa26*$^{Tomato/+}$ mice were bred in the facilities of YARC. Cre driven tomato expression was induced by application of 20 mg/ml tamoxifen (Sigma-Aldrich, #10540-29-1), which was prepared accordingly (Desk, Williams and Health, 2001; Madisen *et al.*, 2010; Heffner, 2011), on 5 consecutive days. *Ptger4* enhancer knockout mice were derived from microinjection of guide RNAs with the help of the Flavell lab CRISPR Core at Yale. *Ptger4*$^{D/D}$ mice were crossed with males on a 129P3/J background. If not indicated otherwise, mice were maintained on a C57BL/6J genetic background. Mice were housed in standard cages, on a 12-hour day/night cycle and were fed a standard rodent chow. Mice were used for experiments at 8-12 weeks of age unless otherwise indicated. For all experiments littermate, cohoused and sex-matched mice were used. No mice were excluded from the analyses performed. All animal experimentation at Yale was performed in compliance with Yale Institutional Animal Care and Use Committee protocols (Roulis, M. *et al.,* unpublished).

2.2.1. Sectioning of mouse intestinal tissue for immunofluorescence

Col1α2CreERRosa26$^{Tomato/+}$ mice were sacrificed on days 8 and 14 after initial tamoxifen application. The intestine was harvested and flushed in ice-cold PBS. Two pieces (2 cm) of

the duodenum, jejunum, terminal ileum, proximal and distal colon were transferred in 4% paraformaldehyde and left for fixation at 4°C for 4 hours. Tissue pieces were washed once in PBS and placed in 30% sucrose/PBS at 4°C overnight. The following day tissue was placed in cryomolds (Tissue-Tek, #27183) filled with Optimal cutting temperature compound (OCT, Tissue-Tek), which were frozen on dry ice. Sections (10 µm) were taken using a cryostat (Leica) and placed onto glass slides. Sections were washed in PBD and mounted with Fluoroshield™ histology medium containing DAPI (Sigma, #F6057) and imaged at a fluorescence microscope (Leica).

WT and *Apc*$^{Min/+}$ mice for E-cadherin-Vimentin, YAP, E-cadherin-Ly6a, Lysozyme-Ly6a and Vimentin-COX-2 immunostainings were sacrificed accordingly. The intestine was taken out, flushed in ice-cold PBS and dissected. Intestinal tissue, i.e. ileal and colonic parts, were fixed overnight at 4°C in 10% neutral buffered formalin solution before embedding in paraffin (FFPE sections) and taking sections, which was done by the Yale Histology Core.

2.3. Organoid and co-culture experiments

Organoid cultures were derived from murine small intestinal and human colonic crypts. For passaging (in a ratio of 1:6 once per week for maintenance) organoids at day 7 of culture were dissociated in Gentle Cell Dissociation Reagent (Stem Cell Technologies, #07174), incubated at room temperature on a rocker (20 rpm) for 10 minutes and spun at 290 g for 7 minutes. Pellets were washed once in DPBS 2% FBS before resuspending in IntestiCult™ Organoid Growth Medium (Stem Cell Technologies, #06005) for mouse and IntestiCult™ Organoid Growth Medium (Human) (Stem Cell Technologies, #06010) for human organoids. Matrigel® (Corning, #356231) was added in a 1:1 ratio, domes (50 µl) were formed on a pre-warmed 24-well plate (Corning, #3526) at 37°C for 7 to 10 minutes before adding 500 µl IntestiCult per well. Mouse organoids, if applicable, were co-cultured with murine fibroblasts that have been isolated from WT mouse intestine as described in 2.1.2. For this purpose, fibroblasts were either seeded on the evening ($2x10^4$ fibroblasts per well of a 48-well plate) before crypt isolation or directly plated in Matrigel® domes (7500 fibroblasts and 500 crypts) together with crypts (Roulis, M. *et al.,* unpublished).

2.3.1. Murine small intestinal organoids

Crypts, dependent on the experiment, were isolated from the last three fourths of the small intestine of WT, *Ptger4*$^{fl/fl}$, *VillinCrePtger4*$^{fl/fl}$ and *Apc*$^{Min/+}$ mice of 2 to 3 months age. The intestine was flushed, cut longitudinally and villi were scraped off with a glass coverslip. The tissue was cut into 0.5 cm pieces, which were incubated in DPBS containing 5 mM EDTA, 0.2 % FBS for 30 minutes at 4 °C on a rocker. Crypts were released by vigorous shaking and were passed through a 70 µm strainer. Six fractions were obtained after vigorous shaking and the ones enriched for crypts were further processed. Crypts were washed by centrifugation at 200 g, 100 g and 50 g and then used (n=500) for organoid development in domes made by Matrigel® (Corning, #356231) and IntestiCult™ Organoid Growth Medium (Stem Cell Technologies, #06005) according to manufacturer's guidelines. If indicated, 16,16-dimethyl Prostaglandin E2 (Cayman, #14750) dissolved in ethanol was added for the given timepoints at a final concentration of 0.1 µM. Ethanol was used as a vehicle control for untreated organoids. EP4 inhibitor (ONO-AE3-208, Cayman, #14522), if applicable, was added at a final concentration of 10 µM for 1 hour prior to PGE_2 stimulation. DMSO was used as a vehicle control for that. Verteporfin (Cayman, #17334) and DMSO respectively, was added at a final concentration of 1 µM 1 hour prior to stimulation. Forskolin (Sigma-Aldrich, #66575-29-9) was applied at a final concentration of 400 ng/µl for the indicated times, DMSO was used as a vehicle control. ROCK inhibitor (Y-27632, Sigma-Aldrich, #SCM075) was added as indicated at a final concentration of 10 nM, DMSO was used as vehicle control. PI3K inhibitor (wortmannin) was added as indicated, DMSO was used as a vehicle control. If not for stimulation experiments, $dmPGE_2$ was added to organoid cultures daily at 0.1 µM, EP4 inhibitor at 10 µM every second day up to three times (Roulis, M. *et al.,* unpublished). For FFPE sections, organoids and spheroids were fixed overnight in formalin, washed in DPBS 2% FBS, stained with 2% methylene blue solution (Sigma-Aldrich, #M9140) in DPBS for 20 minutes at room temperature. Washing was repeated and 500 µl of 2% agar (Sigma-Aldrich, #9002-18-0) were added on top of the pellet, which after solidifying was plunged into 70% ethanol and sent for histology (paraffinization, sectioning and H&E staining).

2.3.1.1. Stemness assays

Organoids were grown in OGM supplemented with 100% ethanol or 0.1 µM PGE_2 consecutively for 4 days. On day 4 spheroid/organoids structures were mechanically dissociated using 700 µl Gentle Cell Dissociation Reagent (Stem Cell Technologies, #07174), incubated for 10 minutes at room temperature on a rocker (20 rpm) before spinning down. Pellets were washed twice in DPBS and resuspended in 500 µl 1 mg/ml Trypsin-EDTA (0.25%) (Gibco™) in DMEM w/o FBS by Gibco™ (ThermoFisher Scientific) and DNase (in a ratio of 6:4:1). Cells in suspension were incubated at 37°C for 25 minutes and mixed gently every 8 minutes. Afterwards, cells were washed 1x, resuspended in DMEM10, stained with Trypan-blue (Sigma-Aldrich, #T8154) and counted twice. Equal numbers of organoid- and spheroid-derived single cells were plated in new Matrigel domes, cultured in Intesticult containing ROCK inhibitor and monitored on the indicated days.

2.3.1.2. *Apc$^{Min/+}$* loss of heterozygosity assay

Crypts isolated from *Apc$^{Min/+}$* mice (2 to 3 months old) were processed as described above. Organoids were split at a weekly basis (1:6) and kept in culture for up to 8 passages. As indicated organoids were genotyped for *Apc* mutated and wildtype alleles at different passage numbers. DNA was collected in 400 µl TAIL DNA Lysis buffer ('Mouse Tail Lysis Buffer II', 2018) with proteinase K and incubated overnight at 56°C. The following day DNA was heat-inactivated at 95°C for 5 minutes and purified via Phenol extraction. Phenol: chloroform solution (1:1) was added 1:1 to DNA sample, vortexed for 3 minutes and spun at 1200 rpm for 10 minutes. The upper aqueous phase was transferred to a new tube and supplemented 1:1 with isopropanol before spinning at 1200 rpm for 5 minutes. The supernatant was discarded, the pellet was washed sequentially in 100% and 70% ethanol before resuspending in 100-150 µl MilliQ water after air drying the pellet for 10 minutes. For subsequent PCRs primers specific for the site of point mutation (see figure 7.7.) or primers as published (Strauss *et al.*, 1994) were used. For the latter the subsequent restriction assay was performed accordingly (Strauss *et al.*, 1994), i.e. the PCR product was purified via the QIAquick PCR Purification Kit (QIAGEN, #28104), whereof 850 – 1000 ng of DNA were added to 1x NEBuffer™ 2.1 (NEB, #B7202S), HindIII restriction enzyme (NEB, #R0104S) and MilliQ water as described previously (New England Biolabs, https://international.neb.com/

protocols/2012/12/07/optimizing-restriction-endonuclease-reactions). The samples were incubated at 37°C for 1 hour and heat-inactivated at 80°C for 20 minutes before run on a 5% agarose gel. Controls have been used as indicated. Undigested parallels without HindIII administration were included. For primer sequences and PCR program see table 7.1.

2.4. Quantitative real-time PCR analysis

2.4.1. RNA isolation

RNA from organoids, which were dissociated in Gentle Cell Dissociation Reagent (Stem Cell Technologies, #07174) and washed once in DPBS, was isolated using TRIzol™ reagent (Thermo Fisher, #15596026) followed by DNase I treatment (Roche, #04716728001) or the QIAGEN RNA isolation RNeasy plus Mini Kit (QIAGEN, #74134) according to manufacturer's instructions. RNA concentration was determined via NanoDrop™ (Thermo Fisher, ND-2000).

2.4.2. Quantitative real-time PCR

Reverse transcription on RNA samples (200 – 1000 ng) was performed via Maxima H Minus Reverse Transcriptase (Thermo Fisher, #EP0751) and Oligo(dT)$_{18}$ (Thermo Fisher, #SO131) primer according to manufacturer's instructions. RT-program included the following steps: 65°C for 5 minutes, 52°C for 45 minutes, 85°C for 5 minutes and 12°C for 5 minutes. Quantitative real-time PCR reactions were performed using iTaq™ Fast SYBR® Green Supermix (BioRad, #1725100) and a CFX96 Touch™ Real-Time PCR Detection System (BioRad). Relative gene expression was determined with the PFAFFL method (Pfaffl, 2001). Per reaction 2 µl cDNA, 7 µl DEPC-water (Thermo Fisher, #750023), 1 µl primer pair mix (5 µM) and 10 µl SYBR® Green Supermix were combined. Quantitative real-time PCR program is listed in table 7.2. All primers used have been tested in standard curves for efficiency and specificity. Relative gene expression to a control sample was calculated with the RelQuant software (BioRad Laboratories) by normalizing to *B2m* expression (Roulis, M. *et al.,* unpublished). Primer sequences used for RT-qPCR are listed in table 7.3.

2.5. Western Blot analysis

2.5.1. Protein isolation

Total protein was extracted from wildtype murine organoids was extracted with RIPA lysis buffer (Abcam, https://www.abcam.com/protocols/sample-preparation-for-western-blot). Nuclear-cytoplasmic fractions from WT and *Apc*$^{Min/+}$ murine organoids were extracted using NE-PER Nuclear and Cytoplasmic Extraction Reagents (Thermo Fisher, #78833). Phosphatase (Thermo Fisher, #78420) and protease inhibitors (Thermo Fisher, #87786) were included (1:100) in lysis buffers.

2.5.2. Bradford assay

Lysed samples were centrifuged at 4°C for 15 minutes at full speed, after which the supernatant was transferred into a new tube. Protein amount was quantified via a BioRad Protein (Bradford) assay. For standard curves a serial dilution of bovine serum albumin (BSA) (Sigma-Aldrich, #9048-46-8) was prepared, 200 µl of BioRad Protein Assay Dye Reagent Concentrate (BioRad, #5000006), diluted according to manufacturer's instructions, were added to each sample, protein samples (2 µl) were applied on a 96-well plate (F-bottom) in technical duplicates. Protein absorbance was measured by a microplate absorbance reader (BioRad) at wavelength 595 nm.

2.5.3. Western blot

For Western blot analysis 8-10 µg protein were used. 3x loading dye (NuPAGE®) (Invitrogen) was added, samples were put for denaturation at 95°C for 5 minutes, quick-spun and loaded onto a NuPAGE™ Novex®, 1-1.5 mm, 4-12% Bis-Tris gel (Invitrogen™, #NP0321BOX) with Precision Plus Protein Dual Color Standard (BioRad, #1610374). Gels were run for 1 hour at 150 V in 1x NuPAGE™ MOPS SDS Running buffer (Invitrogen™, #NP0001). After protein separation, gels were blotted onto a nitrocellulose membrane (Hybond® ECL™ nitrocellulose membrane, Sigma-Aldrich, #GERPN303D) in 1x NuPAGE™ Transfer buffer (20x) supplement with methanol (1:5) (Invitrogen™, #NP00061) at 200 mA for 2 hours. Membranes were stained in Ponceau S (Sigma-Aldrich, #P7767) solution. For antibody staining membranes

were blocked in 5% non-fat milk powder dissolved in PBST (PBS supplemented with 0.1% Tween20 (Sigma-Aldrich, #P9416)) for 30-60 minutes on a rocker (20 rpm) at room temperature. Primary antibody was added 1:1000 – 1:2000 in 5% BSA (American Bio, #9048-46-8) dissolved in PBST on a rocker (20 rpm) at 4°C overnight. Membranes on the following day were washed three times 10 minutes in PBST on a rocker (20 rpm) at room temperature before adding the secondary antibody (1:2000) at room temperature on a rocker for 1 hour. Membranes were washed three times in PBST again. For detection of total and cytoplasmic protein reagents of the SuperSignal West Pico Chemiluminescent Substrate Kit (Thermo Scientific™, #34580) were applied 1:1 onto the membrane. SuperSignal West Femto Maximum Sensitivity Substrate (Thermo Scientific™, #34095) was added analogously for nuclear protein extracts and if required otherwise. Autoradiographic detection was done on HyBlot Autoradiography film (HyBlot, #E3018) in a dark room. If required, membranes were washed and incubated in Restore™ PLUS Western Blot Stripping Buffer (Thermo Scientific™, #46430) according to manufacturer's instructions for additional antibody staining performed as described above. Primary antibodies used for Western blot analysis included anti-Phospho-YAP (Ser127) (D9W2I) (Cell Signaling, #13008), anti-YAP (D8H1X) (Cell Signaling, #14074), anti-TBP (D5C9H) (Cell Signaling, #44059) and anti-non-phospho (active) β-catenin (Ser45) (D2U8Y) (Cell Signaling, #19807). Anti-rabbit IgG (Cell Signaling, #7074S) was used as secondary antibody.

2.6. Immunohistochemistry and microscopy

For immunostainings on murine tissue sections, the intestine was processed as described in 2.2.2. For immunostainings on human colon FFPE tissue sections, we deparaffinized and hydrated in a box at 55°C for 30 minutes, followed by 3 x 10 minutes in xylene, 2 x 2 minutes in 100% EtOH, 95% EtOH, 70% EtOH, 50% EtOH followed by water. Antigen retrieval was achieved by incubating the slides in boiled 0.01 M Citrate buffer pH 6, 0.05% Tween20 (Sigma-Aldrich, #P9416) for 20 minutes, followed by 15-20 minutes cool-down at room temperature. Subsequently slides were washed in water, 3 x 5 minutes in PBS and permeabilized in PBS 0.3% Triton™ X-100 Surfact-Amps™ Detergent Solution (Thermo Scientific™, #85112) for 10 minutes. Blocking was done in PBS 0.025% Triton X-100, 1% BSA (American Bio, #9048-46-8) at room temperature for 30 minutes. Primary antibodies were

applied in the indicated dilution in blocking buffer (200 µl/slide) in a humidified chamber at 4°C overnight. The following day slides were washed 3 x 5 minutes in PBS 0.025% Triton X-100 and incubated in secondary antibody dissolved in blocking buffer for 1 to 2 hours at room temperature. Slides were washed again sequentially in PBS 0.025% Triton X-100, PBS and water. Slides were mounted in Fluoroshield™ histology medium containing DAPI (Sigma, #F6057) and imaged at a Nikon-Ti confocal microscope equipped with an UltraVox spinning disc (PerkinElmer). Data were acquired with Volocity (PerkinElmer) and further processed in ImageJ. For E-cadherin-Vimentin staining on human and mouse intestine anti-E-cadherin-FITC mouse monoclonal antibody (1:200) (BD, #612130) and anti-Vimentin-Alexa Fluor 647 rabbit monoclonal antibody (1:200) (Cell Signaling, #9856) were used. Vimentin-COX-2 staining on mouse intestine was performed with anti-COX-2 rabbit polyclonal primary antibody (1:150) (Cayman, #160126), anti-rabbit secondary antibody Alexa Fluor 488 (1:1000) (Invitrogen, #A27034) in addition to anti-Vimentin-Alexa Fluor 647 rabbit monoclonal antibody (1:200) (Cell Signaling, #9856). E-cadherin-Ly6a staining on mouse encompassed anti-mouse Ly-6A/E (Sca-1) antibody (1:100) (BioLegend, #108114) and anti-E-cadherin-FITC mouse monoclonal antibody (1:200) (BD, #612130). For lysozyme-Ly6a staining on mouse anti-mouse Ly-6A/E (Sca-1) antibody (1:100) (BioLegend, #108114) and anti-human lysozyme polyclonal rabbit antibody (1:100) (Dako EC 3.2.1.17/FITC Code F0372) were utilized. For YAP stainings on WT and *Apc*$^{Min/+}$ mice anti-YAP antibody (1:50) (Cell Signaling, #14074), goat anti-rabbit biotinylated IgG (1:200) (Vector) and anti-biotin/Streptavidin FITC conjugated antibody (1:500) (Life technologies, #S32354) were used.

2.7. Cloning and viral transduction of human cells

Cloning and plasmid amplification of lentiCRISPRv2-*PTGER4* vector has been completed prior to this thesis by Marlene S. Knapp and cloning procedure for the lentiCRISPRv2-*PTGER4* enhancer plasmid has been performed analogously. Guide RNAs have been ordered and synthesized by Integrated DNA Technologies in geneblocks (500 ng) (see figure 7.5.), which were amplified via PCR reaction (New England Biolabs, https://international.neb.com/protocols/2013/12/13/pcr-using-q5-high-fidelity-dna-polymerase-m0491) using the following primer sequences: DblGuideF (forward) TTTGTAGAAGACTTCACCG and DblGuideR (reverse) TACAACGAAGACACAAAC. PCR-reaction mix (50 µl) consisted of Q5® High-Fidelity

DNA polymerase (final concentration 0.02 u/µl) and 5X Q5® reaction buffer (New England BioLabs, #M0492S), dNTPs (10 mM), forward and reverse primer (10 µM), nuclease-free water and DNA (geneblock) template (2 ng). PCR program is indicated in table 7.4. 5 µl of each reaction were run on a 2% agarose gel, the remnant PCR product was purified using the QIAquick PCR Purification Kit (QIAGEN, #28104). DNA concentration was measured via NanoDrop™ (Thermo Fisher, ND-2000). For subsequent restriction digest BsmbI (10 u) (New England BioLabs, #R0580S) was combined in a 50 µl mix with 10x NEB3.1 buffer (New England BioLabs, #B7203S) and purified geneblock or lentiCRISPRv2 vector (Addgene, #52961) DNA (1 µg). Restriction digest was performed at 55°C for 1.5 hours followed by 5 minutes each at 85°C and 12°C. Products were run on an agarose gel and excised under blue light. Gel pieces were purified using QIAquick Gel Extraction Kit (QIAGEN, #28115), concentration was measured via NanoDrop™. Subsequent ligation was performed combining in a 20 µl reaction mix T4 DNA Ligase (New England BioLabs, #M0202S), 10X T4 DNA Ligase Reaction Buffer (New England BioLabs, #0202S) with insert (geneblock) : vector DNA in a 3:1 ratio, i.e. 60 ng of vector and 5 ng of insert DNA. Ligation was done at room temperature for 30 minutes.

2.7.1. Transformation of bacteria

One Shot™ Stbl3™ Chemically Competent E. coli cells (Invitrogen™, #C7373-03) were thawn on ice. S.O.C. medium (Invitrogen™, #C7373-03) was prewarmed at room temperature, selective LB Ampicillin$^+$ plates were placed at 37°C. 3 µl of DNA (10 pg to 100 ng) (ligated plasmid) and cut lentiCRISPRv2 DNA (negative control) were added into a vial of One Shot™ cells, mixed by flicking and incubated on ice for 30 minutes. Cells were heat-shocked at 37°C for 1 minute and placed on ice for 2 minutes. 500 µl of S.O.C. medium were added per DNA sample. Vials were incubated at 37°C and 225 rpm for 1 hour. Vial contents were spread (50 µl and 450 µl) onto pre-warmed selective LB Amp$^+$ plates, which were incubated inverted at 37°C overnight.

2.7.2. Plasmid isolation and amplification

On the following day >6 bacterial colonies were picked to inoculate 15 ml polypropylene tubes containing 2 ml LB-medium supplemented with Ampicillin (100 µg/ml). Tubes were incubated at 37°C and 225 rpm for > 8 hours until the media becomes turbid. 1 ml per bacterial culture was then transferred to an Eppendorf tube and spun at maximum speed for 2 minutes. Subsequent plasmid DNA purification was performed using the QIAprep Spin Miniprep Kit (QIAGEN, #27104) according to manufacturer's instructions. For this purpose, the pellet was resuspended in 250 µl Buffer P1, 250 µl Buffer P2 were added and tubes were inverted for mixing. 350 µl Buffer N3 were added and mixed with the solution before centrifuging at 13 000 rpm for 10 minutes. 800 µl of the supernatant were applied to a QIAprep 2.0 spin column and centrifuged for 60 seconds. The column was washed by adding 500 µl Buffer PB and centrifuging again. The flow-through was discarded, the column was washed again in 750 µl Buffer PE. The flow-through was discarded, column was spun at full speed for 1 minute and placed in a clean 1.5 ml microcentrifuge tube to elute DNA in 30 µl EB Buffer. DNA concentration was determined via NanoDrop™. Correct ligation was examined via a HindIII (New England BioLabs, #R0104S) mediated restriction digest according to manufacturer's instructions on miniprep plasmid DNA (500 ng) in a 25 µl reaction mix.

For Maxiprep DNA preparation using QIAGEN Plasmid Midi and Maxi Kits (QIAGEN, #12943) 100 µl of the initial bacterial colonies in 15 ml falcons were used to inoculate 2 ml LB Amp^+ medium during 6 hours at 37°C. These 2 ml in turn were then used to inoculate 100 ml LB Amp^+ medium overnight at 37°C and 225 rpm. Of these bacterial cultures 750 µl were added to 750 µl glycerol (50%) and stored at -80°C. The rest of the culture was transferred to conical tubes and processed according to manufacturer's instructions with initial spinning step at 4200 rpm for 30 minutes at 4°C (Beckman coulter centrifuge) and subsequent spinning steps at 4000 rpm and doubled amount of time as suggested. The final pellet was resuspended in 500 µl TE buffer. DNA concentration was determined via NanoDrop™.

2.7.3. Sequencing of plasmid DNA

Purified plasmid DNA from 2.7.2. was sent for Sanger sequencing, combining 500 ng ds plasmid DNA template with 2 µl 4 µM primer in a total volume of 18 µl. Primers for Sanger sequencing included GGGACAGCAGAGATCCAGTT (forward) and GCCAATTCCCACTCCTTTCA (reverse). Sequencing was done by the Keck Sanger Sequencing Core at Yale.

2.7.4. Viral packaging and lentiviral transduction of human cells

Production of viral particles containing the desired lentiCRISPRv2-*PTGER4* enhancer plasmids was performed using Lipofectamine® 3000 Reagent (Thermo Fisher, #L300015) and following manufacturer's instructions (Invitrogen, 2016). HEK-293T cells were seeded (100 000 – 500 000 per well of a 6-well plate) until 80-90% confluency. On the day of transfection cells were equipped with new DMEM10 medium without antibiotics. 125 µl Opti-MEM™ I Reduced Serum Medium (Gibco™, #11524456) and 5 µl Lipofectamine 3000 Reagent were combined and vortexed for 3 seconds. In a separate tube 125 µl Opti-MEM™ were mixed with 10 µl P3000 Reagent (Thermo Fisher), 08.9 lentiviral packaging vector (1 µg) (Addgene, #8455), pVSVG envelope plasmid (0.5 µg) (Addgene, #14888) and lentiCRISPRv2 (Addgene, #52961), lentiCRISPRv2-*PTGER4* knockout or lentiCRISPRv2-*PTGER4* enhancer knockout plasmid (1 µg). The two tubes were combined, vortexed briefly and incubated at room temperature for 25 minutes. 250 µl of that solution were added in a drop-wise manner per well. 12-18 hours later media was aspirated and replaced by fresh DMEM10. After 8 hours media was exchanged for fresh DMEM10 (for subsequent transduction of HEK-293T cells) or RPMI10 (for transduction of THP-1 cells) to collect virus in. Lentivirus containing media was collected after 24 hours, replaced by new media and collected again after 48 hours (4 ml total). Virus-containing media was spun down at 1500 rpm for 10 minutes at 4°C. Supernatant was filtered with a 0.22 µm syringe filter and stored at -80°C or temporarily at 4°C.

For virus infection of THP-1 cells, monocytes were seeded (1 000 000 cells per well of a 12-well plate) in RPMI10 with HEPES (1:50) (StemCell Technologies, #07200). 750 µl of non-concentrated virus (see above) containing lentiCRISPRv2, lentiCRISPRv2-*PTGER4* knockout or lentiCRISPRv2-*PTGER4* enhancer knockout plasmid, and 1.5 µl of 10 mg/ml polybrene (Sigma-Aldrich, #TR-1003) were added. Control THP-1 cells were kept in RPMI10 media only.

Cells were spun at 2500 rpm for 1.5 hours at 37°C (spinfection), washed in DPBS and resuspended in RPMI10 + HEPES. Cells were left for growing for 48 hours and then distributed onto 3 wells of a 12-well plate containing 1 µg/ml puromycin (Sigma Aldrich, #P9620). HEK-293T cells were seeded (200 000 per well of a 12-well plate) and maintained in DMEM10 with HEPES. After viral transduction (spinfection) cells were left for growing for 24 hours before reseeding in media containing puromycin. Cells were subjected to puromycin selection for one week. If required cells were split and reseeded in new media with puromycin accordingly. Cells were expanded afterwards. For single-cell derived clones, a dilution series of the respective bulk population was prepared in a range from 0.5 – 2 cells/well of a 96-well plate. 32 wells of a 96-well plate were used per dilution. Cell growth was marked and monitored. DNA from bulk populations (10^6 cells) and cell clones (if ~90% confluent) was collected in QuickTAIL Lysis buffer with Proteinase K (Sigma Aldrich), incubated at 55°C overnight and heat-inactivated at 95°C for 5 minutes. Primer sequences for genotyping of *PTGER4* knockout clones included AGTGGTAATTTCCGCTCACG (forward) and GTCTTCGCAGCCATCAAGTT or AAACGGAGGGTAGGTCTTCG (reverse). PCR was run with the program indicated in table 7.1. PCR product was loaded onto a 2% agarose gel, cut under UV-light and gel purified using the QIAquick Gel Extraction Kit (QIAGEN, #28115). DNA concentration was measured via NanoDrop™. For Sanger Sequencing (by the Keck Sanger Sequencing Core at Yale) with the above primers (4 µM) purified DNA template was added at 15 ng/200 bp in a total reaction volume of 18 µl. Knockout clones (HEK-293T) were expanded and frozen in DMEM10 with DMSO (10% final).

Guide RNAs used for CRISPR/Cas9 mediated knockout of genetic elements have been designed and proof-read via various softwares ('CRISPR', crispr.mit.edu; Johnson et al., 2008; Bae, Park and Kim, 2014; Park, Bae and Kim, 2015). A list of the guide RNAs used for this project is displayed in table 7.5.

2.7.5. Retroviral transduction of human cells

For transduction of THP-1 monocytes cells were seeded (1 000 000 cells/well of a 12-well plate) in RPMI10 + HEPES (1:50) (StemCell Technologies, #07200). Polybrene (Sigma-Aldrich, #TR-1003) (1.5 µl) and retrovirus (produced in HEK-293T cells via viral packaging (packaging pUMVC vector (Addgene, #8449), envelope pCMV-VSV-G vector (Addgene, #8454)) as done

by Marlene S. Knapp prior to this thesis) (7.5 µl) containing MG-Cas9-EGFP-recombinant plasmid (Flavell lab, unpublished) were added per well and mixed with cell suspension by pipetting. Cells were centrifuged at 37°C for 1.5 hours at 2500 rpm (spinfection) after which the cell suspensions were transferred to falcon tubes, which were spun at 1400 rpm for 4 minutes. Pellets were washed in DPBS and resuspended in RPMI10 + HEPES. Cells were incubated at 37°C and checked for green fluorescence under a fluorescence microscope (Leica) on the next day.

2.8. Data analysis in UCSC Genome Browser

Data for *PTGER4* genetic locus analysis were retrieved from, imported to and visualized in UCSC Genome Browser (Kent et al., 2002; https://genome.ucsc.edu/). The PTGER4 locus as such has been overlaid with ChIP-Seq data for H3K27Ac from the ENCODE project (Consortium *et al.*, 2012; Pervouchine *et al.*, 2015; Sloan *et al.*, 2016)and Human Epigenome Roadmap (Roadmap Epigenomics Project, 2007; http://www.roadmapepigenomics.org/). Conserved H3K27Ac sites between human (GRCh37/hg19) and mouse (NCBI37/mm9) were retrieved via extraction of the associated DNA sequences in human and mouse from UCSC and subsequent alignment via NCBI BLAST (Johnson *et al.*, 2008). IBD-associated GWAS hits have been retrieved from Jostins *et al.* (2012). IBD-finemapping SNP data are derived from Huang *et al.* (2017). YY1 datasets have been retrieved from Weintraub *et al.* (2017). Other data indicated on UCSC plots have been retrieved from UCSC datasets.

2.9. Statistical analyses

Statistical analyses were performed with GraphPad Prism 6. Normality was tested with the Shapiro-Wilk W test. In case of non-gaussian distribution means were tested for statistical significance with the Kruskal-Wallis test. In case of gaussian distribution unpaired two-tailed Student's t-test or one-way ANOVA was applied. P-values <0.05 were considered as statistically significant and are indicated in the respective images.

2.10. Image processing

Images included in this master thesis have been processed in Adobe Photoshop CC 2015 by the author if not indicated otherwise.

3. Results

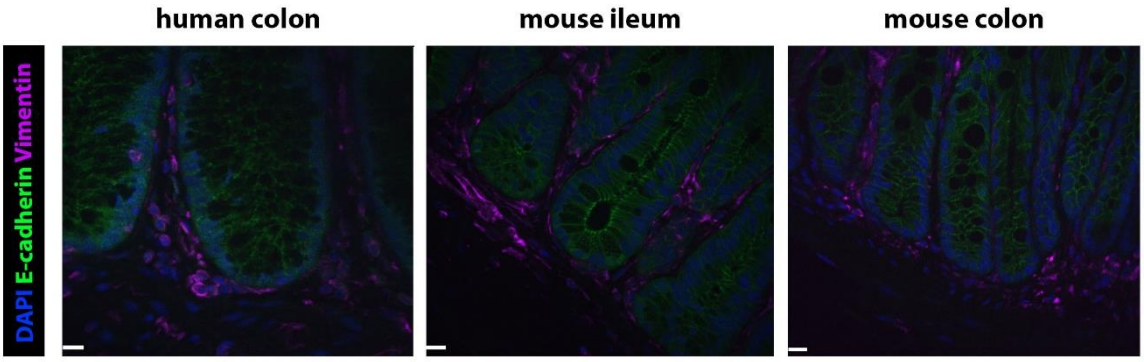

Figure 3.1. Pericryptal mesenchymal network in proximity to human and mouse intestinal epithelium. Immunostaining for epithelial E-cadherin (AF-488) and mesenchymal Vimentin (AF-647) in healthy human colon as well as murine ileum and colon. Scale bar 20 µm.

Mesenchymal cells reside in tight association with the intestinal epithelium, forming an extensive network along the crypt-villus axis, particularly gathering around the crypt base harboring the stem cell niche (see figure 3.1. and supplementary figure 7.1.). Separated merely by layers of extracellular matrix on a µm-scale, fibroblasts represent pronounced modulators of self-renewal and proliferative mechanisms as exerted by undifferentiated progenitor and stem cells (Stzepourginski *et al.*, 2017; Degirmenci *et al.*, 2018; Greicius *et al.*, 2018). Therefore, they are likely to be involved in regenerative processes on the one, and tumorigenic processes on the other hand, both of which have been revealed in association with prostaglandin signaling.

3.1. IBD-associated genetic variants overlap with a putative enhancer region upstream of the candidate gene *PTGER4*

As retrieved from GWA studies on cohorts of IBD patients, *PTGER4* ranks among the most significant associations with both forms of IBD. Interestingly, a substantial amount of genetic variants, including additional hits from subsequent finemapping studies, overlaps with non-coding elements upstream of the gene, though, residing within a ~400 kb region from bases

40 250 000 to 40 650 000 on chromosome 5 (see figure 3.2.(boxes A, B and C)). When overlaying these data with histone 3 lysine 27 acetylation (H3K27Ac) marks, indicative of potential transcriptionally active and enhancer sites, H3K27Ac peaks were particularly found in datasets of intestinal tissue alongside immune cell lines from the Human Epigenome Roadmap project, suggesting a putative enhancer role of the region Chr5.:40 380 000 – 40 630 000 in the intestine. Overall, 9 histone peaks, subdivided into three major clusters, were identified, with the first one being linked to *PTGER4* directly via the transcriptional regulator YY1, linking enhancer-promoter complexes, as inferred from HiChIP data on human Jurkat cells, i.e. a T-lymphocyte cell line (supplementary figure 7.2.). More importantly, however, the three H3K27Ac clusters were shown to be conserved via alignment alongside sequence similarity between human and mouse, where H3K27Ac peaks appear in opposite order within a region from bases 5 380 000 – 5 480 000 on the murine chromosome 15. This supports the notion of region 40 380 000 – 40 480 000 specifically as an enhancer element for *PTGER4* expression, likely applicable to multiple vertebrate species and thus of supposedly high importance.

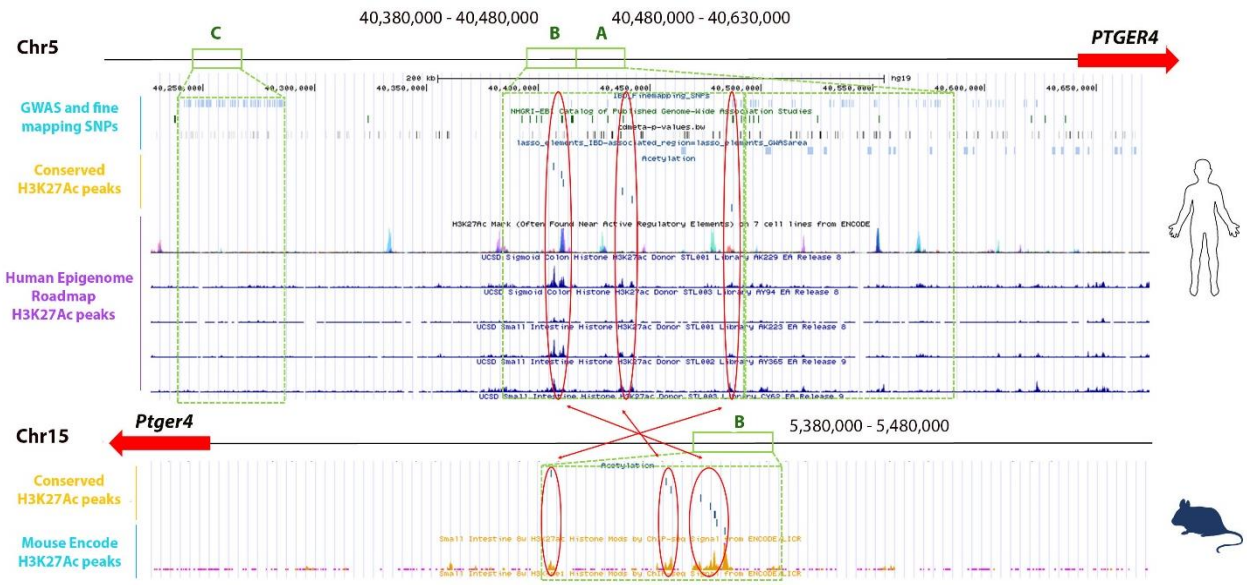

Figure 3.2. An IBD-associated risk region upstream of *PTGER4* overlaps with enhancer marks in human and mouse. Visualization of the 400 kb locus upstream of the *PTGER4* gene, a highly significant risk area in IBD GWAS, in the genomic assembly of human and mouse. Three core clusters of histone acetylation marks (encircled in red), indicative of potentially active enhancer function, particularly in intestinal tissue of human and mouse, could be identified within a subset of this risk locus. Dataset overlay was performed in the UCSC Genome Browser (Kent et al., 2002; https://genome.ucsc.edu/). Data for histone acetylation (H3K27Ac) peaks were obtained from Roadmap Epigenomics project (Roadmap Epigenomics Project, 2007; http://www.roadmapepigenomics.org/) and Mouse ENCODE project (Consortium *et al.*, 2012; Pervouchine *et al.*, 2015; Sloan *et al.*, 2016).

3.1.1. Setting up a system to genetically ablate GWAS-indicated regions in human cells

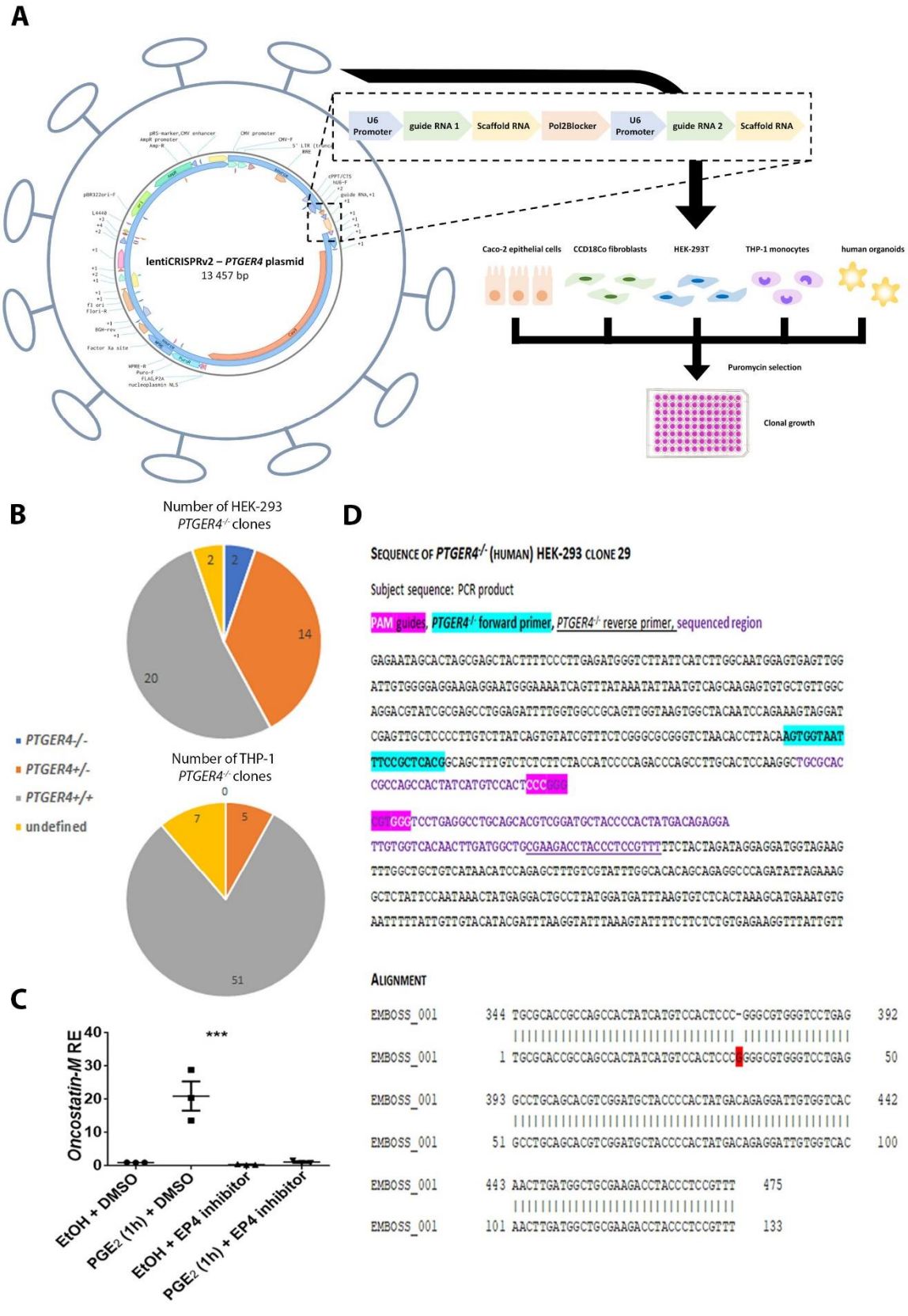

Figure 3.3. A CRISPR/Cas9-mediated *in vitro* system to knockout genetic elements in human cell lines. (A) Scheme of the lentiviral transduction system in human cell lines. Plasmid map of the lentiCRISPRv2-*PTGER4* vector to knockout the *PTGER4*

gene is shown, including a zoom-into the geneblock containing two guide RNAs specific for the gene and additional scaffold and promoter elements (Sanjana, Shalem and Zhang, 2014). Vector map has been designed and obtained from Benchling (Benchling, 2018; https://benchling.com) **(B)** Evaluation of deletion efficiency of the *PTGER4* gene via a two-guide RNA approach in HEK-293 cells and in THP-1 cells **(C)** THP-1 cell line readout for *PTGER4* deletion, resulting in a significant increase of *Oncostatin-M* expression upon PGE_2 stimulation. *** p-value < 0.001 **(D)** Sanger sequencing results from one out of 2 HEK-293 *PTGER4*$^{-/-}$ clones.

To be able to study effects and function of GWAS-indicated risk genes alongside their associated genetic variants, we established, reliant upon experimental work conducted prior to this study, a CRISPR/Cas9-mediated *in vitro* system to knock out designated genetic elements in human cell lines of physiological relevance to the studied genetic element. Using a lentiviral transduction approach (see figure 3.3.A) the *PTGER4* gene itself was initially targeted via a two-guide RNA strategy in HEK-293 cells, due to their generally high transfectability, and THP-1 monocytes, depicting a physiologically relevant immune cell line (figure 3.3.B), for which we had established a reliable readout of genetic deletion, viewing an EP4-mediated upregulated expression of *Oncostatin-M* upon stimulation with PGE_2 (16,16-dimethyl PGE_2) as published before (Ganesh *et al.*, 2012) (figure 3.3.C). Transduction of further cell lines, encompassing epithelial cells of a colon cancer line (Caco-2), colonic fibroblasts (CCD18Co) and human organoids is planned to be conducted for future genetic deletion of putative regulatory elements. Whilst lentiviral transduction of HEK-293 within subsequent single-cell derived clonal growth resulted in 2 knockout clones, as confirmed by Sanger sequencing (figure 3.3.D), merely heterozygous deletion could be achieved in THP-1 cells. The optimization of transduction, genetic ablation and clonal growth will be of interest for follow-up experiments, particularly focusing on the deletion of non-coding elements. Alternatively to the lentiviral system, retroviral transduction, adopting the MG-Cas9-EGFP-recombinant plasmid developed in the lab (Flavell lab, unpublished), of HEK-293 was performed viewing successful transfection according to GFP fluorescence (supplementary figure 7.4.). This approach was not continued, though, based upon prior results of inefficient transfectability of other cell lines (CCD18Co).

3.1.2. Genetic ablation of putative enhancer elements in human cells and mice

Based upon the *in vitro* system established and described before, two guide RNAs were subsequently designed for each designated enhancer block, i.e. Chr5:40 380 000 – 40 480 000 and Chr5: 40 480 000 – 40 630 000, referred to as enhancer blocks 40 380 and 40 480

(figure 3.4.A and supplementary figure 7.5.). Whilst the first element, block 40 380, encompasses the three conserved H3K27Ac clusters alongside multiple IBD-GWAS SNPs, the second one represents a region harboring additional genetic variants, partially replicated during finemapping studies, together with remnant H3K27Ac marks. Analogously to making the lentiCRISPRv2-*PTGER4* knockout plasmid in 3.1.1., guide RNAs were ordered and synthesized in geneblock version, including scaffold, Pol2 blocker and U6 promoter sequences (figure 3.4.B) and cloned into the lentiCRISPRv2 vector backbone (supplementary figure 7.3.). The plasmid was packaged into lentivirus again, which will be utilized for prospective transduction experiments of the indicated cell lines, was beyond the scope of this project, though.

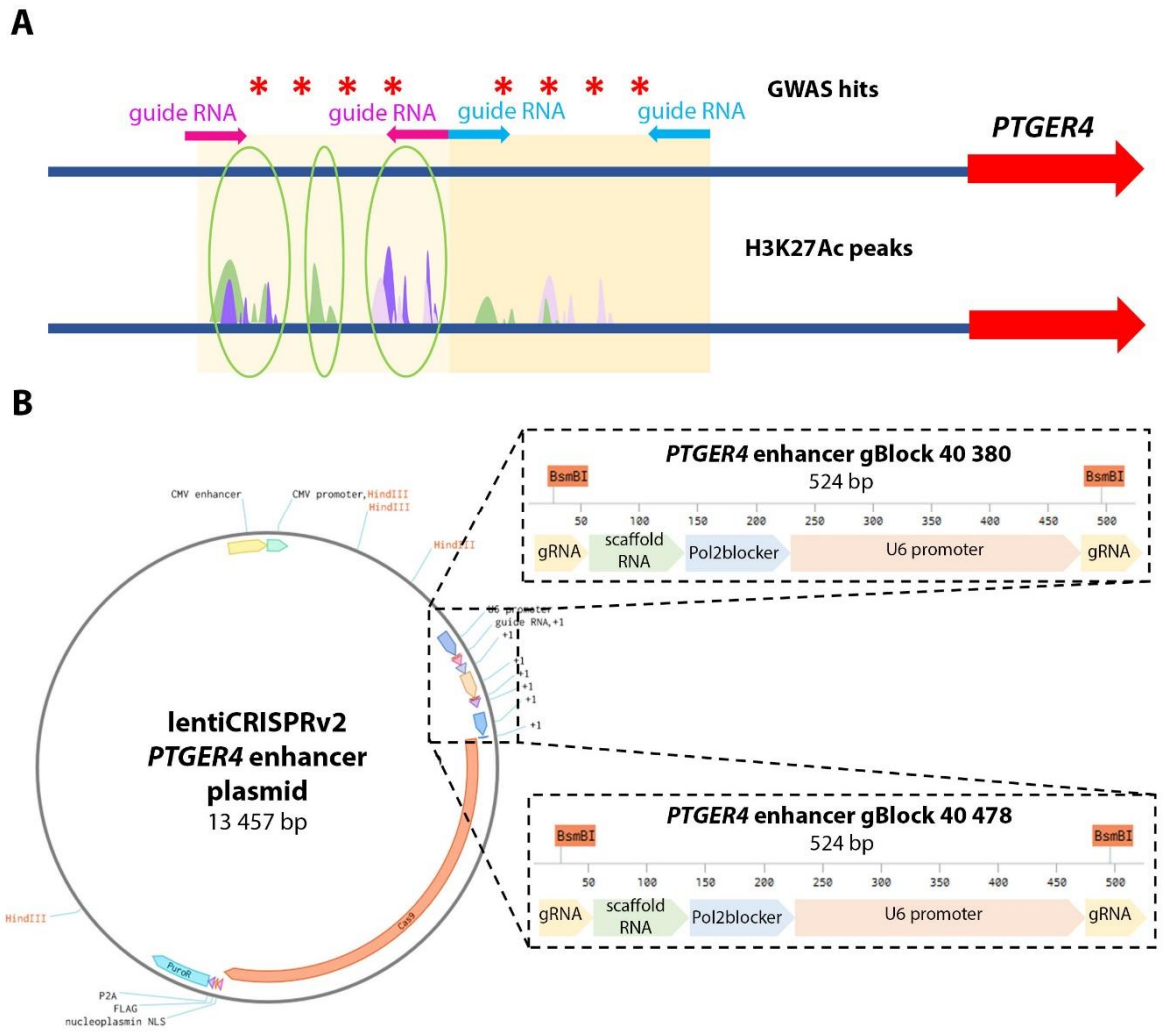

Figure 3.4. Design of a CRISPR/Cas9 mediated system to knockout enhancer elements in human cell lines. (A) Schematic view of the genetic regions upstream of *PTGER4* in humans, which overlap with IBD GWAS hits (*) and H3K27Ac peaks, some of which (encircled in green) are conserved between human and mouse. Guide RNAs in pink target the chromosomal region of Chr5: 40 380 000 – 40 481 000, blue ones target a region around Chr5:40 478 000 – 40 630 000 **(B)** Representative vector map of a lentiCRISPRv2-*PTGER4* enhancer plasmid to knockout designated enhancer elements upstream of the

PTGER4 gene via a two-guide RNA strategy as set up in the lab before. *PTGER4* enhancer geneblock 40 380 targeting a potential enhancer region ranging from Chr5:40 380 000 – 40 481 000, which was introduced to the lentiCRISPRv2 plasmid (Sanjana, Shalem and Zhang, 2014) and geneblock 40 478 targeting the region around Chr5:40 478 000 – 40 630 000, are shown. Vector and geneblock maps were partially obtained from Benchling (Benchling, 2018; https://benchling.com/).

In parallel to that, the complementary enhancer region covering the conserved H3K27Ac peaks in mouse, ranging from Chr15: 5 440 000 – 5 540 000, was selected for guide RNA design as well. For the *Ptger4* enhancer knockout mouse, two guide RNAs (figure 3.5.) demarcating the aforementioned region were synthesized adjacent to scaffold sequences (supplementary figure 7.6.A) and subsequently delivered to murine zygotes together with the Cas9 enzyme and non-homologous end joining inhibitor via microinjection. Heterozygous enhancer knockouts were backcrossed to wildtype animals before crossing. Full enhancer knockouts were confirmed by Sanger sequencing (supplementary figure 7.6.C). No pronounced phenotype was noted. Knockouts will be subjected to DSS tests of colitis as well as crossed to $Tnf^{DARE/+}$ mice to examine their performance in two models of IBD.

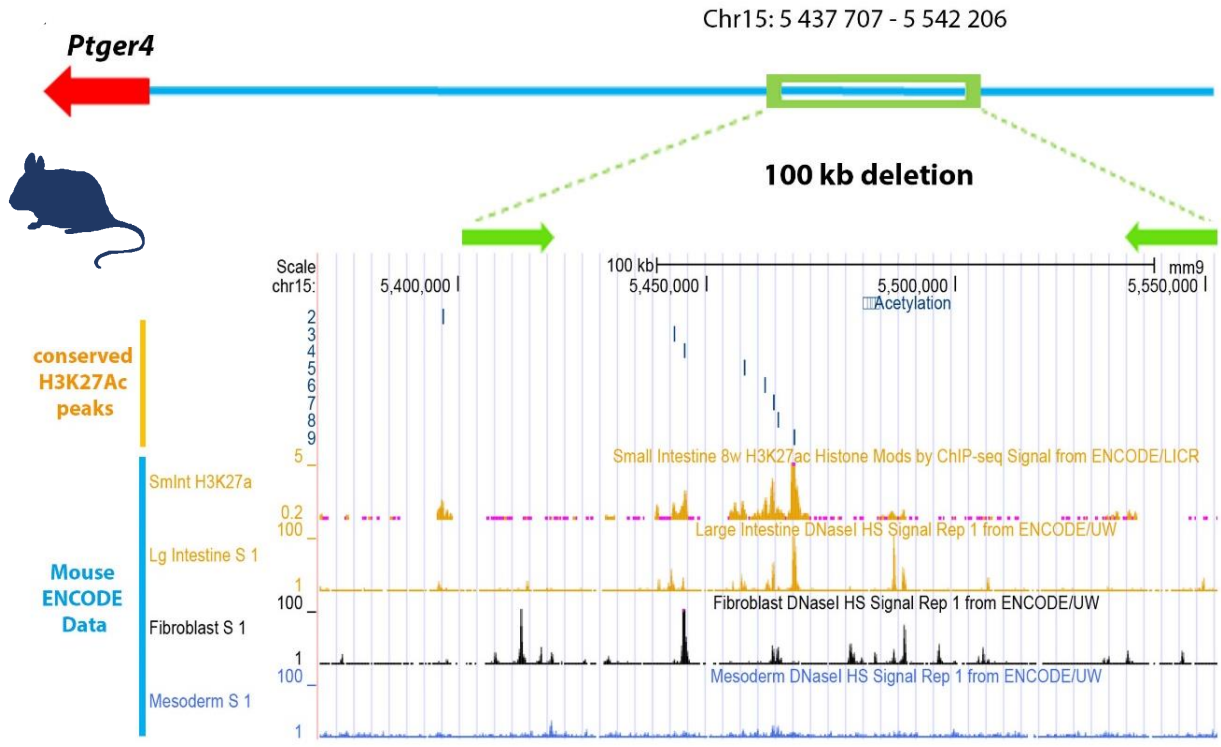

Figure 3.5. *In vivo* deletion of a potential enhancer region upstream of *Ptger4*, as indicated by conserved H3K27Ac marks between human and mouse. Visualization of the enhancer region upstream of *Ptger4* in the mouse, which overlaps with a region high in IBD GWAS hits and H3K27Ac marks in the respective human genetic locus. Histone acetylation pattern in this region was shown to be conserved between human and mouse. As shown above, a 100 kb region encompassing these traits has been selected to be knocked out in a CRISPR/Cas9 system, based upon guide RNA microinjection into murine zygotes.

3.2. Studying mesenchymal-epithelial cell interactions

Given the proinflammatory role of PGE_2 signaling, to a great extent mediated by fibroblasts within the context of an inflammatory microenvironment, but the emanant elusiveness of the exact mechanisms involved, we set up an *in vitro* model to study multicellular interactions as seen in the intestine. Based upon immunostainings (supplementary figure 7.1.) in combination with our preliminary data (figures 1.4.and 1.5.) we hypothesized prostaglandin signaling to be pronounced between the epithelial and mesenchymal compartment. As a result, we developed an organotypic system, isolating murine small intestinal crypts and growing them into organoids, mimicking the intestinal crypt-villus architecture including all relevant epithelial cell populations at a smaller scale *in vitro.* We cultured crypts in organoid growth media (OGM) supplemented with 16,16-dimethyl PGE_2, exhibiting a prolonged half-life compared to its *in vivo* equivalent, for 7 consecutive days. Morphologically, the typical budding process resulting in organoid structure within 7 days (Kretzschmar and Clevers, 2016) was omitted upon PGE_2 treatment, having crypts transform into so-called spheroid structures, lacking the characteristic epithelial compartmentalization into crypts and villi (figure 3.6.A). To test whether this effect was EP4-mediated, we developed organoids from crypts of *VillinCrePtger4*$^{fl/fl}$ and *Ptger4*$^{fl/fl}$ mice (figure 3.6.B). Using mesenchymal cells, isolated from the small intestine of wildtype mice, as an alternative PGE_2 source, spheroid formation was inhibited in *VillinCrePtger4*$^{fl/fl}$-derived organoids lacking the EP4 receptor in the intestinal epithelium. We thus propose prostaglandin signaling to occur in an interactive mesenchymal-epithelial network, viewing stromal cells as primary PGE_2 producing niche, signaling towards the intestinal epithelium via EP4. The thereby established 3D-coculture system of mesenchymal and epithelial cells was subsequently refined, either plating crypts on top of a fibroblast layer (figure 3.6.B) or combining all cell types within Matrigel domes (figure 3.6.C and D). When using EP4 inhibitor (ONO-AE3-208) as a substituent for genetic ablation, spheroid formation similarly to *VillinCrePtger4*$^{fl/fl}$ organoids was prohibited (figure 3.6.D and F), with morphological features of organoid or spheroid structure being distinguishable from day 2 on (figure 3.6.D). Overall, fibroblasts seemed to delay organoid/spheroid development, as the crypt-villus architecture on day 4 of non-co-cultured organoids (figure 3.6.E) was increasingly pronounced, whilst in organoids co-cultured with fibroblasts a merely advanced crypt structure (figure 3.6.D) could be identified.

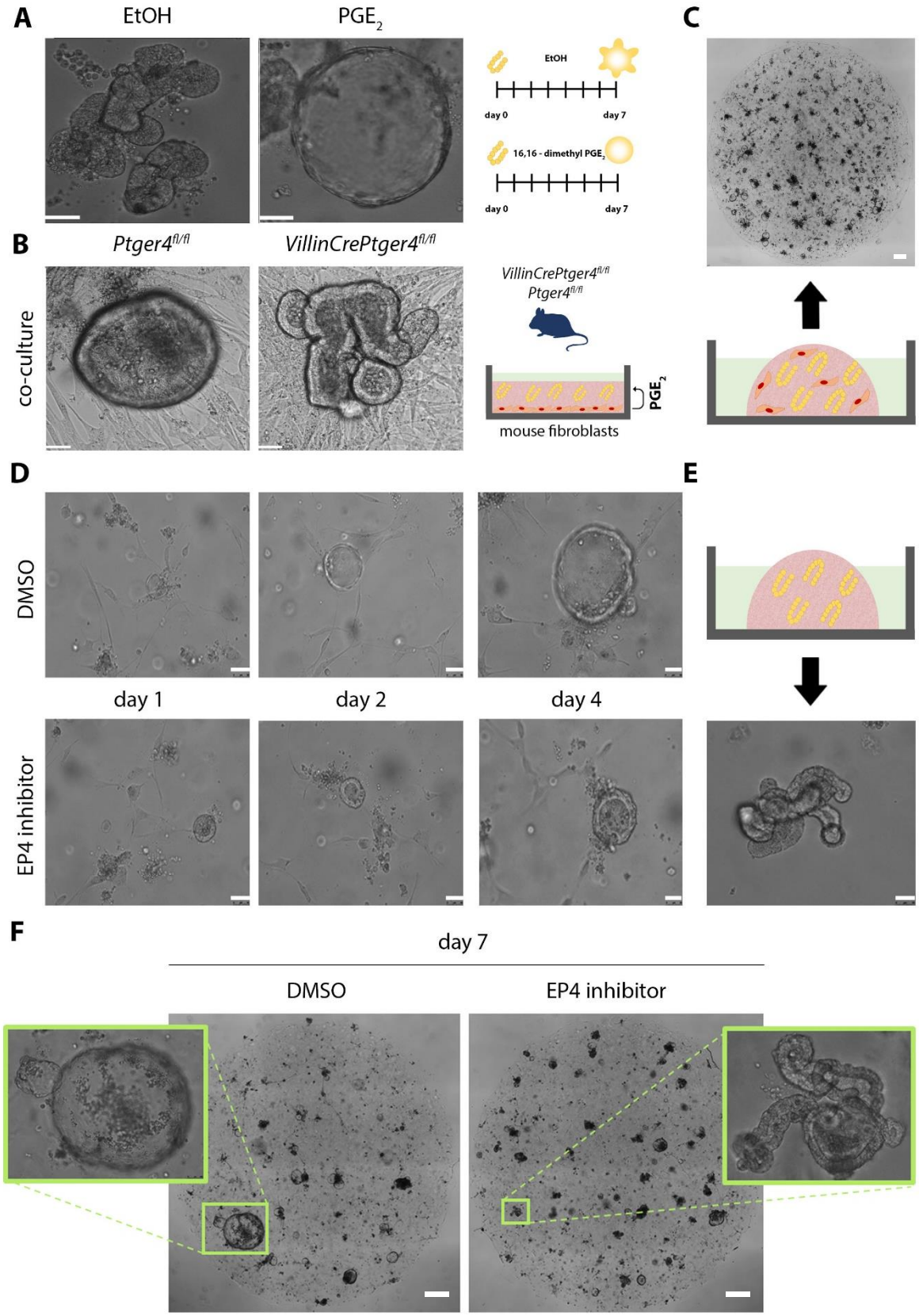

Figure 3.6. Setting up an *in vitro* organoid system to model mesenchymal-epithelial interactions. (A) Crypts isolated from wildtype murine small intestine were grown into organoids in Organoid Growth Medium (OGM) daily supplemented with ethanol or 0.1 µM 16,16-dimethyl PGE_2 ($dmPGE_2$), resulting in spheroid formation as schematically indicated. Scale bar 50 µm **(B)** Organoids were grown from small intestinal crypts of *Ptger4*$^{fl/fl}$ and *VillinCrePtger4*$^{fl/fl}$ mice in OGM on top of a

murine fibroblast layer as indicated on the right. Scale bar 50 µm **(C)** Tile scan of a three-dimensional crypt-fibroblast co-culture network in Matrigel domes cultured in OGM on day 2. Scale bar 300 µm **(D)** Crypt-fibroblast co-cultures as described in (C) cultured in OGM supplemented with dimethyl sulfoxide (DMSO) or 10 µM EP4 inhibitor (ONO-AE3-208) on days 1, 2 and 4. Scale bar 50 µm **(E)** Organoid culture derived from wildtype small intestinal crypts of mice cultured in OGM on day 4 for comparison. Scale bar 50 µm **(F)** Tile scans and detailed representative images of spheroid/organoid co-cultures, as described in (C), following culturing in OGM with or without EP4 inhibitor (ONO-AE3-208). Scale bar 500 µm.

3.2.1. Mesenchymal-epithelial cell interactions in an *Apc$^{Min/+}$* model of tumorigenesis

Spheroid formation is closely associated with poor differentiation (Sato *et al.*, 2010; Mustata *et al.*, 2013) and may thus allude to incomplete differentiation of epithelial lineages. Dysregulation in differentiation, frequently coinciding with overemphasized stemness potential, are common hallmarks of cancer development. Therefore, we decided to investigate the mechanisms underlying spheroid formation in a tumor-associated context, employing the *Apc$^{Min/+}$* mouse model of intestinal adenoma formation. Germline mutations in the *APC* gene in humans have reportedly been assigned to familial adenomatous polyposis, a dominantly inherited syndrome inducing intestinal adenoma development (Bülow, 1987). Somatic mutations, in comparison, have been mapped to sporadic colorectal tumors, attributing mutation in *APC* with a relevant function in early colorectal cancer (Strauss *et al.*, 1994). The APC protein as such represents a component of the destruction complex downstream of the Wnt-signaling pathway, which leads to β-catenin degradation in the absence of Wnt signal. In the murine *Apc$^{Min/+}$* model, a point mutation in one allele of the *Apc* gene truncates and inactivates the protein, resulting in constitutive activation and nuclear translocation of β-catenin, inducing Wnt-target gene transcription. Adenoma formation typically succeeds loss of the second intact wildtype allele, i.e. loss of heterozygosity (Strauss *et al.*, 1994; Lugli *et al.*, 2017). Crypts for organoid cultures were isolated from *Apc$^{Min/+}$* mice and initially validated on genetic level (supplementary figure 7.7.) for the presence of mutated (Min) and wildtype (WT) alleles. Loss of the WT allele in *Apc$^{Min/+}$* organoids is typically expected from passage 2 on, coinciding with persistent spherically shaped structures (Germann *et al.*, 2014). To our surprise, the variety in morphological structures, encompassing preliminary forms of organoid development like cysts and crypts alongside spheroids and organoids (figure 3.7.A) was maintained at substantial level, though (figure 3.7.B). Additionally, retention of the WT allele was still observed around passages 6-8 (figure 3.7.C). Co-culturing organoids on top of a layer of murine fibroblasts resulted in the same effect as seen for WT organoids, triggering spheroid

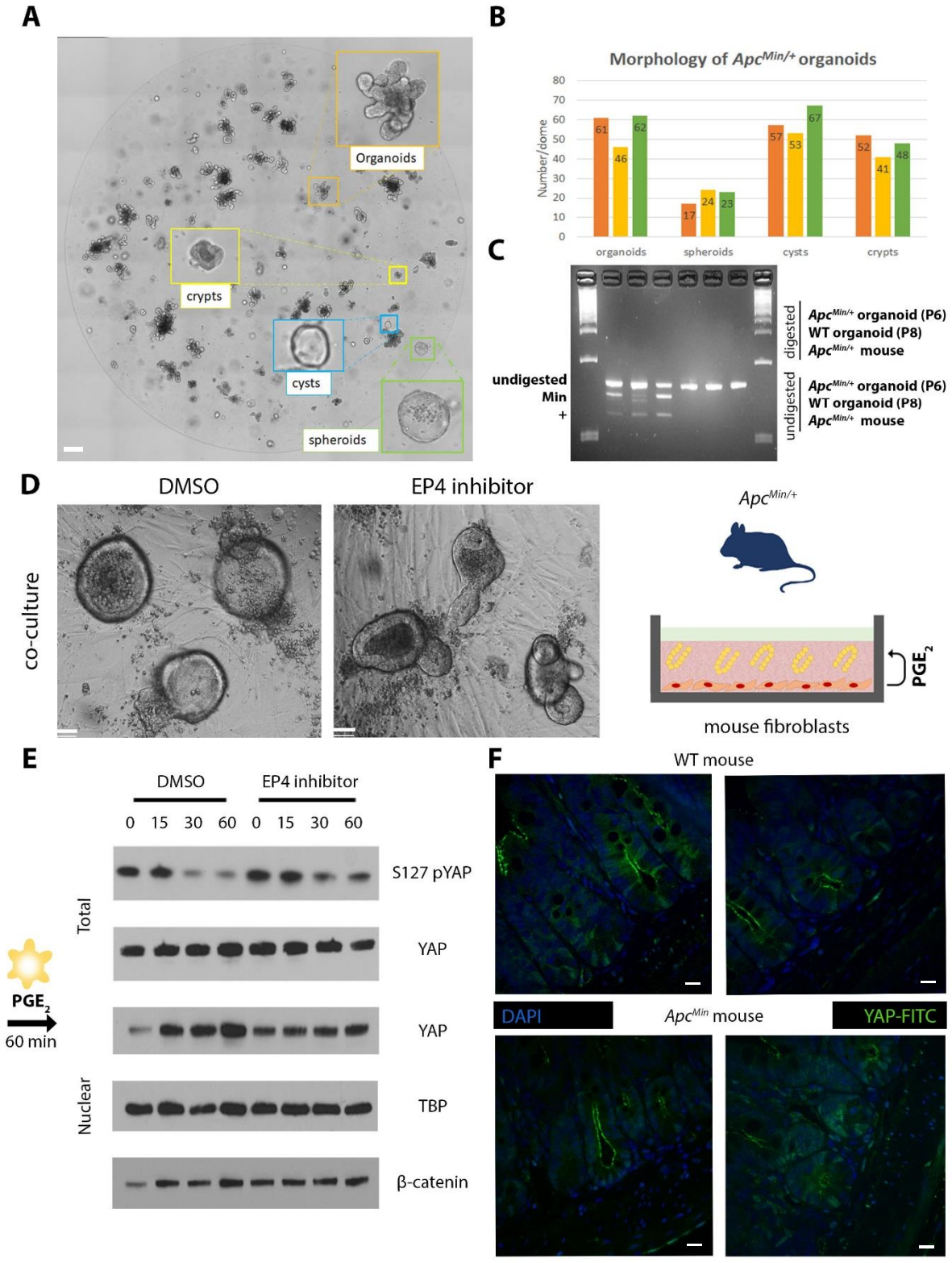

Figure 3.7. Studying epithelial-mesenchymal interactions and their implications towards tumorigenesis in *Apc*$^{Min/+}$ organoids. (A) Tile scan of organoids derived from *Apc*$^{Min/+}$ small intestinal crypts on day 7. Organoids were cultured in OGM. Morphological variety is indicated by the zoom-ins. Scale bar 250 µm **(B)** Quantification of the morphological structures viewed in (A). Numbers have been derived from 3 disparate organoid culture domes **(C)** Loss-of-heterozygosity assay to determine the presence or absence of the *Apc* wildtype allele following the approach by Strauss J. *et al* (1994). Samples loaded are indicated on the right **(D)** Representative pictures of organoids derived from small intestinal crypts of *Apc*$^{Min/+}$ mice, as indicated on the right, co-cultured with murine fibroblasts in OGM with or without 10 µM EP4 inhibitor (ONO-AE3-208) on day 4. Scale bar 50 µm **(E)** Western blot results showing cytoplasmic dephosphorylation of Yap protein

(S127 pYAP) in murine *Apc*$^{Min/+}$ organoid samples upon prolonged stimulation with 0.1 µM dmPGE$_2$. This is consistent with nuclear entry of Yap upon PGE$_2$ stimulation as shown in the nuclear protein fractions. Treatment with 10 µM EP4 inhibitor (ONO-AE3-208) reduced the aforementioned effect. Moreover, PGE$_2$ appears to affect nuclear deposition of β-catenin as well, whose nuclear levels ought to be elevated on account of the *Apc*$^{Min/+}$ genetic background of the utilized organoids **(F)** Immunostainings for Yap (AF-488) in small intestinal sections, specifically in the pericryptal region, of wildtype versus *Apc*$^{Min/+}$ mice. Scale bar 40 µm.

formation if not blocked by EP4 inhibitor administration. Reinstalled organoid structures following inhibitor treatment appeared to be less pronounced in budding phenotype, though, compared to WT organoids (figure 3.7.D).

3.2.2. PGE$_2$ from fibroblasts induces spheroid morphology in intestinal organoids via inhibiting the Hippo kinase cascade

Spheroid morphology, as observed upon PGE$_2$ treatment or fibroblast-co-culture, has been linked to a decline in terminal differentiation of epithelial cells, which display highly proliferative potential throughout spheroid surface, whilst in organoids proliferation is restricted, analogously to the *in vivo* situation, to crypt region (Stzepourginski *et al.*, 2017). Single cell RNA-seq analysis data of intestinal epithelial cells of spheroids and organoids, co-cultured with fibroblasts supplemented with DMSO (vehicle) or EP4 inhibitor, generated by our lab (Roulis, M. *et al.*, unpublished) confirmed that. A noticeably different distribution of cells obtained from PGE$_2$-mediated spherical structures compared to organoids (supplementary figure 7.8.) elicited a decrease in abundance of terminally differentiated enterocytes and actively cycling stem/progenitor cells (Lgr5+) in spheroids and an expansion of slowly cycling or quiescent cells, commonly identified as reserve stem cells (RSCs) based upon established markers (mTert+). Reportedly, myofibroblasts have been shown to upregulate cell cycle regulators and markers of intestinal progenitor cells in small intestinal organoids, while differentiated and canonical stem cell markers remained unaffected (Pastuła, 2016). In our lab's RNA-seq data an overlap in expression levels between slow-cycling stem/progenitor cells and an early *Apc*$^{Min/+}$ tumorigenesis program, retrieved via metagene analysis from publicly available bulk and single cell RNA-seq datasets (supplementary figure 7.8.D), was observed. Surprisingly this program signature did not align with the β-catenin program, though and instead mapped to a Yap gene signature (supplementary figures 7.8. E and F).

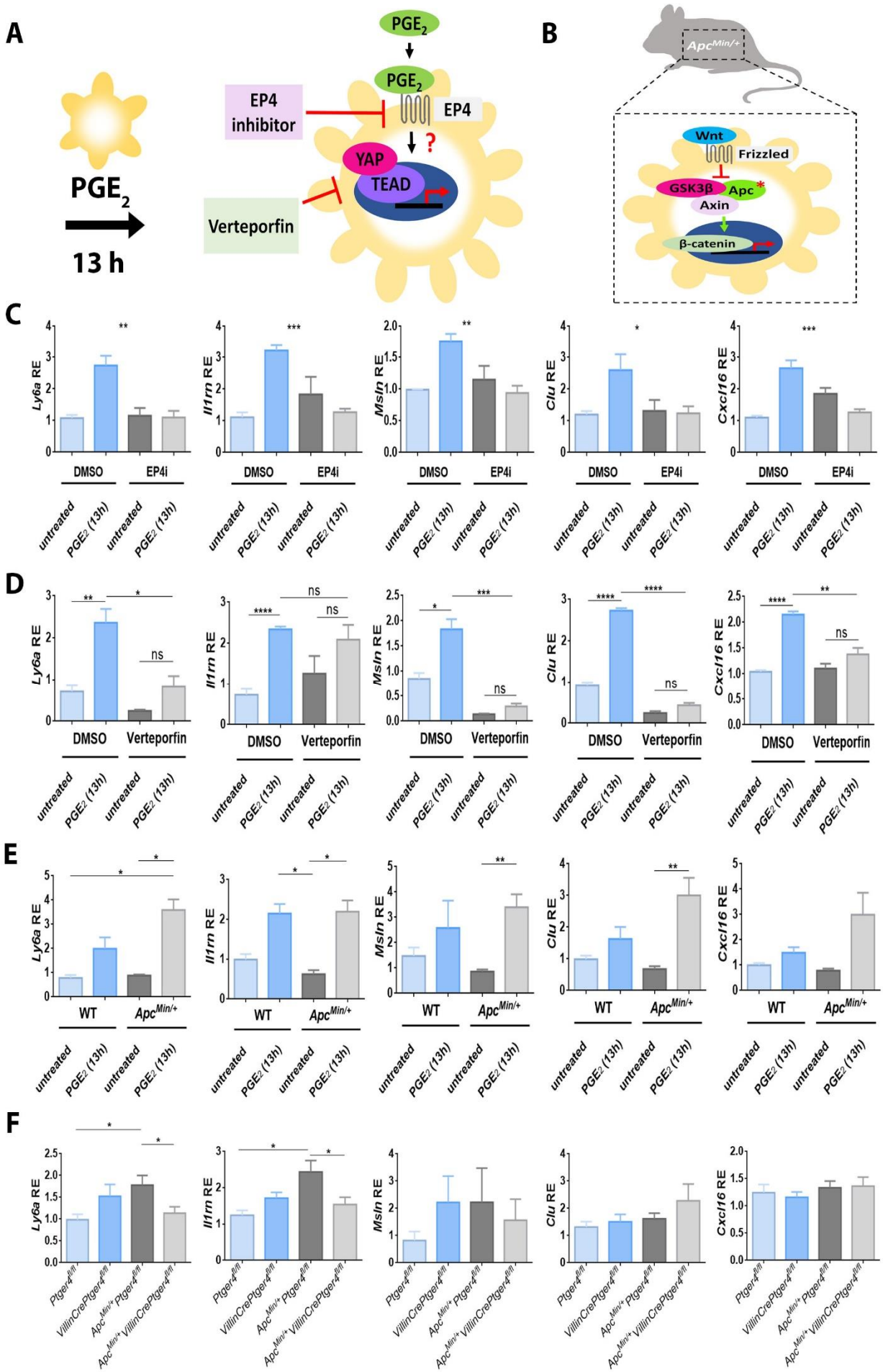
A
PGE2
13 h
PGE2
PGE2
EP4
EP4 inhibitor
?
YAP
TEAD
Verteporfin
B
ApcMin/+
Wnt
Frizzled
GSK3β
Apc*
Axin
β-catenin
C
Ly6a RE
Il1rn RE
Msln RE
Clu RE
Cxcl16 RE
DMSO
EP4i
untreated
PGE2 (13h)
D
DMSO
Verteporfin
ns
E
WT
ApcMin/+
F
Ptger4fl/fl
VillinCrePtger4fl/fl
ApcMin/+ Ptger4fl/fl
ApcMin/+ VillinCrePtger4fl/fl

Figure 3.8. Relative expression levels of Yap target genes upon PGE_2 stimulation in organoid samples. (A) Organoids were stimulated with 0.1 µM 16,16-dimethyl PGE_2 for 13 hours. EP4 inhibitor (ONO-AE3-208) and Yap inhibitor Verteporfin, inhibiting YAP-TEAD binding, were used to interfere with signaling pathways as indicated above **(B)** Organoids derived from $Apc^{Min/+}$ mice ((E) – (F)) owing to a point mutation (*) in the Apc protein (green) are expected to display constitutively active Wnt signaling **(C)** Organoids derived from wildtype mice at day 7 were stimulated with 0.1 µM $dmPGE_2$ for 13 hours following treatment with or without 10 µM EP4 inhibitor (ONO-AE3-208) before RNA was collected for RT-qPCR analysis. Relative expression levels of various established Yap target genes are shown. **(D)** Analysis analogous to what was described in (A) following treatment with or without 1 µM Yap inhibitor Verteporfin **(E)** Relative expression levels of Yap target genes upon treatment with or without 0.1 µM $dmPGE_2$ in samples derived from wildtype versus $Apc^{Min/+}$ organoids **(F)** Relative expression levels of Yap target genes analyzed in intestinal RNA samples obtained from $Ptger4^{fl/fl}$, $VillinCrePtger4^{fl/fl}$, $Apc^{Min/+}Ptger4^{fl/fl}$ and $Apc^{Min/+}VillinCrePtger4^{fl/fl}$ mice. Data represent mean ± SEM. ns, non-significant, * p-value < 0.05, ** p-value < 0.01, *** p-value < 0.001, **** p-value < 0.0001

YAP protein, if translocated to the nucleus, acts as a transcription factor downstream of the HIPPO kinase core cascade. YAP/TAZ transcriptional co-activator signaling has been associated with various human tumors, categorized as essential for cancer initiation, progression or metastasis (Zanconato, Cordenonsi and Piccolo, 2016). Elevated expression of YAP or TAZ appears to be correlative with poor tumor differentiation (Noh *et al.*, 2017) and in RNA-seq data was particularly amassed in quiescent stem/progenitor cells, or RSCs. RSCs in $Apc^{Min/+}$ mice were assessed as tumor-initiating stem cells but of minor function during steady state (Nakanishi *et al.*, 2013). To see whether Yap signaling in our $Apc^{Min/+}$ organoids is active upon PGE_2 stimulation we performed Western blots subdividing protein into nuclear and cytoplasmic fractions (figure 3.7.E). On cytoplasmic level Yap was dephosphorylated in Ser127 following prolonged PGE_2 treatment, suggestive of an inhibition of the Hippo pathway. Consistently, Yap was seen to be translocated to the nucleus within 30-60 minutes of PGE_2 stimulation. Both incidents were partially inhibited via EP4 inhibitor administration. B-catenin mimicked Yap nuclear translocation, which might, however, be determined by abundant Wnt signaling in $Apc^{Min/+}$ organoids. *In vivo*, Yap nuclear abundance, particularly in areas of stem and progenitor cells, was increasingly observed in crypts of $Apc^{Min/+}$ mice compared to WT mice, which mainly exhibited cytoplasmic Yap retention at +4 and CBC stem cell position, as visualized via immunostainings (figure 3.7.F).

In conclusion, these results propose a PGE_2-EP4 mediated downstream activation of Yap transcriptional activity, which made us investigate the expression levels of well-established Yap target genes. To do so we extended PGE2 treatment of WT organoids to 13 hours, when Yap protein itself remained unaffected by PGE_2 signal (supplementary figure 7.10.B). Relative expression levels of a core set of Yap target genes, i.e. *Ly6a, Clu, Il1rn, Cxcl16* and *Msln*, were significantly elevated upon PGE_2 stimulation, which again was EP4 mediated (figure 3.8.C). Similarly, gene expression of those was inhibited upon treatment with verteporfin (figure

3.8.D), interfering with the interaction of co-transcriptional activators Yap and Tead (Liu-Chittenden *et al.*, 2012). Nonetheless, the exact mechanisms underlying PGE_2-Yap signaling axis remain to be determined. Neither cAMP-mediated processes downstream of the PGE_2-EP4 pathway, mimicked by Forskolin application, nor the PI3K subordinate appear to (fully) drive activation of Yap (supplementary figure 7.9.A and B). Rho-associated kinase (ROCK) inhibition partially inhibited PGE_2 driven Yap dephosphorylation, confirming Yap signaling to be dependent on but not entirely regulated by cytoskeletal cues, since ROCK is a prominent actin modulator (Amano, Nakayama and Kaibuchi, 2010) (supplementary figure 7.9.C). Yap immunostainings on murine fibroblasts aligned with that, showing pronounced nuclear translocation in increasingly contracted cells (supplementary figure 7.11.B). Cyclical and static pressure, in comparison, induced both *Cox-2* and *Ctgf* (Yap target) expression in fibroblasts (supplementary figure 7.11.A), did not show a difference on protein levels of Yap, though (data not shown).

When testing for Yap target gene expression in $Apc^{Min/+}$ organoids, results could be replicated (figure 3.8.E) and two of the genes mentioned, *Ly6a* and *Il1rn*, turned out to be significantly downregulated in RNA samples of $Apc^{Min/+}VillinCrePtger4^{fl/fl}$ mice compared to $Apc^{Min/+}Ptger4^{fl/f}$ owing to genetic ablation of the EP4 receptor *in vivo*, whilst in non-tumorigenic animals ($VillinCrePtger4^{fl/fl}$ and $Ptger4^{fl/fl}$) the effect appeared to be less persistent (figure 3.8.F). Overall Yap-mediated gene expression following PGE_2 signaling was more pronounced on the $Apc^{Min/+}$ genetic background, considering a potentially synergistic role of upregulated Wnt signaling activity. Wnt thereby might act in an alternative, non-canonical fashion, since classical target genes showed similar to equivalent expression levels irrelevant of PGE_2 treatment (supplementary figure 7.10.A).

3.2.3. Spheroid morphology reflects an increased stemness potential

To functionally assess these results, suggestive of an extended cluster of undifferentiated, slow-cycling progenitor and stem cells in spherical structures, we treated mouse WT intestinal crypts for 4 consecutive days with or without $dmPGE_2$, thereby inducing spheroid and organoid morphologies. On day 4 we dissociated the obtained structures into single cells, which were plated and monitored for development, number and growth on the indicated days. Strikingly, spheroid-derived single cells resulted in a significantly higher

number of disparate morphological structures, as seen in conventional organoid culture, than organoids (figure 3.9.A), which was confirmed after quantification (figure 3.9.B and supplementary figure 7.13.). Since merely stem cells are capable of giving rise to entire organotypic structures encompassing differentiated epithelial lineages alongside stem and progenitor cells (supplementary figure 7.12.), this increase in number of observed structures is correspondent to an elevated stemness program in PGE_2-induced spheroids.

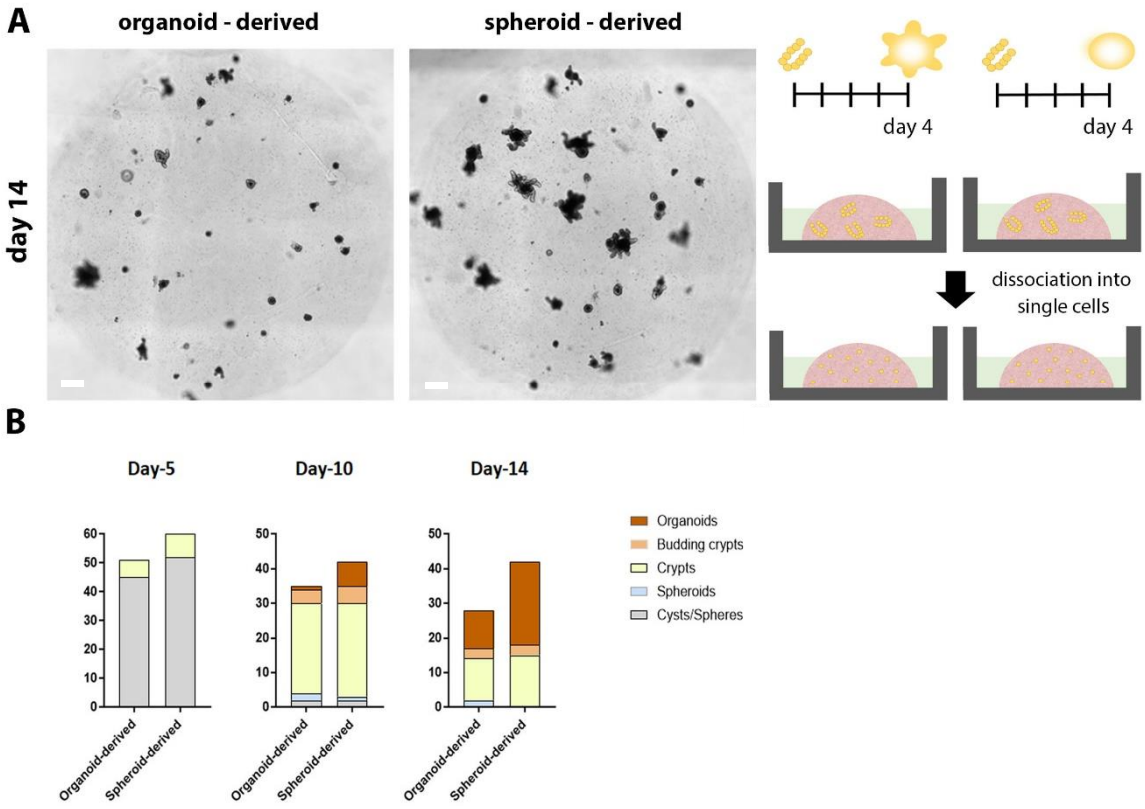

Figure 3.9. PGE_2 signaling activates a stemness program in organoids. (A) Tile scans of organoid structures on day 14 following culturing of single cells obtained from organoid or PGE_2 – induced spheroids as indicated on the right. Scale bar 400 µm **(B)** Quantification of the morphological structures observed in organoid- and spheroid-derived cultures on days 5, 10 and 14.

4. Discussion

In the intestine, epithelial cells largely contribute to intestinal homeostasis, representing an important interface between host and microbiota. Besides coordinating microbially induced immune reactions, they are actively involved in tissue repair upon injury or acute inflammation. Contrarily, following chronic inflammation, as in inflammatory bowel disease, epithelial cells promote intestinal cancer development (Peterson and Artis, 2014). Although

we, in our work, attribute the epithelium with a preemptive role in these conditions, results from experiments in IBD mouse models propose the intestinal mesenchyme to be the eventual driver of proinflammatory mechanisms. Via EP4-mediated prostaglandin E_2 signaling fibroblasts are hypothesized to be activated, thereby exerting ECM remodeling function alongside stimulation of inflammatory processes (figure 4.1.A). A recent single-cell profiling study on colonic mesenchyme confirms that by showing a colitis-associated expansion of a proinflammatory fibroblast subset (Kinchen *et al.*, 2018).

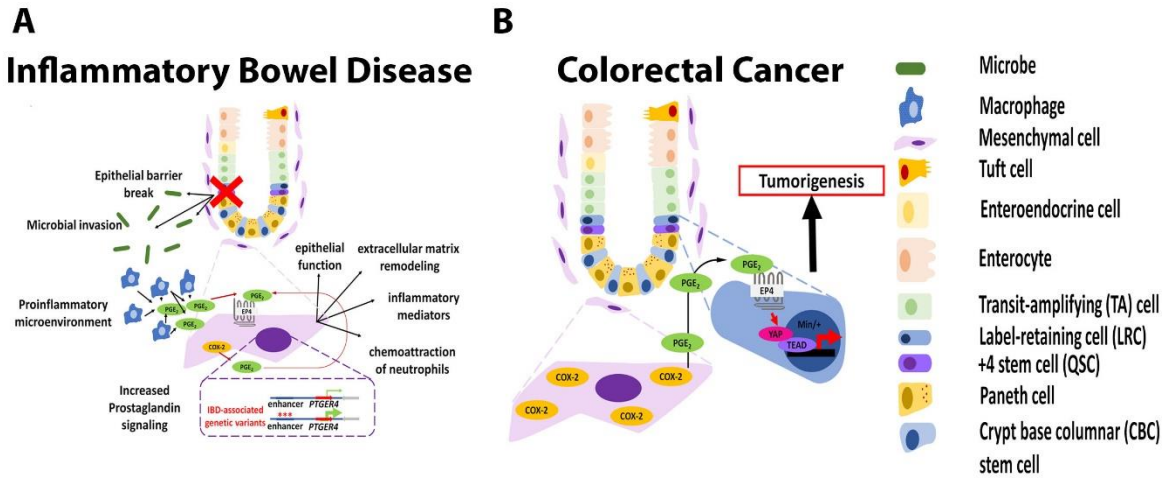

Figure 4.1. Role of PGE_2-EP4 signaling in two intestinal disorders. (A) Within an inflammatory microenvironment, as present upon microbial entry from the intestinal lumen following epithelial disruption, PGE_2 is likely secreted by activated immune cells alongside constitutive production by mesenchymal cells. Via EP4 it specifically activates fibroblasts, which in turn promote immune reaction via proinflammatory modulators **(B)** Given their constitutive PGE_2 production, fibroblasts in proximity to the intestinal crypt niche via EP4 activate a Yap-mediated transcriptional process in progenitor and stem cells, resulting in excessive proliferation and tumorigenesis on a genetically susceptible background ($Apc^{Min/+}$).

It will be interesting to investigate the role of non-coding elements in this context. As addressed in our studies, several of the most significantly IBD-associated genetic variants within GWA studies have been mapped to intergenic areas, including the 400 kb region upstream of *PTGER4*, encoding the EP4 receptor, as prioritized by us. These findings are applicable to association studies for various complex diseases, having single nucleotide polymorphisms being particularly enriched in non-coding but likely functional genetic regions, encompassing enhancer elements, DNase hypersensitivity regions and chromatin marks. While identifying causal mutations and variants within the plethora of hits in coding regions does not seem to pose substantial problems anymore, interpreting the functional impact of non-coding variants in GWAS loci appears to be more challenging. Finemapping studies help by providing high-coverage sequencing information on selected loci and technological advancement exemplified by chromosome conformation capture methods or quantitative trait loci mapping additionally aid in elucidating genetic interactions and effect

on gene expression. Nevertheless, a need for systematic examination of non-coding variants via reporter assays, cell models and model organisms persists (Zhang and Lupski, 2015). Therefore, a substantial part of our studies was dedicated to the establishment and optimization of an *in vitro* lentiviral transduction system, designed to knock out specified (enhancer) genetic elements via CRISPR/Cas9 in human cell lines and organoids alongside the generation of a *Ptger4* enhancer knockout mouse. Subsequent evaluation of the effect of deletions on *PTGER4* gene expression, representing the main candidate target, in reporter assays as well as further prioritization of genetic variants within the designated non-coding regions will be subjects of future experiments. *In vivo*, enhancer knockout mice will be monitored in their development, morphology etc. in murine IBD-models, testing for the physiological relevance of enhancer elements in inflammatory conditions, given the proinflammatory role of prostaglandin signaling and *Ptger4,* specifically in the intestinal mesenchyme.

Through its proinflammatory effect, the COX-2/PGE_2 axis is also hypothesized to drive colorectal cancer, often associated with IBD in humans (Grivennikov, Greten and Karin, 2010). However, in $Apc^{Min/+}$ mice, free from overt intestinal inflammation, tumor development depends on Cox-1 and Cox-2 (Kettunen, Kettunen and Rautonen, 2003), while these enzymes are dispensable for colitis-associated tumorigenesis in mice (Ishikawa and Herschman, 2010). These findings interfere with a simply inflammation-driven effect of Cox-2/PGE_2 to induce cancer and rather suggest non-inflammatory tumorigenic function, as published in several studies already (Wang and DuBois, 2013; Wang *et al.*, 2015). Mechanisms underlying the interaction of tumor cells with their endogenous microenvironment remain poorly investigated, though, thus overlooking the effects of resident cell compartments making up the intestinal tract.

Conditional mice within the onset of tumorigenesis in the $Apc^{Min/+}$ model revealed fibroblasts to be crucial drivers of tumor-initiating prostaglandin E_2 signaling. Commonly associated with wound-healing and inflammatory responses (Kalluri, 2016), fibroblasts in our studies have been shown to mediate crypt cell turnover by inducing a PGE_2-EP4 dependent stemness program in the crypt niche. As recapitulated in an *in vitro* organoid system, mesenchymal cells depict the main source of prostaglandin E_2 signaling, which via EP4 receptors expressed in the intestinal epithelium, similarly to what was shown for the Wnt pathway before, drives

the development of spherical structures lacking terminal differentiation. This coincides with a prominent role of mesenchymal cells in maintaining adult tissue stem cell niches at homeostatic stage, including the intestine (Greicius *et al.*, 2018) and underscores its assigned interaction with Wnt signaling (Goessling *et al.*, 2009).

Single-cell RNA-seq analyses revealed a correlative expression of a Yap program in spheroids consistent with an expansion of stem/progenitor cells distinct from actively cycling Lgr5+ ones. Kinchen and his colleagues (2018) termed those label-retaining cells (LRCs), which had been proposed to escape quiescence and re-establish their clonogenic potential upon epithelial injury in the intestine (Buczacki *et al.*, 2013). LRC identifying markers include markers characterizing the slow-cycling progenitor population at the "+4 position" in the crypt (Mustata *et al.*, 2013) or tuft cells (Dclk1+). In lineage tracing studies in murine adenomas, mice showed a decrease in tumor volume upon ablation of Dclk1+ cells, which was not amenable to Lgr5+ cell removal. This aligns either with the dedifferentiation of committed progenitors or the existence of an alternative stem cell niche in the intestinal crypt base of quiescent character during homeostasis, which re-enter the cell cycle upon injury (Vermeulen and Snippert, 2014). In fact, both events may be applicable, given that LRCs are dynamic over time, demarcating a secretory progenitor cell population, whilst reserve stem cells (RSC), as addressed in our work, depict a quiescent (G0 phase) stem cell population with inactive Wnt signaling (Li *et al.*, 2016). Wnt signaling has been identified as a crucial pathway maintaining the intestinal stem cell niche, often linked to tumorigenesis if deregulated. In our studies we, however, classify Wnt signaling as a subordinate axis, which is essential but not sufficient for intestinal cancer development. Rather, we propose the prostaglandin E_2 – EP4 pathway via downstream activation of Yap signaling to drive excessive proliferation, particularly in cells of quiescent stem cell character. Besides its association with human carcinogenesis, Yap as a transcriptional activator has been revealed to promote proliferation as well as differentiation of intestinal stem and progenitor cells (Imajo, Ebisuya and Nishida, 2014). We hypothesize, based on our results, that on a genetically susceptible basis, as illustrated in the murine $Apc^{Min/+}$ model, upregulated (non-canonical) Wnt signaling synergizes with PGE_2 signals from the tightly associated mesenchymal niche in pericryptal region, which via epithelial EP4 receptors specifically in progenitor and stem cells activate a Yap program (figure 4.1.B). Primary intestinal adenomas preceding colorectal cancer, reportedly depend on the presence of stem-like cells (Schepers *et al.*, 2012). Reacquisition of

stem cell properties, i.e. proliferative potential and self-renewal, thus defines a prerequisite for tumorigenesis, the exact identity of stem or progenitor cells involved remains to be determined, though.

5. Conclusion

In our studies we revealed EP4-mediated prostaglandin E_2 signaling to be a prerequisite for two kinds of intestinal disorders, i.e. IBD and colorectal cancer. While the mesenchymal niche appears to play a regulatory role in both conditions, the implicated local mechanisms differ. In an inflammatory microenvironment PGE_2 signaling is believed to primarily target fibroblasts themselves, which in turn promote a proinflammatory aggravation. During cancer, when secreted by the stroma, PGE_2 can activate a downstream pro-proliferative Yap-regulated transcriptional program in cryptal progenitor and stem cells, supposedly reserve stem cells. As a result, mesenchymal cells subjacent to the intestinal epithelium, involved in modulating homeostasis and regenerative processes, here have been shown to affect immune- and differentiation-related mechanisms in pericryptal region, which establishes them as main contributors to chronic inflammatory and carcinogenic pathogenesis.

6. References

Abcam (2018) 'RIPA Lysis buffer'. Available at: https://www.abcam.com/protocols/sample-preparation-for-western-blot.

Amano, M., Nakayama, M. and Kaibuchi, K. (2010) 'Rho-kinase/ROCK: A key regulator of the cytoskeleton and cell polarity', *Cytoskeleton (Hoboken, N.J.)*. 2010/08/10. John Wiley & Sons, Inc., 67(9), pp. 545–554. doi: 10.1002/cm.20472.

Armaka, M., Apostolaki, M., Jacques, P., Kontoyiannis, D. L., Elewaut, D. and Kollias, G. (2008) 'Mesenchymal cell targeting by TNF as a common pathogenic principle in chronic inflammatory joint and intestinal diseases', *The Journal of Experimental Medicine*, 205(2), p. 331 LP-337. Available at: http://jem.rupress.org/content/205/2/331.abstract.

Bae, S., Park, J. and Kim, J.-S. (2014) 'Cas-OFFinder: a fast and versatile algorithm that searches for potential off-target sites of Cas9 RNA-guided endonucleases', *Bioinformatics*, 30(10), pp. 1473–1475. Available at: http://dx.doi.org/10.1093/bioinformatics/btu048.

Bamba, S., Andoh, A., Yasui, H., Araki, Y., Bamba, T. and Fujiyama, Y. (2003) 'Matrix metalloproteinase-3 secretion from human colonic subepithelial myofibroblasts: role of interleukin-17', *Journal of Gastroenterology*, 38(6), pp. 548–554. doi: 10.1007/s00535-002-1101-8.

Barker, N., van Oudenaarden, A. and Clevers, H. (2012) 'Identifying the Stem Cell of the Intestinal Crypt: Strategies and Pitfalls', *Cell Stem Cell*, 11(4), pp. 452–460. doi: https://doi.org/10.1016/j.stem.2012.09.009.

'Benchling' (2018). Available at: https://benchling.com/.

Boyapati, R., Satsangi, J. and Ho, G.-T. (2015) 'Pathogenesis of Crohn's disease', *F1000Prime Reports*. Faculty of 1000 Ltd, 7, p. 44. doi: 10.12703/P7-44.

Brown, S. L., Riehl, T. E., Walker, M. R., Geske, M. J., Doherty, J. M., Stenson, W. F. and Stappenbeck, T. S. (2007) 'Myd88-dependent positioning of Ptgs2-expressing stromal cells maintains colonic epithelial proliferation during injury', *The Journal of Clinical Investigation*. The American Society for Clinical Investigation, 117(1), pp. 258–269. doi: 10.1172/JCI29159.

Buchanan, F. G. and DuBois, R. N. (2006) 'Connecting COX-2 and Wnt in cancer', *Cancer Cell*, 9(1), pp. 6–8. doi: https://doi.org/10.1016/j.ccr.2005.12.029.

Buczacki, S. J. A., Zecchini, H. I., Nicholson, A. M., Russell, R., Vermeulen, L., Kemp, R. and Winton, D. J. (2013) 'Intestinal label-retaining cells are secretory precursors expressing lgr5', *Nature*, 495(7439), pp. 65–69. doi: 10.1038/nature11965.

Bülow, S. (1987) 'Incidence of associated diseases in familial polyposis coli', *Seminars in Surgical Oncology*. Wiley-Blackwell, 3(2), pp. 84–87. doi: 10.1002/ssu.2980030207.

Castellone, M. D., Teramoto, H., Williams, B. O., Druey, K. M. and Gutkind, J. S. (2005) 'Prostaglandin E2 Promotes Colon Cancer Cell Growth Through a Gs-Axin-ß-Catenin Signaling Axis', *Science*, 310(5753), p. 1504 LP-1510. Available at: http://science.sciencemag.org/content/310/5753/1504.abstract.

Chassaing, B., Aitken, J. D., Malleshappa, M. and Vijay-Kumar, M. (2014) 'Dextran sulfate sodium (DSS)-induced colitis in mice', *Current Protocols in Immunology*, (SUPPL.104), pp. 1–14. doi: 10.1002/0471142735.im1525s104.

Chell, S. D., Witherden, I. R., Dobson, R. R., Moorghen, M., Herman, A. A., Qualtrough, D., Williams, A. C. and Paraskeva, C. (2006) 'Increased EP4 Receptor Expression in Colorectal Cancer Progression Promotes Cell Growth and Anchorage Independence', *Cancer Research*, 66(6), p. 3106 LP-3113. Available at: http://cancerres.aacrjournals.org/content/66/6/3106.abstract.

Cho, J. H. and Brant, S. R. (2011) 'Recent Insights Into the Genetics of Inflammatory Bowel Disease', *Gastroenterology*, 140(6), pp. 1704–1712. doi: 10.1053/j.gastro.2011.02.046.

Consortium, T. E. P., Dunham, I., Kundaje, A., Aldred, S. F., Collins, P. J., Davis, C. A., Doyle, F., Epstein, C. B., Frietze, S., Harrow, J., Kaul, R., Khatun, J., Lajoie, B. R., Landt, S. G., Lee, B.-K., Pauli, F., Rosenbloom, K. R., Sabo, P., Safi, A., Sanyal, A., Shoresh, N., Simon, J. M., Song, L., Trinklein, N. D., Altshuler, R. C., Birney, E., Brown, J. B., Cheng, C., Djebali, S., Dong, X., Dunham, I., Ernst, J., Furey, T. S., Gerstein, M., Giardine, B., Greven, M., Hardison, R. C., Harris, R. S., Herrero, J., Hoffman, M. M., Iyer, S., Kellis, M., Khatun, J., Kheradpour, P., Kundaje, A., Lassmann, T., Li, Q., Lin, X., Marinov, G. K., Merkel, A., Mortazavi, A., Parker, S. C. J., Reddy, T. E., Rozowsky, J., Schlesinger, F., Thurman, R. E., Wang, J., Ward, L. D., Whitfield, T. W., Wilder, S. P., Wu, W., Xi, H. S., Yip, K. Y., Zhuang, J., Bernstein, B. E., Birney, E., Dunham, I., Green, E. D., Gunter, C., Snyder, M., Pazin, M. J., Lowdon, R. F., Dillon, L. A. L., Adams, L. B., Kelly, C. J., Zhang, J., Wexler, J. R., Green, E. D., Good, P. J., Feingold, E. A., Bernstein, B. E., Birney, E., Crawford, G. E., Dekker, J., Elnitski, L., Farnham, P. J., Gerstein, M., Giddings, M. C., Gingeras, T. R., Green, E. D., Guigó, R., Hardison, R. C., Hubbard, T. J., Kellis, M., Kent, W. J., Lieb, J. D., Margulies, E. H., Myers, R. M., Snyder, M., Stamatoyannopoulos, J. A., Tenenbaum, S. A., Weng, Z., White, K. P., Wold, B., Khatun, J., Yu, Y., Wrobel, J., Risk, B. A., Gunawardena, H. P., Kuiper, H. C., Maier, C. W., Xie, L., Chen, X., Giddings, M. C., Bernstein, B. E., Epstein, C. B., Shoresh, N., Ernst, J., Kheradpour, P., Mikkelsen, T. S., Gillespie, S., Goren, A., Ram, O., Zhang, X., Wang, L., Issner, R., Coyne, M. J., Durham, T., Ku, M., Truong, T., Ward, L. D., Altshuler, R. C., Eaton, M. L., Kellis, M., Djebali, S., Davis, C. A., Merkel, A., Dobin, A., Lassmann, T., Mortazavi, A., Tanzer, A., Lagarde, J., Lin, W., Schlesinger, F., Xue, C., Marinov, G. K., Khatun, J., Williams, B. A., Zaleski, C., Rozowsky, J., Röder, M., Kokocinski, F., Abdelhamid, R. F., Alioto, T., Antoshechkin, I., Baer, M. T., Batut, P., Bell, I., Bell, K., Chakrabortty, S., Chen, X., Chrast, J., Curado, J., Derrien, T., Drenkow, J., Dumais, E., Dumais, J., Duttagupta, R., Fastuca, M., Fejes-Toth, K., Ferreira, P., Foissac, S., Fullwood, M. J., Gao, H., Gonzalez, D., Gordon, A., Gunawardena, H. P., Howald, C., Jha, S., Johnson, R., Kapranov, P., King, B., Kingswood, C., Li, G., Luo, O. J., Park, E., Preall, J. B., Presaud, K., Ribeca, P., Risk, B. A., Robyr, D., Ruan, X., Sammeth, M., Sandhu, K. S., Schaeffer, L., See, L.-H., Shahab, A., Skancke, J., Suzuki, A. M., Takahashi, H., Tilgner, H., Trout, D., Walters, N., Wang, H., Wrobel, J., Yu, Y., Hayashizaki, Y., Harrow, J., Gerstein, M., Hubbard, T. J., Reymond, A., Antonarakis, S. E., Hannon, G. J., Giddings, M. C., Ruan, Y., Wold, B., Carninci, P., Guigó, R., Gingeras, T. R., Rosenbloom, K. R., Sloan, C. A., Learned, K., Malladi, V. S., Wong, M. C., Barber, G. P., Cline, M. S., Dreszer, T. R., Heitner, S. G., Karolchik, D., Kent, W. J., Kirkup, V. M., Meyer, L. R., Long, J. C., Maddren, M., Raney, B. J., Furey, T. S., Song, L., Grasfeder, L. L., Giresi, P. G., Lee, B.-K., Battenhouse, A., Sheffield, N. C., Simon, J. M., Showers, K. A., Safi, A., London, D., Bhinge, A. A., Shestak, C., Schaner, M. R., Ki Kim, S., Zhang, Z. Z., Mieczkowski, P. A., Mieczkowska, J. O., Liu, Z., McDaniell, R. M., Ni, Y., Rashid, N. U., Kim, M. J., Adar, S., Zhang, Z., Wang, T., Winter, D., Keefe, D., Birney, E., Iyer, V. R., Lieb, J. D., Crawford, G. E., Li, G., Sandhu, K. S., Zheng, M., Wang, P., Luo, O. J., Shahab, A., Fullwood, M. J., Ruan, X., Ruan, Y., Myers, R. M., Pauli, F., Williams, B. A., Gertz, J., Marinov, G. K., Reddy, T. E., Vielmetter, J., Partridge, E., Trout, D., Varley, K. E., Gasper, C., Bansal, A., Pepke, S., Jain, P., Amrhein, H., Bowling, K. M., Anaya, M., Cross, M. K., King, B., Muratet, M. A., Antoshechkin, I., Newberry, K. M., McCue, K., Nesmith, A. S., Fisher-Aylor, K. I., Pusey, B., DeSalvo, G., Parker, S. L., Balasubramanian, S., Davis, N. S., Meadows, S. K., Eggleston, T., Gunter, C., Newberry, J. S., Levy, S. E., Absher, D. M., Mortazavi, A., Wong, W. H., Wold, B., Blow, M. J., Visel, A., Pennachio, L. A., Elnitski, L., Margulies, E. H., Parker, S. C. J., Petrykowska, H. M., Abyzov, A., Aken, B., Barrell, D., Barson, G., Berry, A., Bignell, A., Boychenko, V., Bussotti, G., Chrast, J., Davidson, C., Derrien, T., Despacio-Reyes, G., Diekhans, M., Ezkurdia, I., Frankish, A., Gilbert, J., Gonzalez, J. M., Griffiths, E., Harte, R., Hendrix, D. A., Howald, C., Hunt, T., Jungreis, I., Kay, M., Khurana, E., Kokocinski, F., Leng, J., Lin, M. F., Loveland, J., Lu, Z., Manthravadi, D., Mariotti, M., Mudge, J., Mukherjee, G., Notredame, C., Pei, B., Rodriguez, J. M., Saunders, G., Sboner, A., Searle, S., Sisu, C., Snow, C., Steward, C., Tanzer, A., Tapanari, E., Tress,

M. L., van Baren, M. J., Walters, N., Washietl, S., Wilming, L., Zadissa, A., Zhang, Z., Brent, M., Haussler, D., Kellis, M., Valencia, A., Gerstein, M., Reymond, A., Guigó, R., Harrow, J., Hubbard, T. J., Landt, S. G., Frietze, S., Abyzov, A., Addleman, N., Alexander, R. P., Auerbach, R. K., Balasubramanian, S., Bettinger, K., Bhardwaj, N., Boyle, A. P., Cao, A. R., Cayting, P., Charos, A., Cheng, Y., Cheng, C., Eastman, C., Euskirchen, G., Fleming, J. D., Grubert, F., Habegger, L., Hariharan, M., Harmanci, A., Iyengar, S., Jin, V. X., Karczewski, K. J., Kasowski, M., Lacroute, P., Lam, H., Lamarre-Vincent, N., Leng, J., Lian, J., Lindahl-Allen, M., Min, R., Miotto, B., Monahan, H., Moqtaderi, Z., Mu, X. J., O'Geen, H., Ouyang, Z., Patacsil, D., Pei, B., Raha, D., Ramirez, L., Reed, B., Rozowsky, J., Sboner, A., Shi, M., Sisu, C., Slifer, T., Witt, H., Wu, L., Xu, X., Yan, K.-K., Yang, X., Yip, K. Y., Zhang, Z., Struhl, K., Weissman, S. M., Gerstein, M., Farnham, P. J., Snyder, M., Tenenbaum, S. A., Penalva, L. O., Doyle, F., Karmakar, S., Landt, S. G., Bhanvadia, R. R., Choudhury, A., Domanus, M., Ma, L., Moran, J., Patacsil, D., Slifer, T., Victorsen, A., Yang, X., Snyder, M., White, K. P., Auer, T., Centanin, L., Eichenlaub, M., Gruhl, F., Heermann, S., Hoeckendorf, B., Inoue, D., Kellner, T., Kirchmaier, S., Mueller, C., Reinhardt, R., Schertel, L., Schneider, S., Sinn, R., Wittbrodt, B., Wittbrodt, J., Weng, Z., Whitfield, T. W., Wang, J., Collins, P. J., Aldred, S. F., Trinklein, N. D., Partridge, E. C., Myers, R. M., Dekker, J., Jain, G., Lajoie, B. R., Sanyal, A., Balasundaram, G., Bates, D. L., Byron, R., Canfield, T. K., Diegel, M. J., Dunn, D., Ebersol, A. K., Frum, T., Garg, K., Gist, E., Hansen, R. S., Boatman, L., Haugen, E., Humbert, R., Jain, G., Johnson, A. K., Johnson, E. M., Kutyavin, T. V, Lajoie, B. R., Lee, K., Lotakis, D., Maurano, M. T., Neph, S. J., Neri, F. V, Nguyen, E. D., Qu, H., Reynolds, A. P., Roach, V., Rynes, E., Sabo, P., Sanchez, M. E., Sandstrom, R. S., Sanyal, A., Shafer, A. O., Stergachis, A. B., Thomas, S., Thurman, R. E., Vernot, B., Vierstra, J., Vong, S., Wang, H., Weaver, M. A., Yan, Y., Zhang, M., Akey, J. M., Bender, M., Dorschner, M. O., Groudine, M., MacCoss, M. J., Navas, P., Stamatoyannopoulos, G., Kaul, R., Dekker, J., Stamatoyannopoulos, J. A., Dunham, I., Beal, K., Brazma, A., Flicek, P., Herrero, J., Johnson, N., Keefe, D., Lukk, M., Luscombe, N. M., Sobral, D., Vaquerizas, J. M., Wilder, S. P., Batzoglou, S., Sidow, A., Hussami, N., Kyriazopoulou-Panagiotopoulou, S., Libbrecht, M. W., Schaub, M. A., Kundaje, A., Hardison, R. C., Miller, W., Giardine, B., Harris, R. S., Wu, W., Bickel, P. J., Banfai, B., Boley, N. P., Brown, J. B., Huang, H., Li, Q., Li, J. J., Noble, W. S., Bilmes, J. A., Buske, O. J., Hoffman, M. M., Sahu, A. D., Kharchenko, P. V, Park, P. J., Baker, D., Taylor, J., Weng, Z., Iyer, S., Dong, X., Greven, M., Lin, X., Wang, J., Xi, H. S., Zhuang, J., Gerstein, M., Alexander, R. P., Balasubramanian, S., Cheng, C., Harmanci, A., Lochovsky, L., Min, R., Mu, X. J., Rozowsky, J., Yan, K.-K., Yip, K. Y. and Birney, E. (2012) 'An integrated encyclopedia of DNA elements in the human genome', *Nature*. The Author(s), 489, p. 57. Available at: http://dx.doi.org/10.1038/nature11247.

'CRISPR' (2018). Available at: crispr.mit.edu.

Dalerba, P., Dylla, S. J., Park, I.-K., Liu, R., Wang, X., Cho, R. W., Hoey, T., Gurney, A., Huang, E. H., Simeone, D. M., Shelton, A. A., Parmiani, G., Castelli, C. and Clarke, M. F. (2007) 'Phenotypic characterization of human colorectal cancer stem cells', *Proceedings of the National Academy of Sciences*, 104(24), p. 10158 LP-10163. Available at: http://www.pnas.org/content/104/24/10158.abstract.

Degirmenci, B., Valenta, T., Dimitrieva, S., Hausmann, G. and Basler, K. (2018) 'GLI1-expressing mesenchymal cells form the essential Wnt-secreting niche for colon stem cells', *Nature*. Springer US, 558(7710), pp. 449–453. doi: 10.1038/s41586-018-0190-3.

Desaki, J. and Shimizu, M. (2000) 'A re-examination of the cellular reticulum of fibroblast-like cells in the rat small intestine by scanning electron microscopy', *Journal of Electron Microscopy*, 49(1), pp. 203–208. Available at: http://dx.doi.org/10.1093/oxfordjournals.jmicro.a023787.

Desk, R., Williams, L. and Health, K. (2001) 'Temporally Regulated and Tissue-Specific Gene Manipulations in the Adult and Embryonic Heart Using a Tamoxifen-Inducible Cre Protein Dawinder S. Sohal, Mai Nghiem, Michael A. Crackower, Sandra A. Witt, Thomas R. Kimball, Kevin M. Tymitz, Josef M. Penninge', *Circulation Research*. doi: 10.1161/hh1301.092687.

Drost, J. and Clevers, H. (2018) 'Organoids in cancer research', *Nature Reviews Cancer*, 18(7), pp. 407–418. doi: 10.1038/s41568-018-0007-6.

Van der Flier, L. G., Sabates–Bellver, J., Oving, I., Haegebarth, A., De Palo, M., Anti, M., Van Gijn, M. E., Suijkerbuijk, S., Van de Wetering, M., Marra, G. and Clevers, H. (2007) 'The Intestinal Wnt/TCF Signature', *Gastroenterology*. Elsevier, 132(2), pp. 628–632. doi: 10.1053/j.gastro.2006.08.039.

Fujino, H., West, K. A. and Regan, J. W. (2002) 'Phosphorylation of Glycogen Synthase Kinase-3 and Stimulation of T-cell Factor Signaling following Activation of EP2 and EP4 Prostanoid Receptors by Prostaglandin E2 ', *Journal of Biological Chemistry* , 277(4), pp. 2614–2619. doi: 10.1074/jbc.M109440200 .

Ganesh, K., Das, A., Dickerson, R., Khanna, S., Parinandi, N. L., Gordillo, G. M., Sen, C. K. and Roy, S. (2012) 'Prostaglandin E_2 induces oncostatin M expression in human chronic wound macrophages through Axl receptor tyrosine kinase pathway', *Journal of immunology (Baltimore, Md. : 1950)*. 2012/07/27, 189(5), pp. 2563–2573. doi: 10.4049/jimmunol.1102762.

Germann, M., Xu, H., Malaterre, J., Sampurno, S., Huyghe, M., Cheasley, D., Fre, S. and Ramsay, R. G. (2014) 'Tripartite interactions between Wnt signaling, Notch and Myb for stem/progenitor cell functions during intestinal tumorigenesis', *Stem Cell Research*. The Authors, 13(Part A), pp. 355–366. doi: 10.1016/j.scr.2014.08.002.

Goessling, W., North, T. E., Loewer, S., Lord, A. M., Lee, S., Stoick-Cooper, C. L., Weidinger, G., Puder, M., Daley, G. Q., Moon, R. T. and Zon, L. I. (2009) 'Genetic interaction of PGE2 and Wnt signaling regulates developmental specification of

stem cells and regeneration', *Cell*, 136(6), pp. 1136–1147. doi: 10.1016/j.cell.2009.01.015.

Grégoire, C., Lechanteur, C., Briquet, A., Baudoux, Baron, F., Louis, E. and Beguin, Y. (2017) 'Review article: mesenchymal stromal cell therapy for inflammatory bowel diseases', *Alimentary Pharmacology and Therapeutics*, 45(2), pp. 205–221. doi: 10.1111/apt.13864.

Greicius, G., Kabiri, Z., Sigmundsson, K., Liang, C., Bunte, R., Singh, M. K. and Virshup, D. M. (2018) '*PDGFRα* $^{+}$ pericryptal stromal cells are the critical source of Wnts and RSPO3 for murine intestinal stem cells in vivo', *Proceedings of the National Academy of Sciences*, p. 201713510. doi: 10.1073/pnas.1713510115.

Grivennikov, S. I., Greten, F. R. and Karin, M. (2010) 'Immunity, inflammation, and cancer', *Cell*, 140(6), pp. 883–899. doi: 10.1016/j.cell.2010.01.025.

Gupta, R. A. and DuBois, R. N. (2001) 'Colorectal cancer prevention and treatment by inhibition of cyclooxygenase-2', *Nature Reviews Cancer*. Nature Publishing Group, 1, p. 11. Available at: http://dx.doi.org/10.1038/35094017.

Heffner, C. (2011) 'Intraperitoneal injection of tamoxifen for inducible Cre-driver lines.' Available at: https://www.jax.org/research-and-faculty/resources/cre-repository/tamoxifen.

Holla, V. R., Mann, J. R., Shi, Q. and DuBois, R. N. (2006) 'Prostaglandin E2 Regulates the Nuclear Receptor NR4A2 in Colorectal Cancer', *Journal of Biological Chemistry* , 281(5), pp. 2676–2682. doi: 10.1074/jbc.M507752200.

Huang, H., Fang, M., Jostins, L., Umićević Mirkov, M., Boucher, G., Anderson, C. A., Andersen, V., Cleynen, I., Cortes, A., Crins, F., D'Amato, M., Deffontaine, V., Dmitrieva, J., Docampo, E., Elansary, M., Farh, K. K. H., Franke, A., Gori, A. S., Goyette, P., Halfvarson, J., Haritunians, T., Knight, J., Lawrance, I. C., Lees, C. W., Louis, E., Mariman, R., Meuwissen, T., Mni, M., Momozawa, Y., Parkes, M., Spain, S. L., Théâtre, E., Trynka, G., Satsangi, J., Van Sommeren, S., Vermeire, S., Xavier, R. J., Weersma, R. K., Duerr, R. H., Mathew, C. G., Rioux, J. D., McGovern, D. P. B., Cho, J. H., Georges, M., Daly, M. J. and Barrett, J. C. (2017) 'Fine-mapping inflammatory bowel disease loci to single-variant resolution', *Nature*. Nature Publishing Group, 547(7662), pp. 173–178. doi: 10.1038/nature22969.

Hull, M. A., Ko, S. C. W. and Hawcroft, G. (2004) 'Prostaglandin EP receptors: Targets for treatment and prevention of colorectal cancer?', *Molecular Cancer Therapeutics*, 3(8), p. 1031 LP-1039. Available at: http://mct.aacrjournals.org/content/3/8/1031.abstract.

Imajo, M., Ebisuya, M. and Nishida, E. (2014) 'Dual role of YAP and TAZ in renewal of the intestinal epithelium', *Nature Cell Biology*. Nature Publishing Group, 17, p. 7. Available at: https://doi.org/10.1038/ncb3084.

Invitrogen (2016) 'Lipofectamine 3000 Reagent User guide'. Available at: https://tools.thermofisher.com/content/sfs/manuals/lipofectamine3000_protocol.pdf.

Ishikawa, T.-O. and Herschman, H. R. (2010) 'Tumor formation in a mouse model of colitis-associated colon cancer does not require COX-1 or COX-2 expression', *Carcinogenesis*. 2010/01/08. Oxford University Press, 31(4), pp. 729–736. doi: 10.1093/carcin/bgq002.

Johnson, M., Zaretskaya, I., Raytselis, Y., Merezhuk, Y., McGinnis, S. and Madden, T. L. (2008) 'NCBI BLAST: a better web interface', *Nucleic acids research*. 2008/04/24. Oxford University Press, 36(Web Server issue), pp. W5–W9. doi: 10.1093/nar/gkn201.

Jostins, L., Ripke, S., Weersma, R. K., Duerr, R. H., McGovern, D. P., Hui, K. Y., Lee, J. C., Philip Schumm, L., Sharma, Y., Anderson, C. A., Essers, J., Mitrovic, M., Ning, K., Cleynen, I., Theatre, E., Spain, S. L., Raychaudhuri, S., Goyette, P., Wei, Z., Abraham, C., Achkar, J. P., Ahmad, T., Amininejad, L., Ananthakrishnan, A. N., Andersen, V., Andrews, J. M., Baidoo, L., Balschun, T., Bampton, P. A., Bitton, A., Boucher, G., Brand, S., Büning, C., Cohain, A., Cichon, S., D'Amato, M., De Jong, D., Devaney, K. L., Dubinsky, M., Edwards, C., Ellinghaus, D., Ferguson, L. R., Franchimont, D., Fransen, K., Gearry, R., Georges, M., Gieger, C., Glas, J., Haritunians, T., Hart, A., Hawkey, C., Hedl, M., Hu, X., Karlsen, T. H., Kupcinskas, L., Kugathasan, S., Latiano, A., Laukens, D., Lawrance, I. C., Lees, C. W., Louis, E., Mahy, G., Mansfield, J., Morgan, A. R., Mowat, C., Newman, W., Palmieri, O., Ponsioen, C. Y., Potocnik, U., Prescott, N. J., Regueiro, M., Rotter, J. I., Russell, R. K., Sanderson, J. D., Sans, M., Satsangi, J., Schreiber, S., Simms, L. A., Sventoraityte, J., Targan, S. R., Taylor, K. D., Tremelling, M., Verspaget, H. W., De Vos, M., Wijmenga, C., Wilson, D. C., Winkelmann, J., Xavier, R. J., Zeissig, S., Zhang, B., Zhang, C. K., Zhao, H., Silverberg, M. S., Annese, V., Hakonarson, H., Brant, S. R., Radford-Smith, G., Mathew, C. G., Rioux, J. D., Schadt, E. E., Daly, M. J., Franke, A., Parkes, M., Vermeire, S., Barrett, J. C., Cho, J. H., Barclay, M., Peyrin-Biroulet, L., Chamaillard, M., Colombel, J. F., Cottone, M., Croft, A., D'Incà, R., Halfvarson, J., Hanigan, K., Henderson, P., Hugot, J. P., Karban, A., Kennedy, N. A., Azam Khan, M., Lémann, M., Levine, A., Massey, D., Milla, M., Montgomery, G. W., Evelyn Ng, S. M., Oikonomou, I., Peeters, H., Proctor, D. D., Rahier, J. F., Roberts, R., Rutgeerts, P., Seibold, F., Stronati, L., Taylor, K. M., Törkvist, L., Ublick, K., Van Limbergen, J., Van Gossum, A., Vatn, M. H., Zhang, H., Zhang, W., Andrews, J. M., Bampton, P. A., Barclay, M., Florin, T. H., Krishnaprasad, K., Krishnaprasad, K., Lawrance, I. C., Mahy, G., Montgomery, G. W., Radford-Smith, G., Roberts, R. L., Simms, L. A., Amininijad, L., Cleynen, I., Dewit, O., Franchimont, D., Georges, M., Laukens, D., Peeters, H., Rahier, J. F., Rutgeerts, P., Theatre, E., Van Gossum, A., Vermeire, S., Aumais, G., Baidoo, L., Barrie, A. M., Beck, K., Bernard, E. J., Binion, D. G., Bitton, A., Brant, S. R., Cho, J. H., Cohen, A., Croitoru, K., Daly, M. J., Datta, L. W., Deslandres, C., Duerr, R. H.,

Dutridge, D., Ferguson, J., Fultz, J., Goyette, P., Greenberg, G. R., Haritunians, T., Jobin, G., Katz, S., Lahaie, R. G., McGovern, D. P., Nelson, L., Ng, S. M., Ning, K., Oikonomou, I., Paré, P., Proctor, D. D., Regueiro, M. D., Rioux, J. D., Ruggiero, E., Philip Schumm, L., Schwartz, M., Scott, R., Sharma, Y., Silverberg, M. S., Spears, D., Hillary Steinhart, A., Stempak, J. M., Swoger, J. M., Tsagarelis, C., Zhang, W., Zhang, C., Zhao, H., Aerts, J., Ahmad, T., Arbury, H., Attwood, A., Auton, A., Ball, S. G., Balmforth, A. J., Barnes, C., Barrett, J. C., Barroso, I., Barton, A., Bennett, A. J., Bhaskar, S., Blaszczyk, K., Bowes, J., Brand, O. J., Braund, P. S., Bredin, F., Breen, G., Brown, M. J., Bruce, I. N., Bull, J., Burren, O. S., Burton, J., Byrnes, J., Caesar, S., Cardin, N., Clee, C. M., Coffey, A. J., Connell, J. M. C., Conrad, D. F., Cooper, J. D., Dominiczak, A. F., Downes, K., Drummond, H. E., Dudakia, D., Dunham, A., Ebbs, B., Eccles, D., Edkins, S., Edwards, C., Elliot, A., Emery, P., Evans, D. M., Evans, G., Eyre, S., Farmer, A., Nicol Ferrier, I., Flynn, E., Forbes, A., Forty, L., Franklyn, J. A., Frayling, T. M., Freathy, R. M., Giannoulatou, E., Gibbs, P., Gilbert, P., Gordon-Smith, K., Gray, E., Green, E., Groves, C. J., Grozeva, D., Gwilliam, R., Hall, A., Hammond, N., Hardy, M., Harrison, P., Hassanali, N., Hebaishi, H., Hines, S., Hinks, A., Hitman, G. A., Hocking, L., Holmes, C., Howard, E., Howard, P., Howson, J. M. M., Hughes, D., Hunt, S., Isaacs, J. D., Jain, M., Jewell, D. P., Johnson, T., Jolley, J. D., Jones, I. R., Jones, L. A., Kirov, G., Langford, C. F., Lango-Allen, H., Mark Lathrop, G., Lee, J., Lee, K. L., Lees, C., Lewis, K., Lindgren, C. M., Maisuria-Armer, M., Maller, J., Mansfield, J., Marchini, J. L., Martin, P., Massey, D. C. O., McArdle, W. L., McGuffin, P., McLay, K. E., McVean, G., Mentzer, A., Mimmack, M. L., Morgan, A. E., Morris, A. P., Mowat, C., Munroe, P. B., Myers, S., Newman, W., Nimmo, E. R., O'Donovan, M. C., Onipinla, A., Ovington, N. R., Owen, M. J., Palin, K., Palotie, A., Parnell, K., Pearson, R., Pernet, D., Perry, J. R. B., Phillips, A., Plagnol, V., Prescott, N. J., Prokopenko, I., Quail, M. A., Rafelt, S., Rayner, N. W., Reid, D. M., Renwick, A., Ring, S. M., Robertson, N., Robson, S., Russell, E., St Clair, D., Sambrook, J. G., Sanderson, J. D., Sawcer, S. J., Schuilenburg, H., Scott, C. E., Scott, R., Seal, S., Shaw-Hawkins, S., Shields, B. M., Simmonds, M. J., Smyth, D. J., Somaskantharajah, E., Spanova, K., Steer, S., Stephens, J., Stevens, H. E., Stirrups, K., Stone, M. A., Strachan, D. P., Su, Z., Symmons, D. P. M., Thompson, J. R., Thomson, W., Tobin, M. D., Travers, M. E., Turnbull, C., Vukcevic, D., Wain, L. V., Walker, M., Walker, N. M., Wallace, C., Warren-Perry, M., Watkins, N. A., Webster, J., Weedon, M. N., Wilson, A. G., Woodburn, M., Paul Wordsworth, B., Yau, C., Young, A. H., Zeggini, E., Brown, M. A., Burton, P. R., Caulfield, M. J., Compston, A., Farrall, M., Gough, S. C. L., Hall, A. S., Hattersley, A. T., Hill, A. V. S., Mathew, C. G., Pembrey, M., Satsangi, J., Stratton, M. R., Worthington, J., Hurles, M. E., Duncanson, A., Ouwehand, W. H., Parkes, M., Rahman, N., Todd, J. A., Samani, N. J., Kwiatkowski, D. P., McCarthy, M. I., Craddock, N., Deloukas, P., Donnelly, P., Blackwell, J. M., Bramon, E., Casas, J. P., Corvin, A., Jankowski, J., Markus, H. S., Palmer, C. N. A., Plomin, R., Rautanen, A., Trembath, R. C., Viswanathan, A. C., Wood, N. W., Spencer, C. C. A., Band, G., Bellenguez, C., Freeman, C., Hellenthal, G., Giannoulatou, E., Pirinen, M., Pearson, R., Strange, A., Blackburn, H., Bumpstead, S. J., Dronov, S., Gillman, M., Jayakumar, A., McCann, O. T., Liddle, J., Potter, S. C., Ravindrarajah, R., Ricketts, M., Waller, M., Weston, P., Widaa, S. and Whittaker, P. (2012) 'Host-microbe interactions have shaped the genetic architecture of inflammatory bowel disease', *Nature*. Nature Publishing Group, 491(7422), pp. 119–124. doi: 10.1038/nature11582.

Kabashima, K., Saji, T., Murata, T., Nagamachi, M., Matsuoka, T., Segi, E., Tsuboi, K., Sugimoto, Y., Kobayashi, T., Miyachi, Y., Ichikawa, A. and Narumiya, S. (2002) 'The prostaglandin receptor EP4 suppresses colitis, mucosal damage and CD4 cell activation in the gut', *The Journal of Clinical Investigation*. American Society for Clinical Investigation, 109(7), pp. 883–893. doi: 10.1172/JCI14459.

Kalluri, R. (2016) 'The biology and function of fibroblasts in cancer', *Nature Reviews Cancer*. Nature Publishing Group, a division of Macmillan Publishers Limited. All Rights Reserved., 16, p. 582. Available at: https://doi.org/10.1038/nrc.2016.73.

Kaser, A., Zeissig, S. and Blumberg, R. S. (2010) 'Inflammatory Bowel Disease', *Annual Review of Immunology*. Annual Reviews, 28(1), pp. 573–621. doi: 10.1146/annurev-immunol-030409-101225.

Kent, W. J., Sugnet, C. W., Furey, T. S., Roskin, K. M., Pringle, T. H., Zahler, A. M. and Haussler, and D. (2002) 'The Human Genome Browser at UCSC', *Genome Research* , 12(6), pp. 996–1006. doi: 10.1101/gr.229102.

Kettunen, H. L., Kettunen, A. S. L. and Rautonen, N. E. (2003) 'Intestinal Immune Responses in Wild-Type and ApcMin/+ Mouse, a Model for Colon Cancer', *Cancer Research*, 63(16), p. 5136 LP-5142. Available at: http://cancerres.aacrjournals.org/content/63/16/5136.abstract.

Kinchen, J., Chen, H. H., Parikh, K. and Antanaviciute, A. (2018) 'Structural Remodeling of the Colonic Mesenchyme in Inflammatory Bowel Disease', *Cell*. Elsevier Inc., 175(2), pp. 1–64. doi: 10.1016/j.cell.2018.08.067.

Krause, W. and DuBois, R. N. (2000) 'Eicosanoids and the large intestine☆', *Prostaglandins & Other Lipid Mediators*, 61(3), pp. 145–161. doi: https://doi.org/10.1016/S0090-6980(00)00069-1.

Kretzschmar, K. and Clevers, H. (2016) 'Organoids: Modeling Development and the Stem Cell Niche in a Dish', *Developmental Cell*, 38(6), pp. 590–600. doi: https://doi.org/10.1016/j.devcel.2016.08.014.

Landi, D., Gemignani, F., Barale, R. and Landi, S. (2007) 'A Catalog of Polymorphisms Falling in MicroRNA-Binding Regions of Cancer Genes', *DNA and Cell Biology*. Mary Ann Liebert, Inc., publishers, 27(1), pp. 35–43. doi: 10.1089/dna.2007.0650.

de Lange, K. M., Moutsianas, L., Lee, J. C., Lamb, C. A., Luo, Y., Kennedy, N. A., Jostins, L., Rice, D. L., Gutierrez-Achury, J., Ji, S.-G., Heap, G., Nimmo, E. R., Edwards, C., Henderson, P., Mowat, C., Sanderson, J., Satsangi, J., Simmons, A., Wilson, D. C., Tremelling, M., Hart, A., Mathew, C. G., Newman, W. G., Parkes, M., Lees, C. W., Uhlig, H., Hawkey, C., Prescott, N. J., Ahmad, T., Mansfield, J. C., Anderson, C. A. and Barrett, J. C. (2017) 'Genome-wide association study implicates immune

activation of multiple integrin genes in inflammatory bowel disease', *Nature genetics*, 49(2), pp. 256–261. doi: 10.1038/ng.3760.

Le, Y. and Sauer, B. (2001) 'Conditional gene knockout using cre recombinase', *Molecular Biotechnology*, 17(3), pp. 269–275. doi: 10.1385/MB:17:3:269.

Li, N., Nakauka-Ddamba, A., Tobias, J., Jensen, S. T. and Lengner, C. J. (2016) 'Mouse Label-Retaining Cells Are Molecularly and Functionally Distinct From Reserve Intestinal Stem Cells', *Gastroenterology*. Elsevier, 151(2), p. 298–310.e7. doi: 10.1053/j.gastro.2016.04.049.

Liu-Chittenden, Y., Huang, B., Shim, J. S., Chen, Q., Lee, S.-J., Anders, R. A., Liu, J. O. and Pan, D. (2012) 'Genetic and pharmacological disruption of the TEAD–YAP complex suppresses the oncogenic activity of YAP', *Genes & Development* , 26(12), pp. 1300–1305. doi: 10.1101/gad.192856.112 .

Liu, T.-C. and Stappenbeck, T. S. (2016) 'Genetics and Pathogenesis of Inflammatory Bowel Disease', *Annual Review of Pathology: Mechanisms of Disease*, 11(1), pp. 127–148. doi: 10.1146/annurev-pathol-012615-044152.

Lugli, N., Dionellis, V. S., Ordóñez-Morán, P., Kamileri, I., Sotiriou, S. K., Huelsken, J. and Halazonetis, T. D. (2017) 'Enhanced Rate of Acquisition of Point Mutations in Mouse Intestinal Adenomas Compared to Normal Tissue', *Cell Reports*, 19(11), pp. 2185–2192. doi: 10.1016/j.celrep.2017.05.051.

Madisen, L., Zwingman, T. A., Sunkin, S. M., Oh, S. W., Zariwala, H. A., Gu, H., Ng, L. L., Palmiter, R. D., Hawrylycz, M. J., Jones, A. R., Lein, E. S. and Zeng, H. (2010) 'A robust and high-throughput Cre reporting and characterization system for the whole mouse brain', *Nature neuroscience.* 2009/12/20, 13(1), pp. 133–140. doi: 10.1038/nn.2467.

Madison, B. B., Braunstein, K., Kuizon, E., Portman, K., Qiao, X. T. and Gumucio, D. L. (2005) 'Epithelial hedgehog signals pattern the intestinal crypt-villus axis', *Development*, 132(2), p. 279 LP-289. Available at: http://dev.biologists.org/content/132/2/279.abstract.

McGovern, D., Kugathasan, S. and Cho, J. H. (2015) 'Genetics of Inflammatory Bowel Diseases', *Gastroenterology*, 149(5), p. 1163–1176.e2. doi: 10.1053/j.gastro.2015.08.001.

Miura, S. and Suzuki, A. (2017) 'Generation of Mouse and Human Organoid-Forming Intestinal Progenitor Cells by Direct Lineage Reprogramming', *Cell Stem Cell*. Elsevier Inc., 21(4), p. 456–471.e5. doi: 10.1016/j.stem.2017.08.020.

Morteau, O., Morham, S. G., Sellon, R., Dieleman, L. A., Langenbach, R., Smithies, O. and Sartor, R. B. (2000) 'Impaired mucosal defense to acute colonic injury in mice lacking cyclooxygenase-1 or cyclooxygenase-2', *The Journal of Clinical Investigation*. The American Society for Clinical Investigation, 105(4), pp. 469–478. doi: 10.1172/JCI6899.

Moser, A. R., Luongo, C., Gould, K. A., McNeley, M. K., Shoemaker, A. R. and Dove, W. F. (1995) 'Apc^{Min}: A mouse model for intestinal and mammary tumorigenesis', *European Journal of Cancer*. Elsevier, 31(7), pp. 1061–1064. doi: 10.1016/0959-8049(95)00181-H.

'Mouse Tail Lysis Buffer II' (2018) *Cold Spring Harbor Protocols* , 2018(2), p. pdb.rec095307. doi: 10.1101/pdb.rec095307 .

Mustata, R. C., Vasile, G., Fernandez-Vallone, V., Strollo, S., Lefort, A., Libert, F., Monteyne, D., Pérez-Morga, D., Vassart, G. and Garcia, M. I. (2013) 'Identification of Lgr5-Independent Spheroid-Generating Progenitors of the Mouse Fetal Intestinal Epithelium', *Cell Reports*, 5(2), pp. 421–432. doi: 10.1016/j.celrep.2013.09.005.

Nakanishi, Y., Seno, H., Fukuoka, A., Ueo, T., Yamaga, Y., Maruno, T., Nakanishi, N., Kanda, K., Komekado, H., Kawada, M., Isomura, A., Kawada, K., Sakai, Y., Yanagita, M., Kageyama, R., Kawaguchi, Y., Taketo, M. M., Yonehara, S. and Chiba, T. (2013) 'Dclk1 distinguishes between tumor and normal stem cells in the intestine', *Nature Genetics*. Nature Publishing Group, 45(1), pp. 98–103. doi: 10.1038/ng.24813.

New England Biolabs (2018) 'Optimizing Restriction Endonuclease Reactions'. Available at: https://international.neb.com/protocols/2012/12/07/optimizing-restriction-endonuclease-reactions.

New England Biolabs (2018) 'PCR Using Q5® High-Fidelity DNA Polymerase (M0491)'. Available at: https://international.neb.com/protocols/2013/12/13/pcr-using-q5-high-fidelity-dna-polymerase-m0491.

Nishihara, H., Hwang, M., Kizaka-Kondoh, S., Eckmann, L. and Insel, P. A. (2004) 'Cyclic AMP Promotes cAMP-responsive Element-binding Protein-dependent Induction of Cellular Inhibitor of Apoptosis Protein-2 and Suppresses Apoptosis of Colon Cancer Cells through ERK1/2 and p38 MAPK', *Journal of Biological Chemistry* , 279(25), pp. 26176–26183. doi: 10.1074/jbc.M313346200.

Noah, T. K. and Shroyer, N. F. (2013) 'Notch in the Intestine: Regulation of Homeostasis and Pathogenesis', *Annual Review of Physiology*. Annual Reviews, 75(1), pp. 263–288. doi: 10.1146/annurev-physiol-030212-183741.

Noh, M.-G., Kim, S. S., Hwang, E. C., Kwon, D. D. and Choi, C. (2017) 'Yes-Associated Protein Expression Is Correlated to the

Differentiation of Prostate Adenocarcinoma', *Journal of pathology and translational medicine*. 2017/06/09. The Korean Society of Pathologists and the Korean Society for Cytopathology, 51(4), pp. 365–373. doi: 10.4132/jptm.2017.05.04.

Park, J., Bae, S. and Kim, J.-S. (2015) 'Cas-Designer: a web-based tool for choice of CRISPR-Cas9 target sites', *Bioinformatics*, 31(24), pp. 4014–4016. Available at: http://dx.doi.org/10.1093/bioinformatics/btv537.

Park, J. Y., Pillinger, M. H. and Abramson, S. B. (2006) 'Prostaglandin E2 synthesis and secretion: The role of PGE2 synthases', *Clinical Immunology*, 119(3), pp. 229–240. doi: https://doi.org/10.1016/j.clim.2006.01.016.

Pastuła, A. (2016) 'Organoids as a model to study the cellular microenvironment and as a potential tool for personalized cancer medicine'.

Pervouchine, D. D., Djebali, S., Breschi, A., Davis, C. A., Barja, P. P., Dobin, A., Tanzer, A., Lagarde, J., Zaleski, C., See, L.-H., Fastuca, M., Drenkow, J., Wang, H., Bussotti, G., Pei, B., Balasubramanian, S., Monlong, J., Harmanci, A., Gerstein, M., Beer, M. A., Notredame, C., Guigó, R. and Gingeras, T. R. (2015) 'Enhanced transcriptome maps from multiple mouse tissues reveal evolutionary constraint in gene expression', *Nature Communications*. The Author(s), 6, p. 5903. Available at: http://dx.doi.org/10.1038/ncomms6903.

Peterson, L. W. and Artis, D. (2014) 'Intestinal epithelial cells: regulators of barrier function and immune homeostasis', *Nature Reviews Immunology*. Nature Publishing Group, a division of Macmillan Publishers Limited. All Rights Reserved., 14, p. 141. Available at: https://doi.org/10.1038/nri3608.

Pfaffl, M. W. (2001) 'A new mathematical model for relative quantification in real-time RT-PCR', *Nucleic acids research*. Oxford University Press, 29(9), pp. e45–e45. Available at: https://www.ncbi.nlm.nih.gov/pubmed/11328886.

Powell, D. W., Pinchuk, I. V., Saada, J. I., Chen, X. and Mifflin, R. C. (2011) 'Mesenchymal Cells of the Intestinal Lamina Propria', *Annual Review of Physiology*, 73(1), pp. 213–237. doi: 10.1146/annurev.physiol.70.113006.100646.

Pozzi, A., Yan, X., Macias-Perez, I., Wei, S., Hata, A. N., Breyer, R. M., Morrow, J. D. and Capdevila, J. H. (2004) 'Colon Carcinoma Cell Growth Is Associated with Prostaglandin E2/EP4 Receptor-evoked ERK Activation', *Journal of Biological Chemistry* , 279(28), pp. 29797–29804. doi: 10.1074/jbc.M313989200.

Ripke, S. and Brett, T. (2018) *Ricopili*. Available at: https://data.broadinstitute.org/mpg/ricopili/.

Roadmap Epigenomics Project (2007) 'Roadmap Epigenomics Project', *Roadmap Epigenomics Project*. Available at: http://www.roadmapepigenomics.org/.

Rothenberg, M. E., Nusse, Y., Kalisky, T., Lee, J. J., Dalerba, P., Scheeren, F., Lobo, N., Kulkarni, S., Sim, S., Qian, D., Beachy, P. A., Pasricha, P. J., Quake, S. R. and Clarke, M. F. (2012) 'Identification of a cKit^{+} Colonic Crypt Base Secretory Cell That Supports Lgr5^{+} Stem Cells in Mice', *Gastroenterology*. Elsevier, 142(5), p. 1195–1205.e6. doi: 10.1053/j.gastro.2012.02.006.

Roulis, Manolis; Kaklamanos, Aimilios; Schernthanner, Marina; Zhao, Jun; Bielecki, Piotr; Kaffe, Eleanna; Knapp, Marlene S.; Koliaraki, Vasiliki; Breyer, Richard M.; Herschman, Harvey R.; Aidinis, Vassilis; Kluger, Yuval; Kollias, George; Flavell, R. A. (no date) 'Paracrine orchestration of intestinal tumorigenesis at the mesenchymal-epithelial interface (preliminary title)', *unpublished*.

Roulis, M., Armaka, M., Manoloukos, M., Apostolaki, M. and Kollias, G. (2011) 'Intestinal epithelial cells as producers but not targets of chronic TNF suffice to cause murine Crohn-like pathology', *Proceedings of the National Academy of Sciences*, 108(13), p. 5396 LP-5401. Available at: http://www.pnas.org/content/108/13/5396.abstract.

Roulis, M. and Flavell, R. A. (2016) 'Fibroblasts and myofibroblasts of the intestinal lamina propria in physiology and disease', *Differentiation*. Elsevier, 92(3), pp. 116–131. doi: 10.1016/j.diff.2016.05.002.

Roulis, M., Nikolaou, C., Kotsaki, E., Kaffe, E., Karagianni, N., Koliaraki, V., Salpea, K., Ragoussis, J., Aidinis, V., Martini, E., Becker, C., Herschman, H. R., Vetrano, S., Danese, S. and Kollias, G. (2014) 'Intestinal myofibroblast-specific Tpl2-Cox-2-PGE₂ pathway links innate sensing to epithelial homeostasis', *Proceedings of the National Academy of Sciences*, 111(43), p. E4658 LP-E4667. Available at: http://www.pnas.org/content/111/43/E4658.abstract.

Sancho, R., Cremona, C. A. and Behrens, A. (2015) 'Stem cell and progenitor fate in the mammalian intestine: Notch and lateral inhibition in homeostasis and disease', *EMBO reports*, 16(5), p. 571 LP-581. Available at: http://embor.embopress.org/content/16/5/571.abstract.

Sanjana, N. E., Shalem, O. and Zhang, F. (2014) 'Improved vectors and genome-wide libraries for CRISPR screening', *Nature methods*, 11(8), pp. 783–784. doi: 10.1038/nmeth.3047.

Sato, T., van Es, J. H., Snippert, H. J., Stange, D. E., Vries, R. G., van den Born, M., Barker, N., Shroyer, N. F., van de Wetering, M. and Clevers, H. (2010) 'Paneth cells constitute the niche for Lgr5 stem cells in intestinal crypts', *Nature*. Nature Publishing Group, a division of Macmillan Publishers Limited. All Rights Reserved., 469, p. 415. Available at: https://doi.org/10.1038/nature09637.

Sato, T., Stange, D. E., Ferrante, M., Vries, R. G. J., Van Es, J. H., Van Den Brink, S., Van Houdt, W. J., Pronk, A., Van Gorp, J., Siersema, P. D. and Clevers, H. (2011) 'Long-term expansion of epithelial organoids from human colon, adenoma, adenocarcinoma, and Barrett's epithelium', *Gastroenterology*. Elsevier Inc., 141(5), pp. 1762–1772. doi: 10.1053/j.gastro.2011.07.050.

Sato, T., Vries, R. G., Snippert, H. J., van de Wetering, M., Barker, N., Stange, D. E., van Es, J. H., Abo, A., Kujala, P., Peters, P. J. and Clevers, H. (2009) 'Single Lgr5 stem cells build crypt–villus structures in vitro without a mesenchymal niche', *Nature*. Macmillan Publishers Limited. All rights reserved, 459, p. 262. Available at: http://dx.doi.org/10.1038/nature07935.

Schepers, A. G., Snippert, H. J., Stange, D. E., van den Born, M., van Es, J. H., van de Wetering, M. and Clevers, H. (2012) 'Lineage Tracing Reveals Lgr5⁺ Stem Cell Activity in Mouse Intestinal Adenomas', *Science*, 337(6095), p. 730 LP-735. Available at: http://science.sciencemag.org/content/337/6095/730.abstract.

Schipke, K. J., Filip To, S. D. and Warnock, J. N. (2011) 'Design of a Cyclic Pressure Bioreactor for the Ex Vivo Study of Aortic Heart Valves', *Journal of Visualized Experiments*, (54), pp. 3–7. doi: 10.3791/3316.

Shao, J., Jung, C., Liu, C. and Sheng, H. (2005) 'Prostaglandin E2 Stimulates the β-Catenin/T Cell Factor-dependent Transcription in Colon Cancer', *Journal of Biological Chemistry* , 280(28), pp. 26565–26572. doi: 10.1074/jbc.M413056200 .

Sloan, C. A., Chan, E. T., Davidson, J. M., Malladi, V. S., Strattan, J. S., Hitz, B. C., Gabdank, I., Narayanan, A. K., Ho, M., Lee, B. T., Rowe, L. D., Dreszer, T. R., Roe, G., Podduturi, N. R., Tanaka, F., Hong, E. L. and Cherry, J. M. (2016) 'ENCODE data at the ENCODE portal', *Nucleic Acids Research*. Oxford University Press, 44(Database issue), pp. D726–D732. doi: 10.1093/nar/gkv1160.

Sonoshita, M., Takaku, K., Sasaki, N., Sugimoto, Y., Ushikubi, F., Narumiya, S., Oshima, M. and Taketo, M. M. (2001) 'Acceleration of intestinal polyposis through prostaglandin receptor EP2 in ApcΔ716 knockout mice', *Nature Medicine*. Nature Publishing Group, 7, p. 1048. Available at: http://dx.doi.org/10.1038/nm0901-1048.

Spence, J. R., Mayhew, C. N., Rankin, S. A., Kuhar, M. F., Vallance, J. E., Tolle, K., Hoskins, E. E., Kalinichenko, V. V., Wells, S. I., Zorn, A. M., Shroyer, N. F. and Wells, J. M. (2011) 'Directed differentiation of human pluripotent stem cells into intestinal tissue in vitro', *Nature*. Nature Publishing Group, 470(7332), pp. 105–110. doi: 10.1038/nature09691.

Strauss, J., Luongo, C., Marchesi, J. R., Allen-Vercoe, E., Dutilh, B. E., Moser, A. R., Kaplan, G. G., Chadee, K., Hall, N., Beck, P. L., Gledhill, S., Dove, W. F., Peters, W. H. M., Rioux, K., Roelofs, R., Panaccione, R., Boleij, A., Devinney, R., Tjalsma, H. and Lynch, T. (1994) 'Loss of Apc+ in intestinal adenomas from Min mice.', *Cancer research*, 54(22), pp. 5947–5952.

Stzepourginski, I., Nigro, G., Jacob, J.-M., Dulauroy, S., Sansonetti, P. J., Eberl, G. and Peduto, L. (2017) 'CD34 $^{+}$ mesenchymal cells are a major component of the intestinal stem cells niche at homeostasis and after injury', *Proceedings of the National Academy of Sciences*, 114(4), pp. E506–E513. doi: 10.1073/pnas.1620059114.

Tennyson, G. S. and Bucy, R. P. (1994) 'Dextran Sulfate Sodium-Induced Colitis Occurs in Severe Combined Immunodeficient Mice', *Gastroenterology*, 107, pp. 1643–1652. doi: 10.1016/0016-5085(94)90803-6.

Toyoda, H., Ina, K., Kitamura, H., Tsuda, T. and Shimada, T. (1997) 'Organization of the Lamina propria mucosae of Rat Intestinal Mucosa, with Special Reference to the Subepithelial Connective Tissue', *Cells Tissues Organs*, 158(3), pp. 172–184. doi: 10.1159/000147928.

Vermeulen, L. and Snippert, H. J. (2014) 'Stem cell dynamics in homeostasis and cancer of the intestine', *Nature Reviews Cancer*. Nature Publishing Group, 14(7), pp. 468–480. doi: 10.1038/nrc3744.

Verstockt, B., Smith, K. G. C. and Lee, J. C. (2018) 'Genome-wide association studies in Crohn's disease: Past, present and future', *Clinical & Translational Immunology*. Hoboken: John Wiley and Sons Inc., 7(1), p. e1001. doi: 10.1002/cti2.1001.

Wang, D. and DuBois, R. N. (2013) 'Inflammatory mediator prostaglandin E(2) in colorectal cancer', *Cancer journal (Sudbury, Mass.)*, 19(6), pp. 502–510. doi: 10.1097/PPO.0000000000000003.

Wang, D., Fu, L., Sun, H., Guo, L. and DuBois, R. N. (2015) 'Prostaglandin E2 Promotes Colorectal Cancer Stem Cell Expansion and Metastasis in Mice', *Gastroenterology*. 2015/08/07, 149(7), p. 1884–1895.e4. doi: 10.1053/j.gastro.2015.07.064.

Wang, D., Wang, H., Shi, Q., Katkuri, S., Walhi, W., Desvergne, B., Das, S. K., Dey, S. K. and DuBois, R. N. (2004) 'Prostaglandin E2 promotes colorectal adenoma growth via transactivation of the nuclear peroxisome proliferator-activated receptor δ', *Cancer Cell*, 6(3), pp. 285–295. doi: https://doi.org/10.1016/j.ccr.2004.08.011.

Watanabe, K., Kawamori, T., Nakatsugi, S., Ohta, T., Ohuchida, S., Yamamoto, H., Maruyama, T., Kondo, K., Ushikubi, F., Narumiya, S. and Sugimura, T. (1999) 'Role of the Prostaglandin E Receptor Subtype EP 1 in Colon Carcinogenesis', *Cancer Research*, 59, pp. 5093–5096. doi: 10.1158/0008-5472.can-05-4348.

Watanabe, K., Kawamori, T., Nakatsugi, S., Ohta, T., Ohuchida, S., Yamamoto, H., Maruyama, T., Kondo, K., Ushikubi, F., Narumiya, S. and Sugimura, T. (2002) 'Involvement of Prostaglandin E Receptor Subtype EP4 in Colon Carcinogenesis',

Cancer Research, 62, pp. 28–32.

Weintraub, A. S., Li, C. H., Zamudio, A. V., Sigova, A. A., Hannett, N. M., Day, D. S., Abraham, B. J., Cohen, M. A., Nabet, B., Buckley, D. L., Guo, Y. E., Hnisz, D., Jaenisch, R., Bradner, J. E., Gray, N. S. and Young, R. A. (2017) 'YY1 Is a Structural Regulator of Enhancer-Promoter Loops', *Cell*. Elsevier Inc., 171(7), p. 1573–1588.e28. doi: 10.1016/j.cell.2017.11.008.

Wirtz, S., Neufert, C., Weigmann, B. and Neurath, M. F. (2007) 'Chemically induced mouse models of intestinal inflammation', *Nature Protocols*, 2(3), pp. 541–546. doi: 10.1038/nprot.2007.41.

Yokoyama, U., Iwatsubo, K., Umemura, M., Fujita, T. and Ishikawa, Y. (2013) 'The Prostanoid EP4 Receptor and Its Signaling Pathway', *Pharmacological Reviews*, 65(3), pp. 1010–1052. doi: 10.1124/pr.112.007195.

Zanconato, F., Cordenonsi, M. and Piccolo, S. (2016) 'Review YAP / TAZ at the Roots of Cancer', *Cancer Cell*. Elsevier, 29(6), pp. 783–803. doi: 10.1016/j.ccell.2016.05.005.

Zhang, F. and Lupski, J. R. (2015) 'Non-coding genetic variants in human disease', *Human molecular genetics*. 2015/07/07. Oxford University Press, 24(R1), pp. R102–R110. doi: 10.1093/hmg/ddv259.

7. Supplementary material

Supplementary Figures

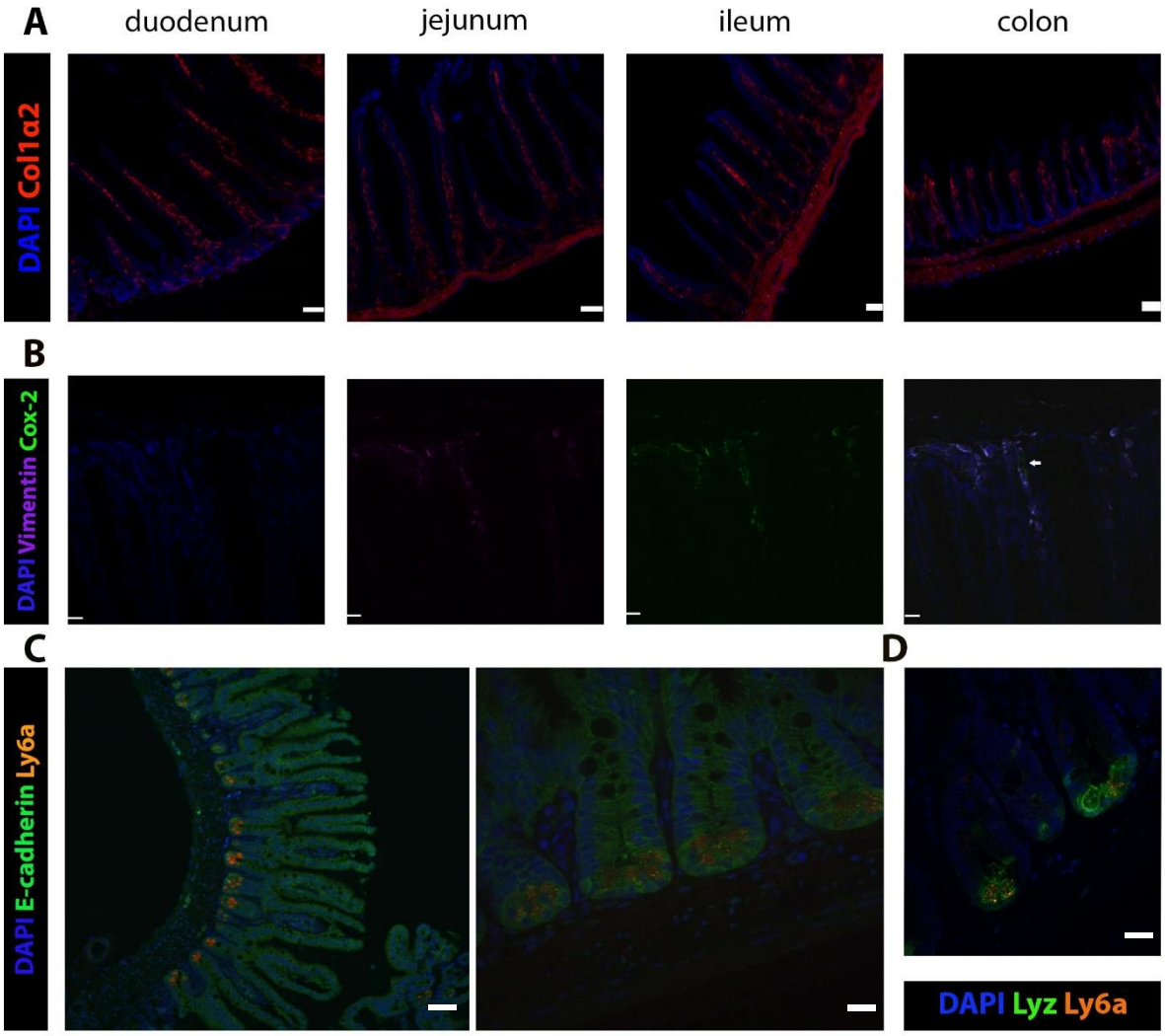

Figure 7.1. Marker-based characterization of intestinal cell populations. (A) Fluorescent imaging of intestinal sections of *Col1α2CreERRosa26Tomato* reporter mice. Col1α2 is a collagen subset showing expression in distinct mesenchymal and smooth muscle cell populations throughout the intestinal mucosal-submucosal interface. Scale bar 50 µm **(B)** Immunostainings on murine small intestinal tissue sections for the mesenchymal markers Vimentin (AF-648) and Cox-2 (AF-488). Cox-2 positive cells specifically show in pericryptal region as indicated by the white arrow. Scale bar 9 µm **(C)** Immunostainings on murine small intestinal tissue sections for the epithelial and stem cell markers E-cadherin (AF-488) and Ly6a (PE-Cy7). Scale bars 100 and 20 µm **(D)** Immunostaining for the Paneth and stem cell markers Lysozyme (AF-488) and Ly6a (PE-Cy7) on murine small intestinal tissue. Scale bar 50 µm.

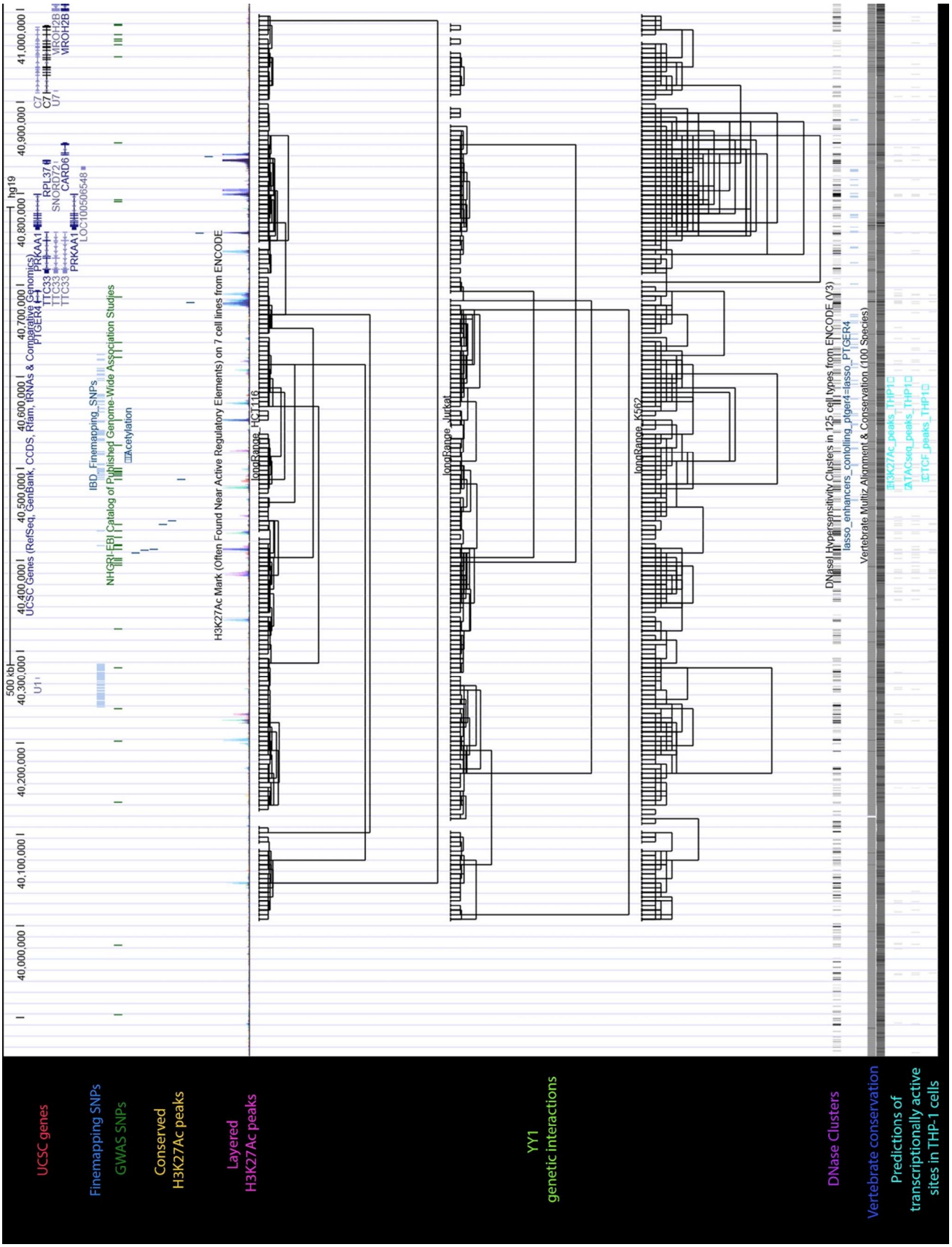

Figure 7.2. *PTGER4* is linked to a potential enhancer element overlapping with IBD GWAS hits. YY1 datasets (Weintraub *et al.*, 2017) have been imported to UCSC Genome Browser (Kent et al., 2002; https://genome.ucsc.edu/) and found *PTGER4* to be linked with parts of the upstream enhancer region as indicated as an IBD-associated risk locus by GWAS. Additional UCSC datasets, suggestive of transcriptional activity (DNase clusters) are included in the above picture in order to refine the

enhancer region, specifically applied to relevant human cell lines, which were also used for CRISPR/Cas9 studies during this project.

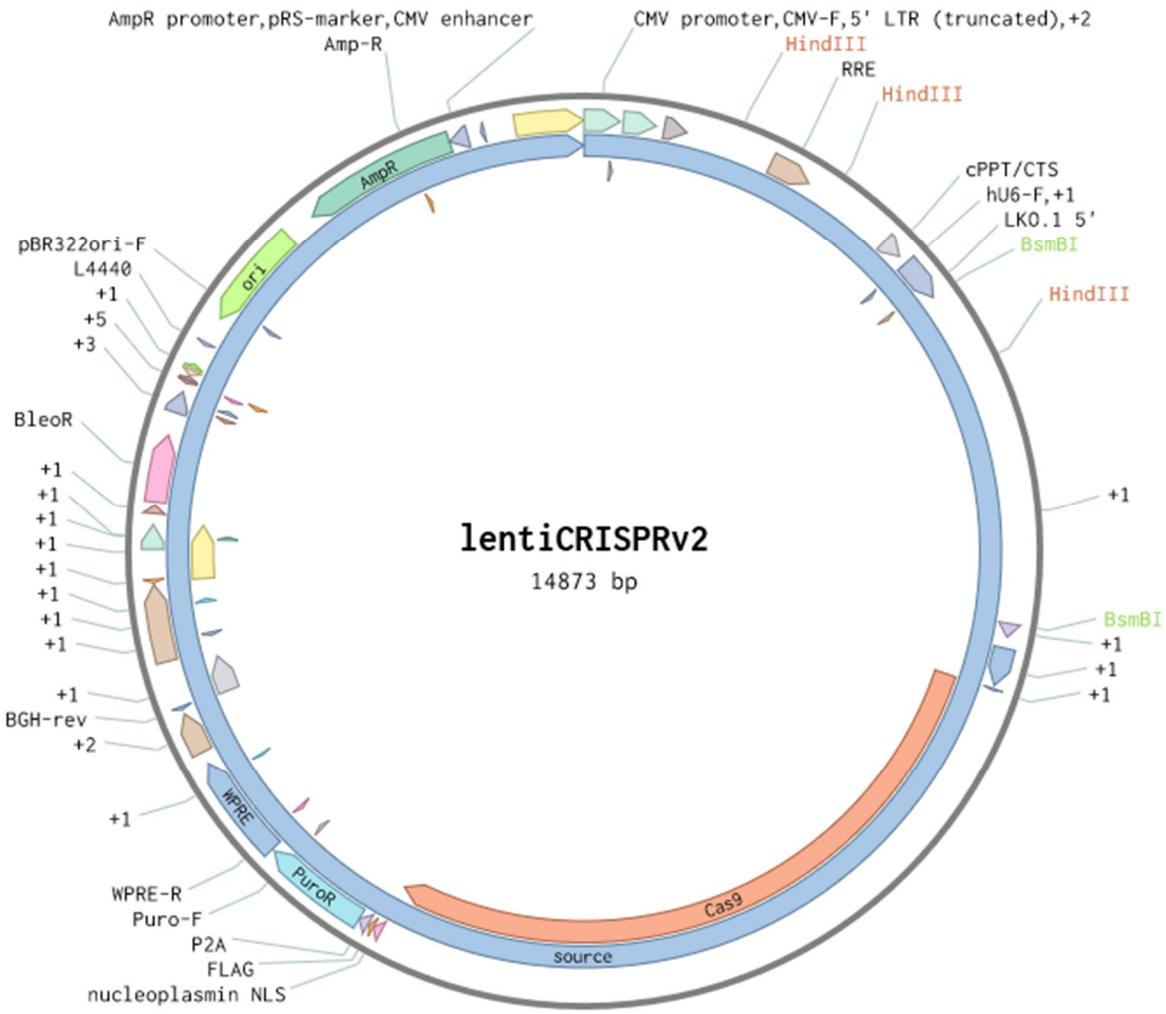

Figure 7.3. Vector map of the lentiCRISPRv2 plasmid used for CRISPR/Cas9 mediated knockout system. lentiCRISPRv2 plasmid (Sanjana, Shalem and Zhang, 2014)**.** Vector map has been designed and obtained from Benchling (Benchling, 2018; https://benchling.com/).

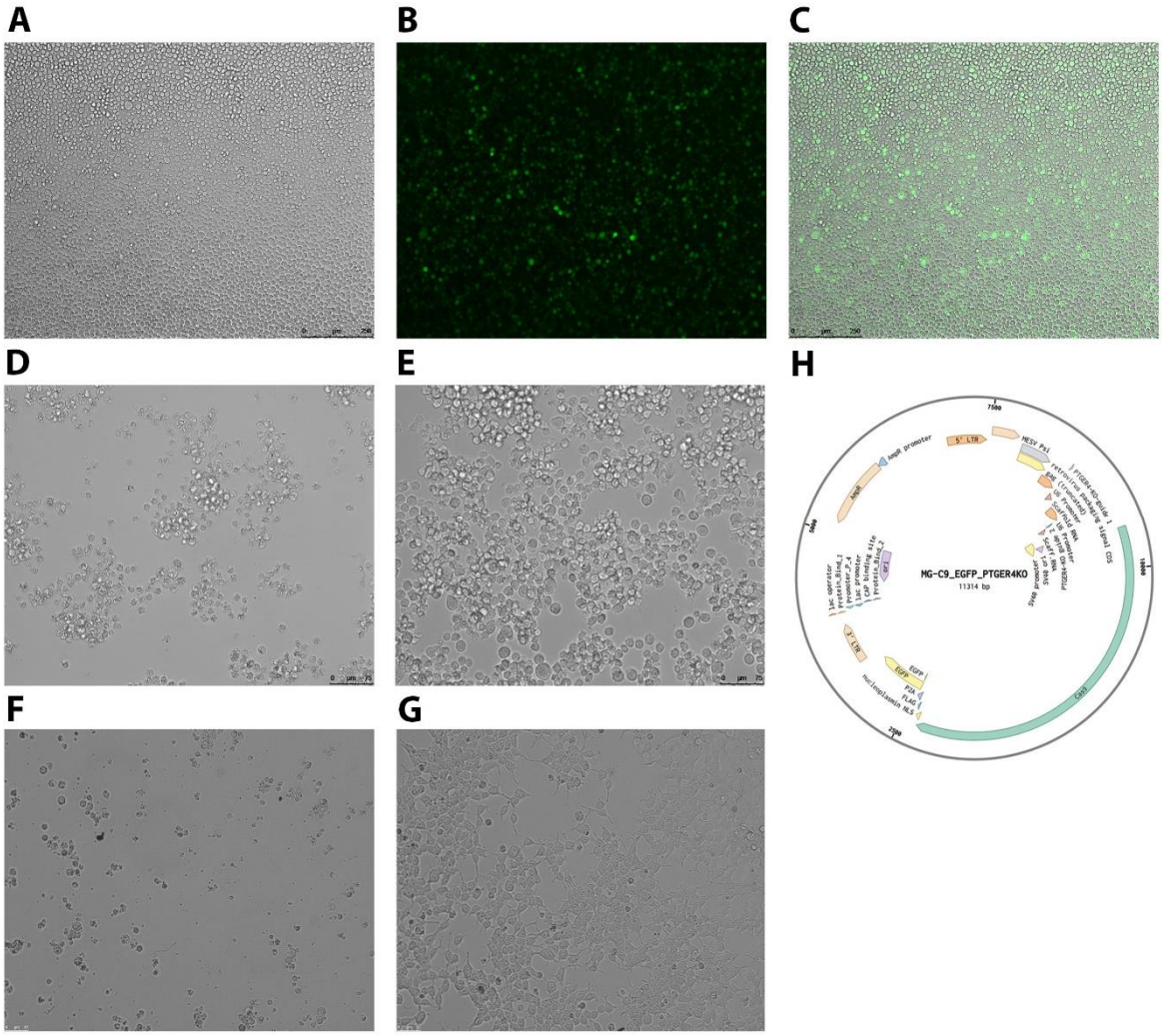

Figure 7.4. Transduction of HEK-293 and THP-1 cells via two viral CRISPR/Cas9 systems. (A) – (C) THP-1 monocytes after retroviral transduction with lentivirus containing MG-Cas9-EGFP-recombinant plasmid (Flavell lab, unpublished). (A) Brightfield (B) Fluorescent (GFP) channel and (C) overlay. Scale bar 250 µm **(D) – (E)** THP-1 monocytes after lentiviral transduction with lentiCRISPRv2 plasmid as shown before after treatment with puromycin. (D) Non-transduced control (E) transduced cells. Scale bar 75 µm **(F) – (G)** HEK-293 cells after transduction with lentiCRISPRv2 plasmid following treatment with puromycin. (F) Non-transduced control (G) Transduced cells. Scale bar 50 µm. **(H)** Vector map of MG-Cas9-EGFP-recombinant plasmid (Flavell lab, unpublished) used in (A) – (C). For *PTGER4* gene knockout this plasmid contains two guide RNAs targeting the gene derived from the same geneblock that was introduced to lentiCRISPRv2 as described elsewhere.

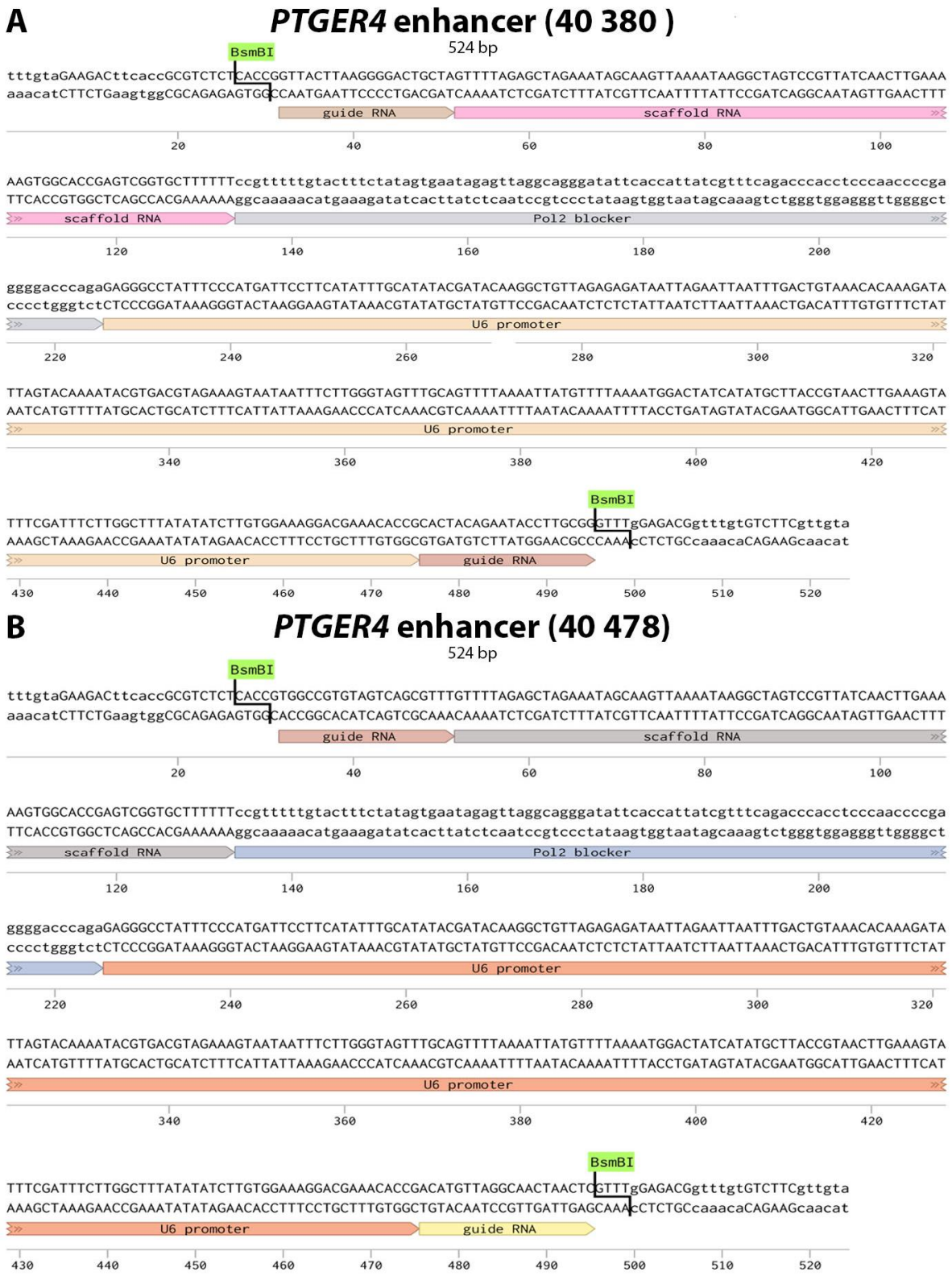

Figure 7.5. Visualization of the two geneblocks targeting different enhancer elements upstream of *PTGER4.* (A) *PTGER4* enhancer geneblock targeting the region Chr5:40 380 000 – 40 481 000 **(B)** *PTGER4* enhancer geneblock targeting the region Chr5:40 478 000 – 40 630 000. Geneblock design as shown above has been obtained from Benchling (Benchling, 2018; https://benchling.com/).

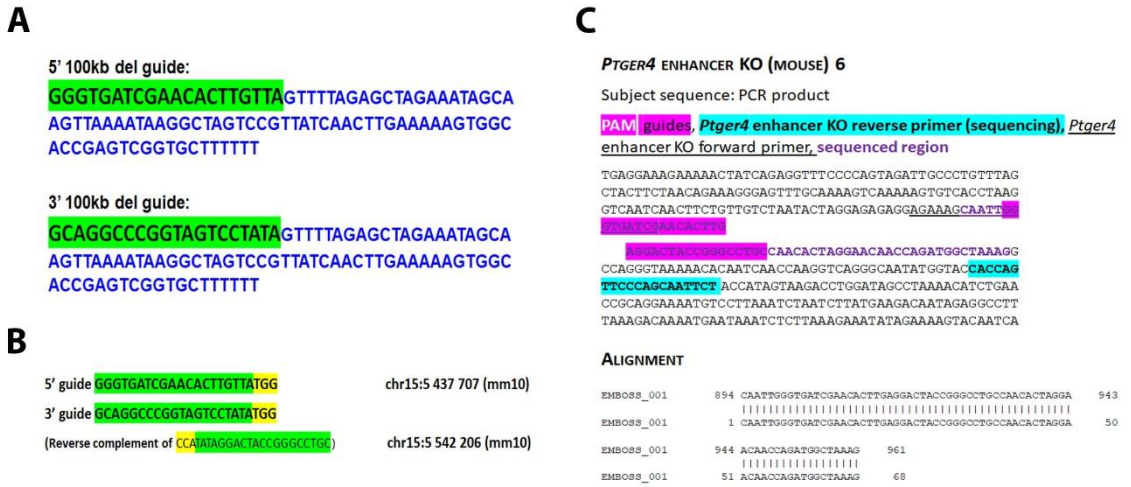

Figure 7.6. Design of a *Ptger4* enhancer knockout mouse (A) Sequences of the two guide RNAs and scaffolds targeting a 100 kb enhancer element upstream of *Ptger4* as they were delivered to murine zygotes via microinjection **(B)** Guide RNA sequences only together with the coordinates of the genetic regions they are targeting. PAM sequences in yellow **(C)** Sanger sequencing results of a *Ptger4* enhancer knockout mouse.

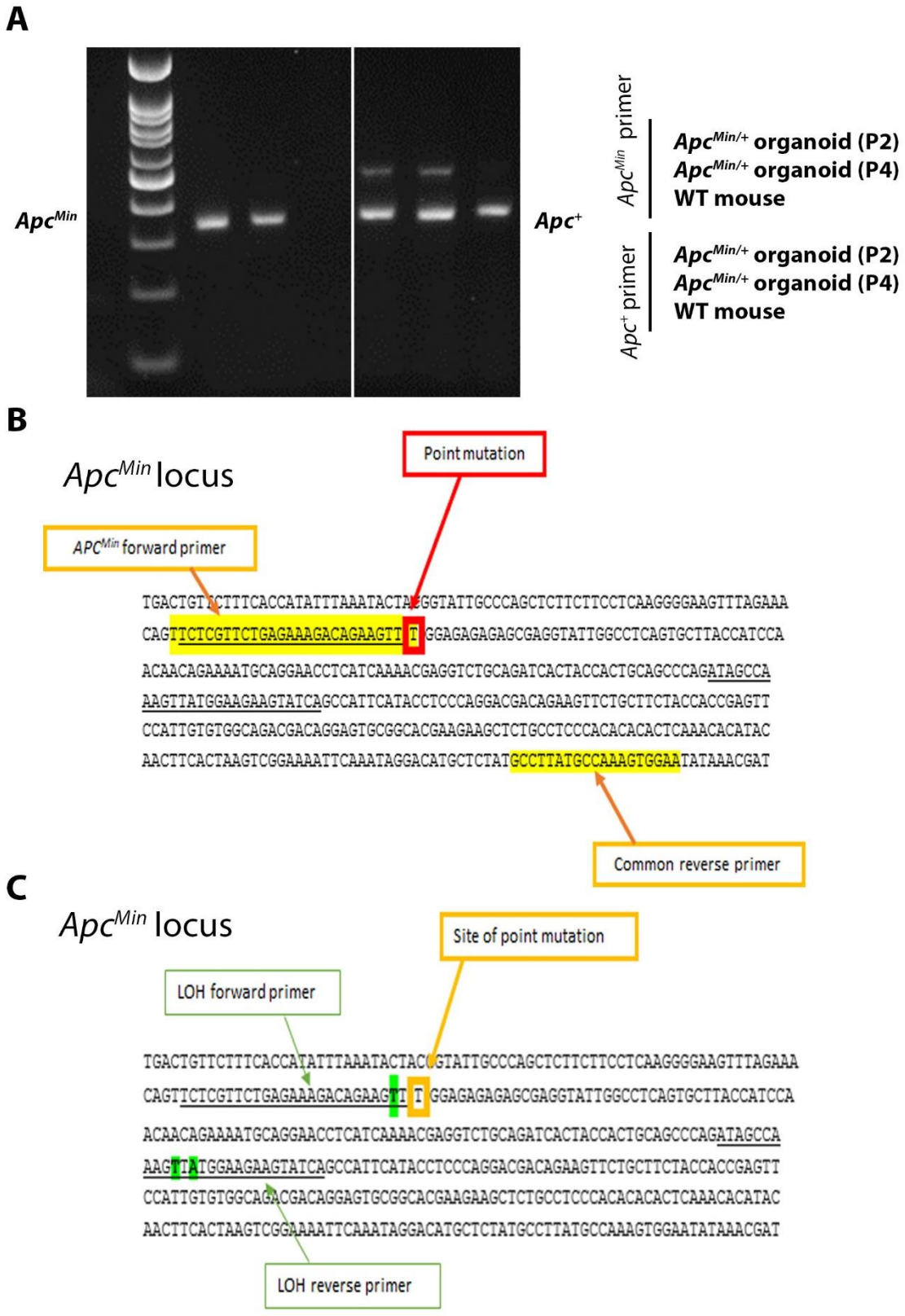

Figure 7.7. Determining the genotype of *Apc*$^{Min/+}$ organoids (A) Alternative genotyping strategy to determine the presence or absence of the wildtype *Apc* allele in organoids by using primers specifically annealing to the mutated and non-mutated gene region, respectively **(B)** Visualization of the *Apc*^{Min} genetic locus with binding sites of the primers used in (A) indicated **(C)** Visualization of the *Apc*^{Min} genetic locus with binding sites of the primers used for the loss-of-heterozygosity restriction assay indicated. Green highlights the bases that ought to be altered via the implemented primer set so that restriction sites for the HindIII enzyme will be created.

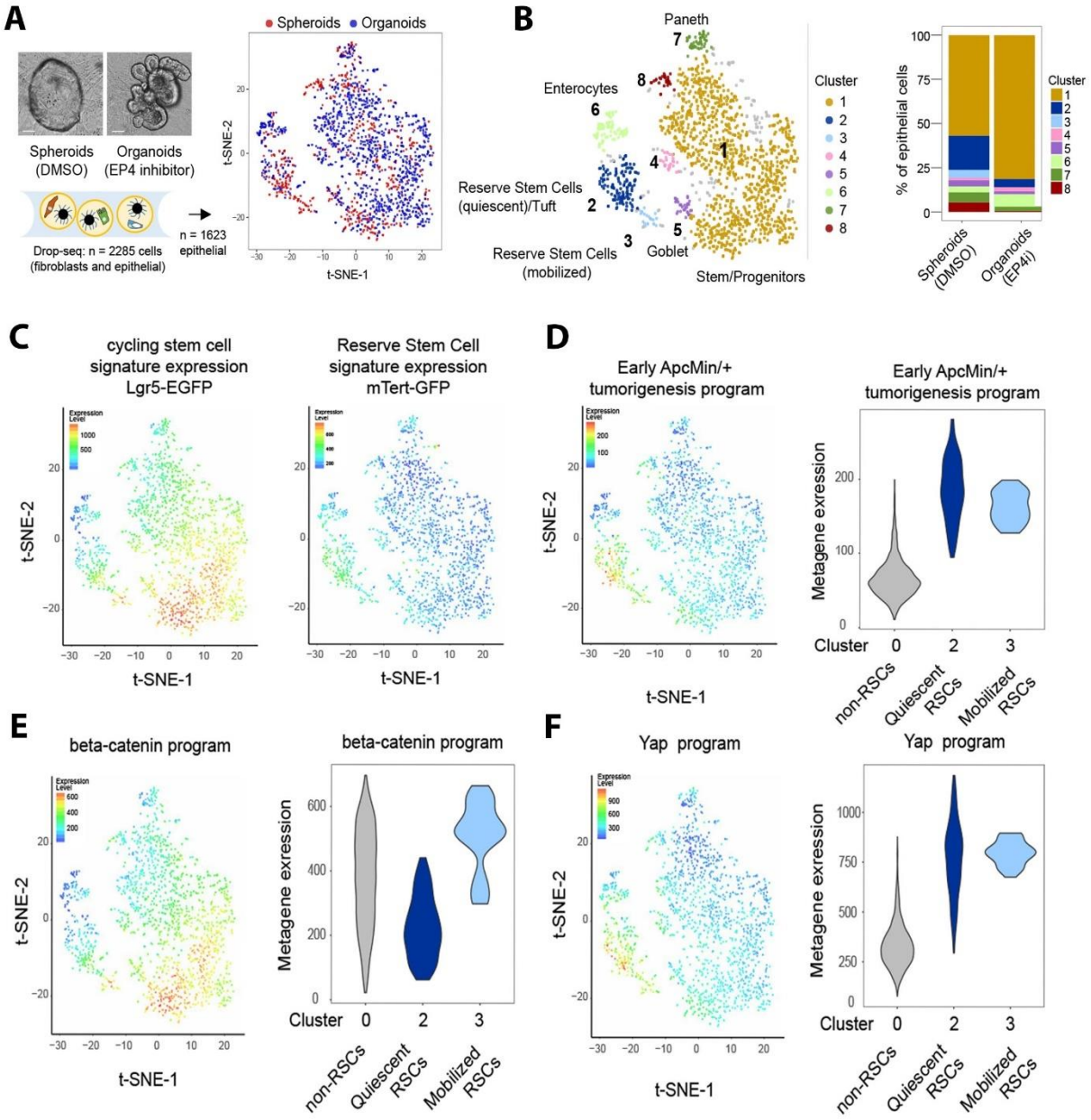

Figure 7.8. Single-cell RNA-seq analysis reveals a Yap-mediated tumorigenic program in non-actively cycling stem cells driven by fibroblast-mediated PGE_2 signaling. (A) Gene expression profiles via droplet-based single-cell RNA-seq (Drop-seq) were obtained from spheroid and organoid structures derived from co-culture experiment of intestinal crypts with fibroblasts supplemented with DMSO (spheroids) or EP4 inhibitor (organoids). 1623 single epithelial cells from both structures are visualized in a t-SNE plot **(B)** Single cells (n=1623) assigned to clusters representing distinct epithelial cell populations on a t-SNE plot and proportionate visualization of those within the total amount of spheroid and organoid cells **(C)** Expression of the transcriptional signature of Lgr5-EGFP+ (actively cycling) and mTert-GFP+ cells (quiescent) stem cells in single epithelial cells as shown via overlay on t-SNE plots **(D)-(F)** Expression levels of molecular programs in single epithelial cells shown via overlay on t-SNE plots and violin plots specifically comparing between actively cycling (non-RSCs), quiescent and mobilized reserve stem cells (RSCs) **(D)** Early (non-tumor) *Apc*$^{Min/+}$ tumorigenesis program **(E)** β-catenin (proliferation) program **(F)** Yap program. Graphs and data were obtained from Roulis, M. *et al.* (unpublished) and shown as supplementary information in the context of this thesis to help better understand the experimental outline and conclusions drawn from it.

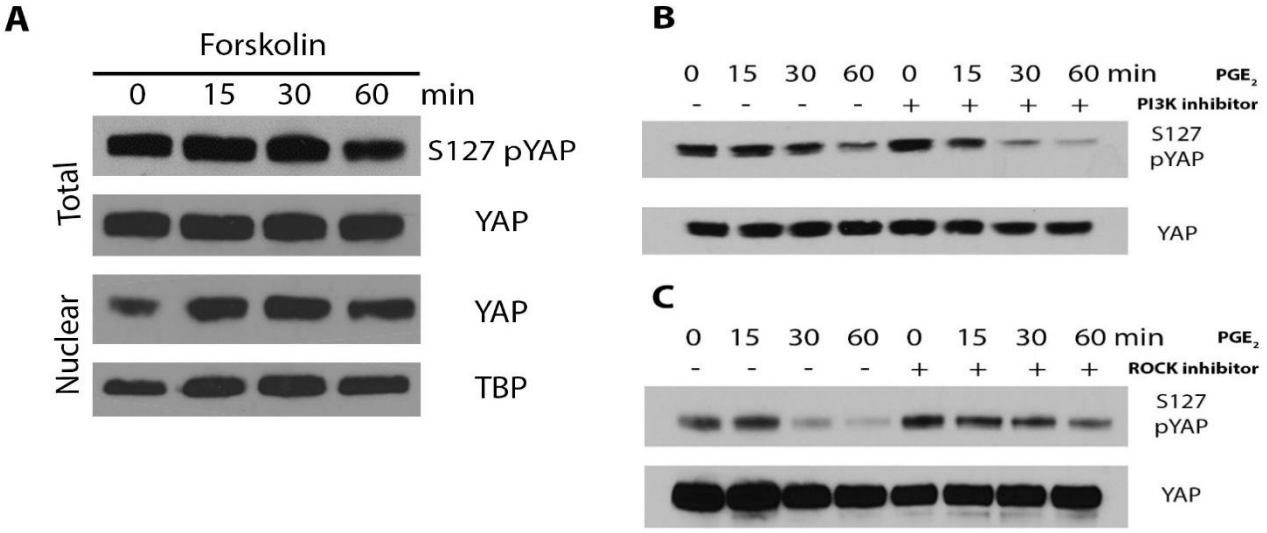

Figure 7.9. Studying signaling axes downstream of PGE_2-YAP signaling (A) Western blot analysis of the effect of Forskolin, an adenylate cyclase activator, on wildtype (WT) organoid samples on YAP signaling **(B)** Western blot analysis of the effect of PI3K inhibitor on YAP signaling downstream of PGE_2. PI3K inhibitor has been applied to WT organoid samples 1 hour prior to PGE_2 stimulation. Total protein lysates are shown **(C)** Western blot analysis of the effect of ROCK inhibitor on YAP signaling downstream of PGE_2. ROCK inhibitor has been applied to WT organoid samples 1 hour prior to PGE_2 stimulation. Total protein lysates are shown.

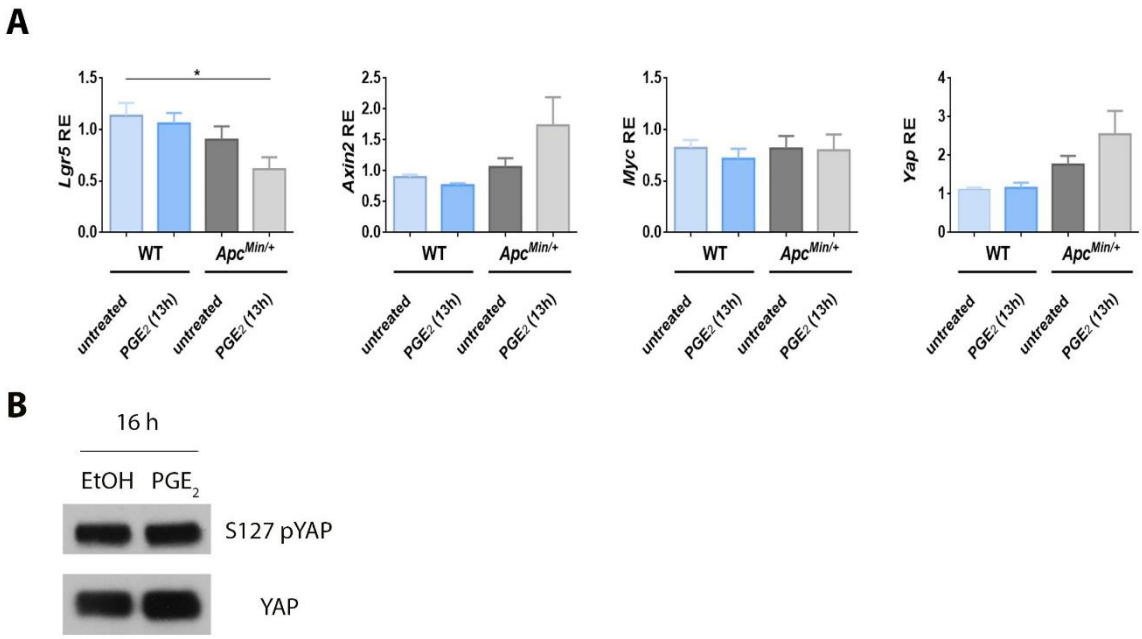

Figure 7.10. Relative expression of β-catenin target genes in wildtype versus *Apc$^{Min/+}$* mouse organoids. (A) RT-qPCR results of genes typically activated by β-catenin in mouse wildtype versus *Apc$^{Min/+}$* organoid samples following 13 hours treatment with or without 0.1 µM dmPGE$_2$. * p-value < 0.05 **(B)** Western blot analysis of phosphorylated and total YAP upon 16 hours PGE$_2$ stimulation in total protein lysates of *Apc$^{Min/+}$* organoids.

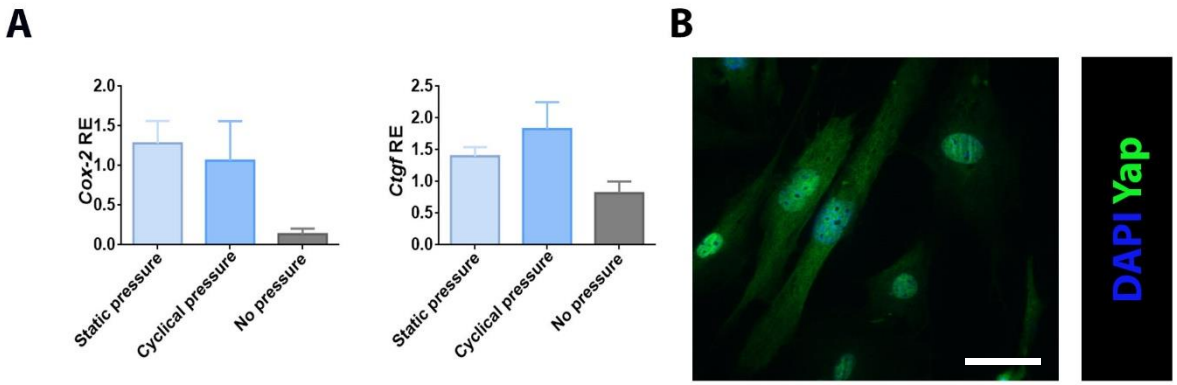

Figure 7.11. Effect of pressure and cytoskeletal cues on PGE_2-Yap signaling. (A) Relative expression levels of *Cox-2* and *Ctgf* as a well-established Yap target in mouse fibroblasts upon treatment with static (30 mmHg for 6 hours), cyclical (55 – 115 mmHg in alternating cycles for 6 hours) or no pressure **(B)** Immunostaining for Yap (AF-488) on murine fibroblasts after *in vitro* culture. Scale bar 50 µm

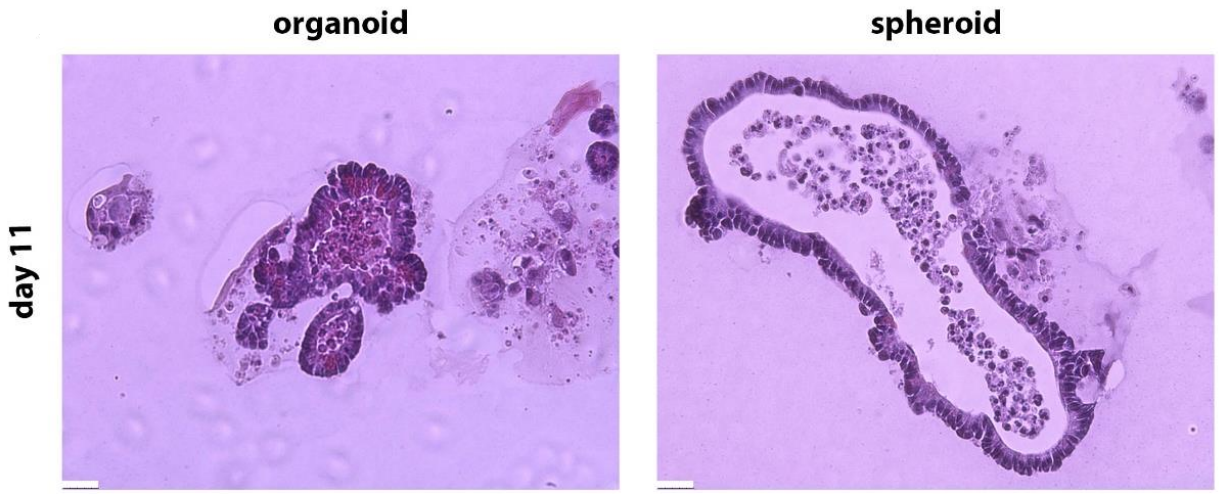

Figure 7.12. H&E stainings on organoids and spheroids. H&E stained histological sections of organoids and spheroids after 11 days with or without co-culture with murine fibroblasts. Scale bar 25 µm.

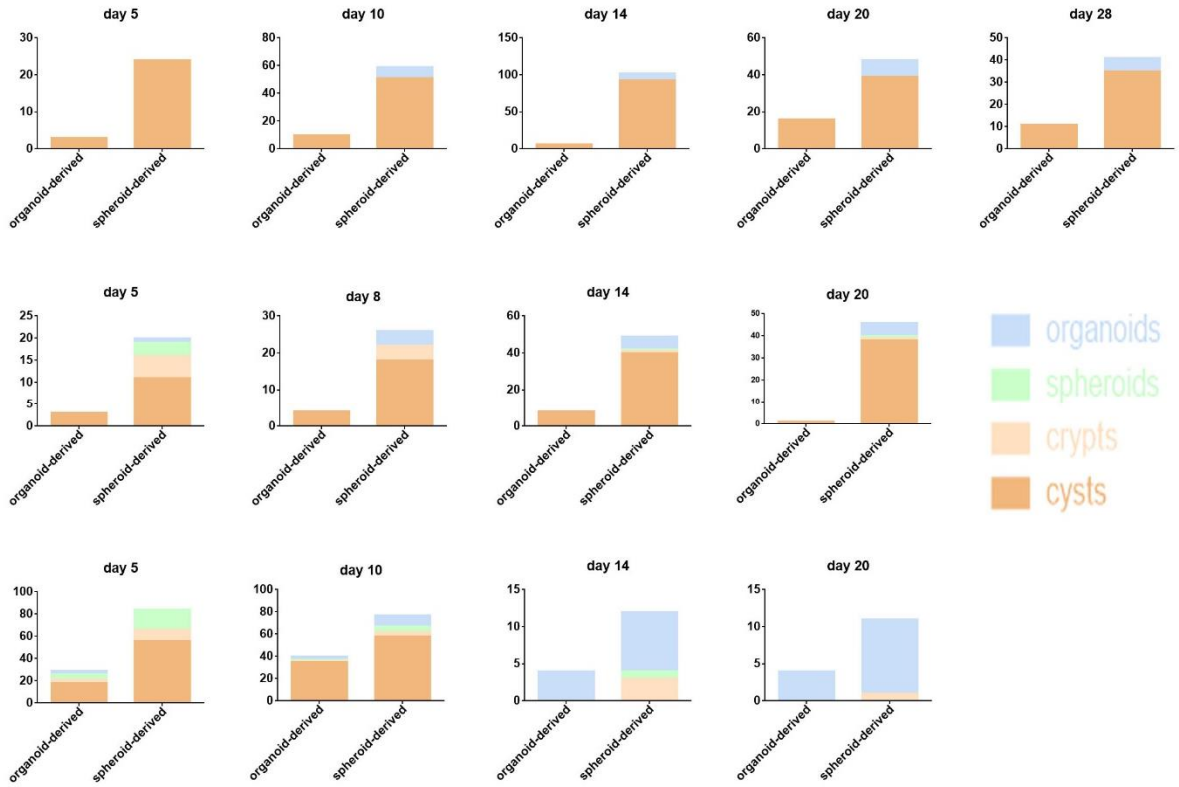

Figure 7.13. Stemness assays on organoids and spheroids. Repeats of the aforementioned stemness assay based upon the quantification of the different morphological structures obtained from organoid- versus spheroid-derived single cells. Structures were counted on the indicated days of culture.

Supplementary Tables

PCR program			Primer sequence	Name
95°C	5 min		TTCTGAGAAAGACAGAAGTTA	*Apc*^{Min} forward primer
95°C	1 min	|	TTCTGAGAAAGACAGAAGTTT	*Apc*$^{+}$ forward primer
57°C	1 min	| x35	TTCCACTTTGGCATAAGGC	common reverse primer
72°C	1 min	|	TCTCGTTCTGAGAAAGACAGAAGCT	LOH forward primer
72°C	5 min		TGATACTTCTTCCAAAGCTTTGGCTAT	LOH reverse primer
4°C	∞			

Table 7.1. List of primer sequences and PCR program for *Apc*$^{Min/+}$ organoid genotyping. HindIII restriction site encompasses AAGCTT. The underlined bases in the LOH primers introduce point mutations to the genetic DNA sequence so as to create additional HindIII restriction sites. Therefore, the WT allele after PCR reaction will display 2, the mutated Min allele 1 HindIII restriction site. Exact product sizes can be derived from Strauss J. *et al.* (1994).

Quantitative real-time PCR program		
95°C	30 seconds	
95°C	5 seconds	x40
60°C	45 seconds	
65°C	+0.5°C/cycle	x60
95°C		

Table 7.2. Quantitative real-time PCR program. Quantitative real-time PCRs were run using CFX96 Touch™ Real-Time PCR Detection System (BioRad).

Primer sequence (forward)	Primer sequence (reverse)	Gene
TTCTGGTGCTTGTCTCACTGA	CAGTATGTTCGGCTTCCCATTC	*B2m*
GAAAGAGCTCAGGGACTGGAGTGTT	TTAGGAGGGCAGATGGGTAAGCAA	*Ly6a*
GCTCATTGCTGGGTACTTACAA	CCAGACTTGGCACAAGACAGG	*Il1rn*
CTTAGTCTTGGGTGGATA	TCTTCTGTCTTACAGCCA	*Msln*
GCTGCTGATCTGGGACAATG	ACCTACTCCCTTGAGTGGACA	*Clu*
CCTTGTCTCTTGCGTTCTTCC	TCCAAAGTACCCTGCGGTATC	*Cxcl16*
AGAACACTGACTTTGAATGG	CACTTGGAGATTAGGTAACTG	*Lgr5*
AAGATCACAAAGAGCCAAAG	GAAAAAGTAGGTGACAACCAG	*Axin2*
AGCTGTTTGAAGGCTGGATT	AATAGGGCTGTACGGAGTCG	*Myc*
GATGTCTCAGGAATTGAGAAC	CTGTATCCATTTCATCCACAC	*Yap1*
QT00165347 (QIAGEN)		*Ptgs2 (Cox-2)*
GGGCCTCTTCTGCGATTTC	ATCCAGGCAAGTGCATTGGTA	*Ctgf*
TCCTTGCACTCCTGTTTC	GATACGTATATAGGGGTCCAG	*OSM* (human)

Table 7.3. List of RT-qPCR primers. Primer sequences are listed in 5'-3' orientation and have been tested for efficiency via standard curves. All primers listed have been utilized to determine murine gene expression.

PCR program for geneblock amplification		
98°C	2 minutes	
98°C	10 seconds	x34
57°C	1 minute	

72°C	1 minute	
72°C	2 minutes	
12°C	5 minutes	

Table 7.4. PCR program for initial geneblock amplification. PCR program for Q5 High-Fidelity DNA Polymerase mediated PCR reaction of *PTGER4* enhancer geneblocks for subsequent cloning procedure.

	guide RNA sequence	**Genetic coordinates (genome assembly)**	
human	GAGGCGGACGAATTGACCCCGGG	Chr5: 40 679 498 (hg38)	***PTGER4***
	ACAATCAAGTTGACTCACGTGGG	Chr5: 40 692 530 (hg38)	
	GTTACTTAAGGGGACTGCTATGG	Chr5: 40 380 280 (hg19)	***PTGER4*** **enhancer**
	CACTACAGAATACCTTGCGGAGG	Chr5: 40 481 479 (hg19)	
	TGGCCGTGTAGTCAGCGTTTTGG	Chr5: 40 478 100 (hg19)	
	ACATGTTAGGCAACTAACTCAGG	Chr5: 40 630 105 (hg19)	
mouse	GGGTGATCGAACACTTGTTATGG	Chr15: 5 437 707 (mm10)	***PTGER4*** **enhancer**
	GCAGGCCCGGTAGTCCTATATGG	Chr15: 5 542 206 (mm10)	

Table 7.5. List of guide RNAs used for CIRSPR/Cas9 systems in human cell lines and mice. Guide RNAs are shown in 5'-3' orientation with PAM-sequences underlined and have been designed and proof-read ('CRISPR', crispr.mit.edu ; Johnson *et al.*, 2008; Bae, Park and Kim, 2014; Park, Bae and Kim, 2015). Genetic coordinates as derived from the indicated genome assembly, i.e. hg38 and hg19 for humans and mm10 for mice, are listed.